

# **For Reference**

---

**NOT TO BE TAKEN FROM THIS ROOM**

EX LIBRIS  
UNIVERSITATIS  
ALBERTAENSIS







Digitized by the Internet Archive  
in 2020 with funding from  
University of Alberta Libraries

<https://archive.org/details/Carola1970>









THE UNIVERSITY OF ALBERTA

EXPERIMENTAL AND THEORETICAL STUDIES

OF  $^{53}\text{Cr}$  AND  $^{55}\text{Fe}$

by



Toussaint Paul Georges CAROLA

A THESIS

SUBMITTED TO THE FACULTY OF GRADUATE STUDIES

IN PARTIAL FULFILMENT OF THE REQUIREMENTS FOR THE DEGREE

OF DOCTOR OF PHILOSOPHY

DEPARTMENT OF PHYSICS

EDMONTON, ALBERTA

FALL, 1970





Thesis  
1970 F  
103

UNIVERSITY OF ALBERTA  
FACULTY OF GRADUATE STUDIES

The undersigned certify that they have read,  
and recommend to the Faculty of Graduate Studies for  
acceptance, a thesis entitled EXPERIMENTAL AND THEORETICAL  
STUDIES OF  $^{53}\text{Cr}$  AND  $^{55}\text{Fe}$  submitted by Toussaint Paul  
Georges Carola in partial fulfilment of the requirements  
for the degree of Doctor of Philosophy.

Date July 13<sup>th</sup>, 1970





## ABSTRACT

This work deals with the experimental and theoretical investigation of  $^{53}\text{Cr}$  and  $^{55}\text{Fe}$ . Excited states of  $^{53}\text{Cr}$  were studied by means of the  $^{52}\text{Cr}(\text{d},\text{p}\gamma)^{53}\text{Cr}$  reaction. In the case of  $^{55}\text{Fe}$ , the  $^{55}\text{Mn}(\text{p},\text{n}\gamma)$  reaction was used. The theoretical calculations based on Nilsson model and the unified model are compared with experiment and other available calculations.

The decay modes of many of the excited states of  $^{53}\text{Cr}$  below 4.25 MeV excitation energy have been determined by means of the  $^{52}\text{Cr}(\text{d},\text{p}\gamma)^{53}\text{Cr}$  reaction. Previous tentative spin assignments of  $5/2^-$ ,  $3/2^-$  and  $9/2^+$  to the 1.006 MeV, 2.324 MeV and 3.715 MeV levels respectively have been confirmed. New spin assignments are the following:  $5/2$  or  $9/2$  to the 2.227 MeV level,  $3/2^-$  to the 3.190 MeV level,  $5/2$  to the 3.271 MeV level and  $1/2$  or  $3/2$  to the 3.971 MeV level. Multipole mixing ratios are given for many of the observed transitions.

The study of the  $^{55}\text{Mn}(\text{p},\text{n}\gamma)^{55}\text{Fe}$  reaction resulted in the determination of decay modes, spin assignments and multipole mixing ratios for levels of  $^{55}\text{Fe}$  between 2.5 and 3.1 MeV excitations. New spin assignments are the following:  $11/2^-$ ,  $(9/2)$  for the 2.542 MeV level,  $9/2$  for the 2.984 MeV level and  $(11/2, 9/2)$  for the 3.076 MeV level. Measurements are in agreement with the  $3/2^-$  assignment of the 3.027 MeV level.

The Nilsson model was used to predict energy levels of  $^{53}\text{Cr}$  and  $^{55}\text{Fe}$



but the fit to experimental results is only fair. Calculations based on the intermediate coupling in the unified model yielded energy levels, electromagnetic transition rates, branching ratios, mixing ratios, lifetimes and spectroscopic factors.

These calculations resulted in an overall agreement with experimental results for most of the levels of  $^{53}\text{Cr}$  and  $^{55}\text{Fe}$  below  $\simeq 2.5$  MeV excitation. Comparison is also made with other available calculations based on the unified model, the "Thankappan and True" model and the shell model.





## ACKNOWLEDGEMENTS

I would like to thank my supervisor, Dr. W.C. Olsen for his support and encouragement during the course of this work.

I am very grateful to Dr. P.J. Twin who played an active role in the initial phase of the project.

I wish to thank Dr. D.M. Sheppard for numerous discussions and comments on all aspects of this work. Thanks also to Dr. B.D. Sowerby and Dr. B. Robertson for their help and comments.

To the members of the "old team", Norm Davison, Bob Humphries, Dave Hutcheon and J.G. Strumpfito, for the many discussions, the fine spirit and the hard work, Thank you.

A special mention to Aadu Pilt, whose help and enthusiasm were precious: Tānan Vāga, Aadu. My sincere thanks to my colleagues who assisted in doing the runs: Peter Green, Paul Gutowski, Ed Wong and Woon Chung.

Je tiens à remercier le Dr. W.K. Dawson sans qui l'utilisation des ordinateurs ne serait qu' incomplète et imparfaite. Many thanks also to Mr. Jim Easton for his help and advice in computer programming.

A large part of this project deals with theoretical work. The help and comments of Dr. H.S. Sherif in this regard were greatly appreciated. I also wish to thank Dr. H. Ohnuma for extending his shell model calculations and for a fruitful correspondence, Dr. J.B. McGrory for his comments on the calculations, and Dr. V.K. Gupta.

The cooperation of the technical staff, in particular, Miss Elsie





Hawirko, Miss Greta Tratt, Jock Elliott, Con Green, Lars Holm, Paul Karvonen, Ron Popik and Harold Fodchuk, has been deeply appreciated.

My sincere thanks to Miss Audrey Forman for the efficient and very careful typing of the manuscript.

The financial assistance of the University of Alberta, in particular in the form of a Dissertation Fellowship for this last year is gratefully acknowledged.

A Roselyne  
Juillet 1970



# TABLE OF CONTENTS

	Page
CHAPTER I MOTIVATION	1
CHAPTER II EXPERIMENTAL INVESTIGATION OF $^{53}\text{Cr}$	5
1. Theory	6
1.1. Gamma-ray distributions for decay of aligned states	6
1.2. Alignment in the case of triple angular correlation	10
1.3. $\chi^2$ fitting of angular distributions	11
1.4. Restriction on the population parameter ratio	12
2. Experimental Procedure	14
2.1. Apparatus	14
2.2. Analysis of the gamma-ray spectra	19
2.3. Angular distribution analysis	19
3. Lifetime Measurements in $^{53}\text{Cr}$	21
4. Experimental Results	24
4.1. The levels below 2.0 MeV	24
4.2. The levels between 2.0 and 3.6 MeV	28
4.3. Levels above 3.6 MeV	34
CHAPTER III THE $^{55}\text{Mn}(p,n\gamma)^{55}\text{Fe}$ REACTION	39
1. The Compound Nuclear Statistical Theory of Gamma-Ray Angular Distributions	40
1.1. Introduction	40
1.2. Conditions for alignment in the $A(a,b)B^*$ experiment	41
1.3. Gamma-ray angular distributions and the statistical model	43



2.	Experimental Procedure	Page 48
2.1.	Apparatus	48
2.2.	Acquisition and analysis of data	48
3.	Experimental Results	54
3.1.	Determination of branching ratios	54
3.2.	The 2.211 MeV level	58
3.3.	The 2.301 MeV level	58
3.4.	The 2.542 MeV level	60
3.5.	The 2.578 MeV level	63
3.6.	The 2.818 MeV level	64
3.7.	The 2.871 MeV level	64
3.8.	The 2.938 MeV level	65
3.9.	The 2.984 MeV level	66
3.10.	The 3.027 MeV level	69
3.11.	The 3.076 MeV level	69
CHAPTER IV	THEORETICAL INVESTIGATION OF $^{53}\text{Cr}$ AND $^{55}\text{Fe}$	71
1.	Motivation	71
2.	Nilsson Model Calculations	74
2.1.	Theory	74
2.2.	Application of Nilsson model to $^{53}\text{Cr}$ and $^{55}\text{Fe}$	82
3.	The Intermediate Coupling in the Unified Model	88
3.1.	Introduction	88
3.2.	Outline of the intermediate coupling model	89



3.3.	Application of the model to the study of $^{53}\text{Cr}$ and $^{55}\text{Fe}$	Page 90
3.4.	Justification of the use of this model	93
4.	The Thankappan and True Model	98
5.	Shell Model Calculations for $N = 29$ Odd-Nuclei	100
6.	Comparison between Theoretical Calculations and Experimental Data	102
6.1.	Energy spectra	103
6.2.	Branching ratios	108
6.3.	Electromagnetic properties	111
6.4.	Spectroscopic factors	118
7.	Concluding Remarks	122
CHAPTER V	CONCLUSION	125
APPENDIX	A description of intermediate coupling calculations in the unified model.	





# LIST OF TABLES

	Page
Table I     A summary of Legendre Polynomials. Coefficients fitted to the angular distributions of transitions observed in the $^{52}\text{Cr} (d,p\gamma)^{53}\text{Cr}$ reaction at a bombarding energy of 4.11 MeV. The value of multipole mixing ratios are given for the spin sequences indicated.	33
Table II    A summary of the measured branching ratios in $^{55}\text{Fe}$ for levels at energies $\geq 2.144$ MeV. The results are compared with those of Pilt (Pi 69) and Fischbeck et al. (Fi 66).	55
Table III $^{55}\text{Mn}(p,n\gamma)^{55}\text{Fe}$ reaction. Values of Legendre polynomial coefficients $a_2$ and $a_4$ for the angular distribution of the 1371 keV gamma ray resulting from the decay of the 2.301 MeV ( $9/2^-$ ) state to the 0.930 MeV ( $5/2^-$ ) state for different proton bombarding energies.	60
Table IV    Legendre polynomial coefficients, corrected for solid angle effects, fitted to angular distributions of gamma rays deexciting levels of $^{55}\text{Fe}$ .	62
Table V     A summary of spin assignments and multipole mixing ratios determined in this study of the $^{55}\text{Mn}(p,n\gamma)^{55}\text{Fe}$ reaction.	68
Table VI    Parameters corresponding to the best fits of the energy levels of $^{53}\text{Cr}$ and $^{55}\text{Fe}$ for Nilsson model calculations.	84
Table VII   Sets of parameters used in the intermediate coupling model calculations.	91



	Page
Table VIII    Expansion coefficients corresponding to states $ E(\text{keV})$ ; $I\pi>$ of $^{53}\text{Cr}$ for the parameters corresponding to set B in Table VII.	94
Table IX       Expansion coefficients corresponding to states $ E(\text{keV})$ ; $I\pi>$ of $^{55}\text{Fe}$ for the parameters corresponding to set E in Table VII.	95
Table X        Calculated and measured branching ratios for some levels in $^{53}\text{Cr}$ . Calculations are based on the intermediate coupling model and the shell model.	109
Table XI       Experimental and theoretical branching ratios for levels of $^{55}\text{Fe}$ up to 2.578 MeV. The theoretical calculations are based on the intermediate coupling model and the shell model.	110
Table XII      Electromagnetic transition strengths and lifetimes in $^{53}\text{Cr}$ calculated from the intermediate coupling model. The cal- culated lifetimes are compared with experimental results when available.	112
Table XIII    Electromagnetic transition strengths and lifetimes in $^{55}\text{Fe}$ calculated from the intermediate coupling model. The cal- culated lifetimes are compared with experimental results.	113
Table XIV      Experimental and theoretical reduced transition probability for electric quadrupole radiation resulting from decay to ground of lower states of $^{53}\text{Cr}$ .	114



	Page
Table XV	Calculated and measured mixing ratios in $^{53}\text{Cr}$ and $^{55}\text{Fe}$ . 115
Table XVI	Calculated and measured static moments in $^{53}\text{Cr}$ and $^{55}\text{Fe}$ . 117
Table XVI	Sample spectroscopic factors, $(2J+1)S$ , for the $^{52}\text{Cr}(d,p)^{53}\text{Cr}$ reaction. The experimental values were obtained by averaging the results given in (An 64, Bo 65, SS 64 and Ra 68), and are compared with theoretical values calculated from different models. 120
Table XVII	Sample spectroscopic factors, $(2J+1)S$ , for the $^{54}\text{Fe}(d,p)^{55}\text{Fe}$ reaction. The experimental values were obtained by averaging the results given in (Ma 64) and (Fu 63), and are compared with theoretical values calculated from different models. 121





## LIST OF FIGURES

	Page
Figure 1 Schematic diagram of target chamber and detector assembly.	15
Figure 2 Block diagram of coincidence electronics used in the correlation measurements.	17
Figure 3 Charged particle spectrum in coincidence with gamma rays for the $^{52}\text{Cr}(d,p\gamma)^{53}\text{Cr}$ reaction at a bombarding energy of 4.11 MeV.	25
Figure 4 A summary of branching ratios and spin assignments of some of the excited states of $^{53}\text{Cr}$ below 4.3 MeV.	26
Figure 5 Gamma rays in coincidence with protons populating the 1.537 MeV level in $^{53}\text{Cr}$ .	29
Figure 6 The 2.227 MeV state: The angular distribution (a) and $\chi^2$ plots (b and c) for the 690 keV transition to the 1.537 MeV ( $7/2^-$ ) level in $^{53}\text{Cr}$ are shown.	30
Figure 7 a) Gamma rays in coincidence with protons populating the triplet in $^{53}\text{Cr}$ at 2.664 MeV, 2.676 MeV and 2.715 MeV. b) Gamma rays in coincidence with protons populating the 3.146 MeV and 3.190 MeV levels in $^{53}\text{Cr}$ .	32
Figure 8 The 3.271 MeV state: The angular distribution (a) and $\chi^2$ plots (b) for the 3271 keV ground state transition are shown.	33



	Page
Figure 9 The 3.715 MeV state: The angular distributions of the 2430 keV and 1285 keV gamma rays in cascade are shown.	37
Figure 10 A schematic diagram of the reaction process involved in the study of the (p,n $\gamma$ ) reaction.	41
Figure 11 A typical gamma-ray spectrum taken at a bombarding energy of 4.35 MeV with the 15 cc Ge(Li) detector.	50
Figure 12 Relative efficiency curve for the 15 cc Ge(Li) detector. The experimental points correspond to measurements taken using a $^{56}\text{Co}$ source.	52
Figure 13 The $^{55}\text{Fe}$ energy level diagram: The branching ratios for levels below 2.144 MeV were determined by Pilt (Pi 69).	57
Figure 14 The 2.211 MeV level: Angular distribution (a) and $\chi^2$ plots (b) for the 801 keV gamma-ray transition to the 1.410 MeV (7/2) level.	59
Figure 15 The 2.542 MeV level: Angular distribution (a) and $\chi^2$ plots (b) for the 1224 keV gamma-ray transition to the 1.318 MeV (7/2 $^-$ ) level.	61
Figure 16 The 2.984 MeV level: Angular distribution (a) and $\chi^2$ plots (b) for the 1574 keV gamma-ray transition to the 1.410 MeV (7/2 $^-$ ) level.	67



- Figure 17 The 3.076 MeV level: Angular distribution (a) and  $\chi^2$  plots (b) for the 1666 keV gamma-ray transition to the 1.410 MeV ( $7/2^-$ ) state. 70
- Figure 18 Nilsson model orbits as a function of the deformation parameter  $\delta$ , for  $\mu = 0.25$  and  $\kappa = 0.085$ . 77
- Figure 19 A schematic diagram describing the different angular momenta involved in the study of a deformed odd-A nucleus. 79
- Figure 20 Nilsson model calculations: Theoretical and experimental spectra are shown for  $^{53}\text{Cr}$  and  $^{55}\text{Fe}$ . 85
- Figure 21 The intermediate coupling model: Energy levels of the total Hamiltonian as a function of the coupling parameter  $\xi$ . 92
- Figure 22 Energy levels and spins in  $^{53}\text{Cr}$  as predicted by intermediate coupling model and shell model calculations are compared with experimental results. 104
- Figure 23 Energy levels and spins of  $^{55}\text{Fe}$  as predicted by intermediate coupling model and shell model calculations are compared with experimental results. 105
- Figure 24 The T.T. model: Calculations of energy levels in  $^{53}\text{Cr}$  (Ph 70) and  $^{55}\text{Fe}$  (La 70) are compared with experimental results obtained in this work. 107



## CHAPTER I

### MOTIVATION

From the measurements of electromagnetic properties in nuclei, it is possible to determine the modes of decay of nuclear levels, their spins, parities, electromagnetic transition rates, static moments, . . . without reference to a particular theory of nuclear interactions. These measurements constitute a good test for the predictions of nuclear models.

In the last decade, there has been great interest shown in the study of odd-A,  $N = 29$  nuclei as they have a simple  $\nu 2p_{3/2}$  configuration and are expected to be easily described by theoretical calculations. There are four nuclei of interest:  $^{49}_{20}\text{Ca}$ ,  $^{51}_{22}\text{Ti}$ ,  $^{53}_{24}\text{Cr}$  and  $^{55}_{26}\text{Fe}$ . All four nuclei have been studied by (d,p) stripping reaction on the nearest even nucleus (K<sub>a</sub> 64, Ba 64, Ra 68, Ma 64 and references therein). These studies have resulted in the determination of energy levels up to 6 to 8 MeV excitation. Comparatively, there has been little work done to determine gamma-ray decay scheme and spin assignments of these levels. This explains why theoretical calculations were mainly concerned with reproducing energy levels and spectroscopic factors rather than with the electromagnetic properties.

Many factors must be taken into consideration before doing gamma-ray work: target-making feasibility, Q-value of the reaction, problem of





contaminants, competing reactions, gamma-ray yield are among the most important. Their evaluation will permit to decide whether or not an experiment is feasible and also what type of method is to be used to extract as much information as possible.

$^{48}\text{Ca}$  targets are difficult to make and oxidize very easily even under good vacuum. The presence of a large amount of oxygen, which is not a major hindrance for study of stripping reactions, virtually eliminates all possibility of the study of the  $(d,p\gamma)$  reaction, if coincidence requirements are imposed, as most of the  $\gamma$ -yield originates from the contaminant. Self-supporting targets of  $^{50}\text{Ti}$  are easy to prepare and the metal does not oxidize too easily. Unfortunately, the gamma yield is too low to permit any  $p\text{-}\gamma$  coincidence study of the  $(d,p\gamma)$  reaction. The study of  $^{53}\text{Cr}$  and  $^{55}\text{Fe}$ , on the other hand, proved to be quite feasible and is the object of the present work.

The stripping reaction  $^{52}\text{Cr}(d,p)^{53}\text{Cr}$  has been extensively studied in the past few years (An 64, Bo 64, Ro 65 and Ra 68). However, only the decay modes of levels below 2.5 MeV had been determined (Ro 65, Ra 68) prior to this work. Assignments of the spins of the excited states of  $^{53}\text{Cr}$  had been based on  $(n,n'\gamma)$  and  $(n,\gamma)$  experiments (Va 62, Ba 65) and on the empirical rules in the analysis of pick-up and stripping reactions (Ra 68, Wh 67). Most of these assignments were tentative.

The level scheme of  $^{55}\text{Fe}$  has been determined from  $(d,p)$  reactions (Fu 63, Ma 65) and little has been done in the study of the gamma-ray decay until the recent work of Pilt (Pi 69) who determined the spins and



gamma decay of most of the levels below 2.6 MeV excitation, using the  $^{55}\text{Mn}(p,n\gamma)^{55}\text{Fe}$  reaction. The shell model predictions of Ohnuma (Oh 66) appeared to be in very good agreement with Pilt's results. These calculations also predicted two high-spin states below 3.0 MeV excitation ( $11/2$  at 2.790 MeV and  $13/2$  at 2.975 MeV) not reported by Pilt. It was therefore decided to extend the study of  $^{55}\text{Fe}$  up to the 3 MeV region in order to investigate the possibility of the existence of such high-spin states.

There are two main approaches to the theoretical study of odd-A  $N = 29$  nuclei. First, shell model calculations in which  $^{48}\text{Ca}$  is considered as an inert core. Effective p-p and p-n interactions are used to describe the different configurations outside this core (Ve 66, Oh 66).

The second approach is based on the intermediate coupling model and considers the coupling of the odd nucleon to the neighbouring even core, which is either in its ground state or in an excited state. If the nature of the excited states of the core is not supposed to be known, the so-called "Thakappan and True" approach is used (Th 65). Such calculations were quite successful in describing the low lying levels of  $^{63}\text{Cu}$  (Th 65). Recently, this type of calculation was used to describe the  $N = 29$  odd nuclei (Ph 70, La 70). In a more specific approach, one considers the even core as capable of performing quadrupole oscillations. This approach was used by Ramavataram (Ra 63) to describe  $N = 29$  odd nuclei.

In the calculations of Ramavataram, only levels with spins up to  $7/2$  were taken into consideration. Moreover, these calculations were done at



a time when very little was known experimentally about  $^{53}\text{Cr}$  and  $^{55}\text{Fe}$ . Similarly the shell model calculations of Ohnuma (Oh 66) and Vervier (Ve 66) dealt mainly with predictions of energy levels and calculations of spectroscopic factors. In order to attempt a quantitative appraisal of the merits of the respective models, more complete calculations were needed. Such calculations based on the intermediate coupling model were undertaken in this work while existing shell model calculations were extended by Ohnuma (Oh 70).

If the odd nucleon is strongly coupled to a deformed core, Nilsson model calculations are then applicable. Such calculations have been fairly successful in describing  $^{57}\text{Fe}$  and  $^{59}\text{Fe}$  (So 67, So 69). As  $^{52}\text{Cr}$  and  $^{54}\text{Fe}$  are not strongly deformed (see e.g. Go 62), Nilsson model calculations for  $^{53}\text{Cr}$  and  $^{55}\text{Fe}$  have very little chance of success. However, it was thought that such calculations might yield some fair results if band mixing was included, and they were consequently attempted.





## CHAPTER II

### EXPERIMENTAL INVESTIGATION OF $^{53}\text{Cr}$

The spins and mixing ratios for many of the levels below 4.3 MeV excitation in  $^{53}\text{Cr}$  were obtained using the  $^{52}\text{Cr}(\text{d},\text{p}\gamma)^{53}\text{Cr}$  reaction, by application of Method II of Litherland and Ferguson (Li 61), with detection of the protons at approximately  $180^\circ$ . Branching ratios were also measured in this experiment. Lifetimes were determined via the  $^{53}\text{Cr}(\text{p},\text{p}'\gamma)^{53}\text{Cr}$  reaction using the Doppler Shift technique, but the results obtained were rather limited.

Section 1 describes the theoretical aspects involved in this study. Detailed theoretical treatment of the study of gamma-ray angular distributions can be found in articles by Litherland and Ferguson (Li 61), Poletti and Warburton (Po 65) and Rose and Brink (Ro 67). Consequently, the presentation of this theory will be limited to general principles. The notation and sign conventions of Rose and Brink will be used throughout. Section 2 describes the experimental procedure associated with the study of angular distributions. A description of the Doppler Shift Attenuation Method can be found in an article by Litherland (Li 64). This method will be outlined in section 3. The experimental results are given in detail in section 4.



## 1. THEORY

### 1.1. Gamma-ray Distributions for Decay of Aligned States

Consider the reaction  $A(a,b)B^*$  where neither the target nucleus  $A$  nor the beam of particles  $a$  is polarized. It is also assumed that the residual nucleus  $B^*$  is an excited state  $|J_1 m_1\rangle$  with definite parity. The state  $|J_1 m_1\rangle$  is said to be aligned if the population parameters  $P(m_1)$  [probability that the  $m_1^{\text{th}}$  substate is populated] satisfy the relation  $P(m_1) = P(-m_1)$ . Because the state  $|J_1 m_1\rangle$  has definite parity, there is symmetry under reflection through a plane normal to the beam direction (Fe 65). Under these conditions, (unpolarized target and beam, intermediate state of definite parity), there is alignment with respect to the beam axis as long as the beam axis remains an axis of cylindrical symmetry.

Consider the state  $|J_1 m_1\rangle$  decaying by emission of a gamma ray to a state  $|J_2 m_2\rangle$ . If  $q$  defines the circular polarization, ( $q = \pm 1$ ) and if  $\vec{k}$  is the wave vector of the gamma ray, the probability amplitude for such a transition may be represented by:

$$A_{m_1 m_2}^q(\vec{k}) = -\sqrt{\frac{k}{h}} \sum_{Lm\pi} q^\pi \langle J_1 m_1 | T_{Lm}^{(\pi)} | J_2 m_2 \rangle \mathcal{D}_{mq}^L(R) \quad (\text{II.1})$$



Where  $D_{mq}^L(R)$  is the rotation matrix describing the rotation  $R = (\alpha\beta\gamma)$  which takes the beam axis  $z$  into the direction  $\vec{k}^\dagger$ ; the operator  $T_{Lm}^{\pi>}$  is the electromagnetic operator of parity  $\pi$  [ $\pi = 0$  for electric and 1 for magnetic multipolarity].

If the orientation of the spin  $J_2$  of the final state is not observed, then the probability of transition from the state  $|J_1 m_1>$  to any substate of  $J_2$  by emission of a photon is

$$\sum_{m_2} |A_{m_1 m_2}^q(\vec{k})|^2 \quad (\text{II.2})$$

Assuming that there is cylindrical symmetry, the total transition probability is then equal to equation (II.2) weighted by the relative probability of population of each substate of the initial state  $|J_1 m_1>$  i.e. it is given by:

$$\sum_{m_1} P(m_1) \sum_{m_2} |A_{m_1 m_2}^q(\vec{k})|^2 \quad (\text{II.3})$$

This expression is proportional to the number of gamma rays emitted in the direction  $\vec{k}$ . For its evaluation, equation (II.1) is substituted into (II.3). In the resulting expression, the product of rotation matrices

---

<sup>†</sup>  $\alpha, \beta$  and  $\gamma$  are the Euler angles of the rotation.



can be expressed in terms of expansions in Legendre Polynomials; the operator matrix elements are reduced by application of the Wigner-Eckart theorem. Finally, the sums involving different Clebsch-Gordan coefficients are reduced by techniques of Racah Algebra. The resulting angular distribution is:

$$\begin{aligned}
 W(J_1 \rightarrow J_2; kq) &= \frac{k}{h} \sum_{\substack{kLL' \\ \pi\pi'}} B_k(J_1) P_k(\cos\theta) (-)^{q+J_1-J_2+L'-L-k} \\
 &\times \sqrt{2J_1+1} (LqL'-q | k0) W(J_1 J_1 LL'; kJ_2) \\
 &\times q^{\langle\pi+\pi'\rangle} \langle J_1 || T_L^{\langle\pi\rangle} || J_2 \rangle \langle J_1 || T_{L'}^{\langle\pi'\rangle} || J_2 \rangle^* \quad (II.4)
 \end{aligned}$$

in which:

$$B_k(J_1) = \sum_{m_1} P(m_1) (-)^{J_1-m_1} \sqrt{2J_1+1} (J_1 m_1 J_1 -m_1 | k0)$$

There are limitations of the multipole order  $L$  of a given transition  $J_1 \rightarrow J_2$ , namely:  $|J_1 - J_2| \leq L < J_1 + J_2$  (conservation of angular momentum) and  $L \neq 0$  (intrinsic spin of photon is 1). Also, for a given  $L$ ,  $\pi$  is restricted to electric or magnetic because parity is conserved in this interaction. In general, only the lowest orders contribute to a transition and it is, in most cases, sufficient to consider the two lowest multipole orders  $L$  and  $L'$ . One then defines the multipole mixing ratio  $\delta$  as:





$$\delta = \frac{\langle J_1 || T_L^{(\pi)} || J_2 \rangle}{\langle J_1 || T_L^{(\pi)} || J_2 \rangle} \sqrt{\frac{2L'+1}{2L+1}} \quad L' > L \quad (\text{II.5})$$

In this study, polarization is not observed. One can then write the angular distribution formula as:

$$W(\theta) = \sum_k B_k(J_1) P_k(\cos\theta) \frac{R_k(LLJ_1J_2) + 2\delta R_k(LL'J_1J_2) + \delta^2 R_k(LLJ_1J_2)}{1 + \delta^2} \quad (\text{II.6})$$

where:

$$R_k(LL'J_1J_2) = (-)^{1+J_1-J_2+L'-L-k} \sqrt{(2J+1)(2L+1)(2L'+1)} (L_1L'-1|k0) \\ \times W(J_1J_1LL';kJ_2) \quad (\text{II.7})$$

Remarks:

a) In equation (II.6), the  $B_k(J_1)$  terms contain all the information on the alignment of the initial state  $|J_1m_1\rangle$ . The  $R_k$  terms depend specifically on the  $J_1 \rightarrow J_2$  gamma-ray cascade. The nuclear properties on the other hand, appear exclusively through the mixing ratio  $\delta$ .

b) In the Racah coefficients of equation (II.7), triangular relations limit  $k$  to  $k \leq \min(2L', 2J_1)$ .

c) As a consequence of alignment

$B_k(J_1) = 0$  if  $k$  is odd. Therefore, the angular distribution is limited to



even order Legendre polynomials and is consequently symmetric about  $90^\circ$ .

d) Equation (II.6) is established for an ideal point detector.

However, because of the finite size of the gamma detector, the distribution is "averaged-out" over the solid angle the detector subtends. For a cylindrical detector this attenuation may be corrected by introducing coefficients,  $Q_k$ , for each order of Legendre polynomial. In equation (II.6), each  $P_k(\cos\theta)$  is to be replaced by  $Q_k P_k(\cos\theta)$ . For standard size gamma detectors these coefficients have been tabulated [see e.g. (Wa 59)].

## 1.2. Alignment in the Case of Triple Correlation

In order to preserve alignment in the  $A(a,b)B^*$  reaction, the particles are detected at either  $0^\circ$  or  $180^\circ$  with respect to the beam axis in the case of triple correlation. Then, strong limitations occur in the number of magnetic substates that are populated (Li 61). Because the orbital angular momenta of the incoming and outgoing particles are perpendicular to the beam axis, only the intrinsic spins of the various particles involved contribute to the population parameters. That is, the largest projection which can be obtained in  $B^*$  is  $m_{\max} = J_A + s_a + s_b$  where  $J_A$ ,  $s_a$  and  $s_b$  are the intrinsic spins of the target, the incoming and outgoing particles respectively. In the  $^{52}\text{Cr}(d,p\gamma)^{53}\text{Cr}$  reaction,  $J_A = 0$ ,  $s_a = 1$  and  $s_b = 1/2$ , therefore  $m_{\max} = 3/2$  i.e. only  $P(3/2)$  and  $P(1/2)$  parameters are non-zero.

Because of the finite size of the detector, which in this experiment, was an annular silicon surface barrier detector situated at  $180^\circ$  with



respect to the beam axis, substates beyond  $m_{\max}$  can actually be populated. Litherland and Ferguson (Li 61) have shown that if  $\xi$  is the half angle subtended by the detector ( $\xi$  in radians), substates ( $m_{\max} + n$ ) are populated proportionally to  $\xi^{2n}$ . For reasonable detector-target distance, this effect is generally negligible as  $\xi$  is small.

### 1.3. $\chi^2$ Fitting of Angular Distributions

As shown earlier, in (d,p) experiments on even nuclei where the protons are detected at  $180^\circ$ , only the magnetic substates  $m = 3/2$  and  $m = 1/2$  are populated. The theoretical angular distribution of the gamma rays is expressed in terms of the population parameters, the mixing ratio  $\delta$  and the spin sequence. A linear least-squares fit of the theoretical distribution to the experimental distribution is made for a discrete set of fixed values of  $\delta$ . For each value of  $\delta$ , the best fit corresponds to those values where  $\chi^2$  is given by:

$$\chi^2 = \frac{1}{n} \sum_i [Y(\theta_i) - W(\theta_i)]^2 / E^2(\theta_i)$$

in which  $E(\theta_i)$  is the uncertainty assigned to the gamma-ray yield  $Y(\theta_i)$  at angle  $\theta_i$ ,  $W(\theta_i)$  is the theoretical yield and  $n$  is the number of degrees of freedom, (number of data points minus number of free parameters in  $W(\theta)$ ). Since  $\delta$  varies between  $-\infty$  and  $+\infty$ , it is more convenient to step through the finite range values of  $\arctan \delta$ . The resulting plots of  $\chi^2$  versus



$\delta$  show dips which correspond to possible solutions for at least one set of the allowed spins  $J_1$  and  $J_2$ . Sets of  $\delta$ ,  $J_1$  and  $J_2$  which correspond to a  $\chi^2$  lower than an assigned confidence limit are kept as possible solutions. The confidence limit is a measure of the probability that, for the correct theoretical expression,  $\chi^2$  will exceed a certain value. For example, with 5 degrees of freedom, the 1% confidence limit is 3.0. This means that  $\chi^2$  is expected to be larger than 3.0 in 1% of the measurements if the correct theory is used (in the present case, the correct spins and mixing ratio). The 0.1% confidence limit criterion is usually applied in the determination of spins and mixing ratios, i.e. solutions for which  $\chi^2$  exceeds the value at the 0.1% limit are rejected. The 0.1% confidence limit criterion was adopted in this work.

#### 1.4. Restriction on the Population Parameter Ratio

The technique described above takes no account of the physical reality of a state except in setting a population parameter to 0 when a negative value is obtained for it in the fitting procedure. The question arises then, whether all possible magnetic substate populations represent physical situations. This has been discussed by Goldfarb and Wong (Go 66) who have calculated the ratio of population parameters  $\xi = \frac{P(3/2)}{P(1/2)}$  in the case of the 2.324 MeV level of  $^{53}\text{Cr}$  excited via the  $^{52}\text{Cr}(d,p)$  reaction for several bombarding energies between 6.6 and 11 MeV. They have shown that, when







protons are detected at  $180^\circ$ ,  $\xi$  varies between 0.31 and 1.11 for the direct interaction mechanism, whereas  $\xi$  remains almost constant and equal to 1.10 for the compound nucleus mechanism. In this experiment, many weak non-stripping states were observed which are formed predominantly through the compound nuclear process. The experimental yield curve showed no strong resonance structure and narrow resonances would have been integrated over by the thick target. Hence it was considered that physically realistic situations would result from limits on  $\xi$  from 0.3 to 3.0. In section 4, this restriction is used to reject certain spin assignments for two states in  $^{53}\text{Cr}$ .



## 2. EXPERIMENTAL PROCEDURE

### 2.1. Apparatus

Deuterons from the University of Alberta CN Van de Graaff accelerator were used to bombard  $150 \mu\text{g}/\text{cm}^2$  thick self-supporting targets of chromium enriched to 99.9% in  $^{52}\text{Cr}$ . Natural chromium targets were also used for preliminary runs at 4.85 MeV bombarding energy. On the basis of the yield curve measurements between 4.0 and 5.5 MeV, deuteron energies of 4.11 MeV and 4.85 MeV were chosen for the experiment since they correspond to optimum excitation of the low lying levels of  $^{53}\text{Cr}$ . The beam current was maintained at about 200 nA. A series of three collimators lined with platinum determined a beam spot of about 1.5 mm diameter on target.

The target chamber is described in fig. 1. The protons were detected by an annular silicon surface barrier detector<sup>†</sup> located at  $180^\circ$  with respect to the beam direction. This detector, which has a resistivity of  $20,000 \Omega\text{-cm}$ , was operated at a bias of 100 volts and the resolution was better than 25 keV in the region of interest. A shield on the detector mount (fig. 1) prevented elastically backscattered deuterons from the tantalum beam stop from striking the detector face.

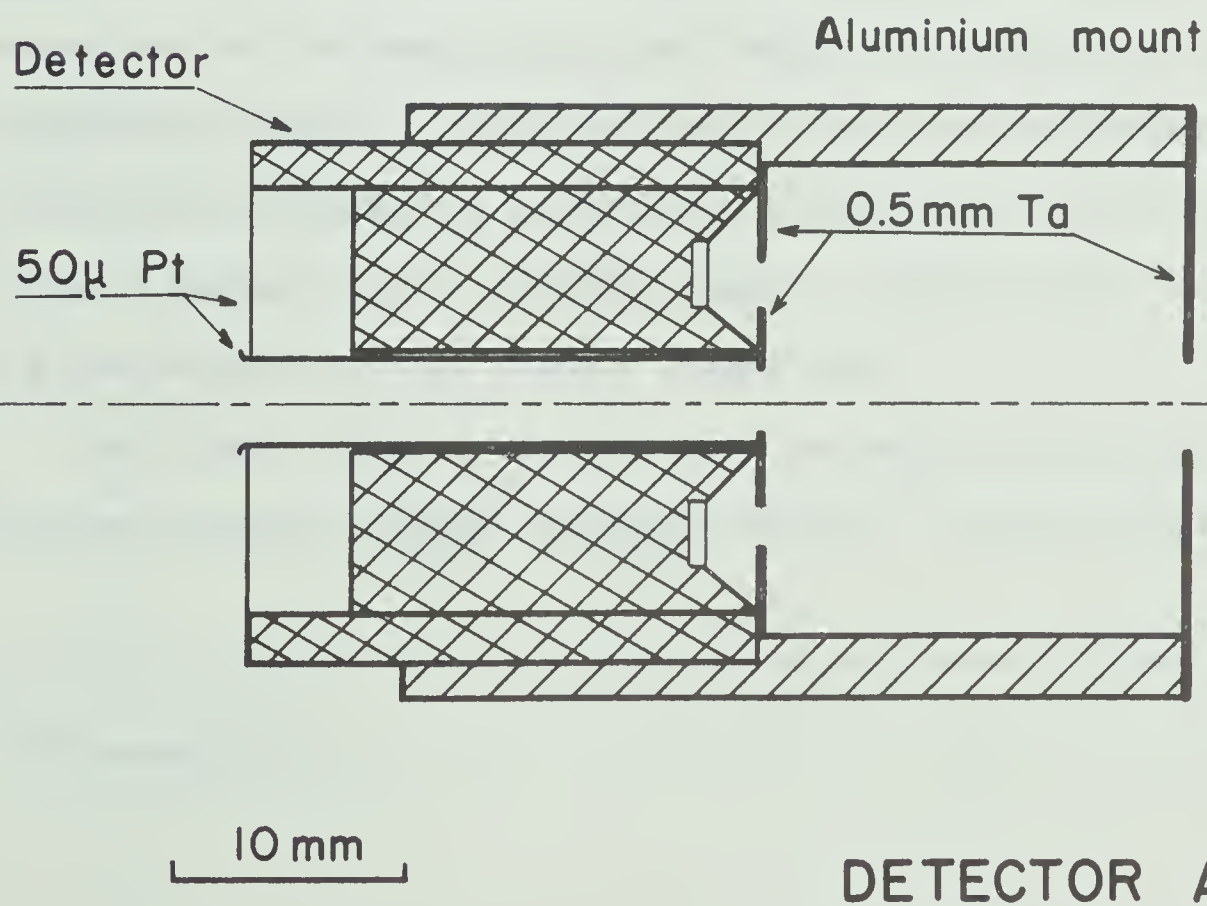
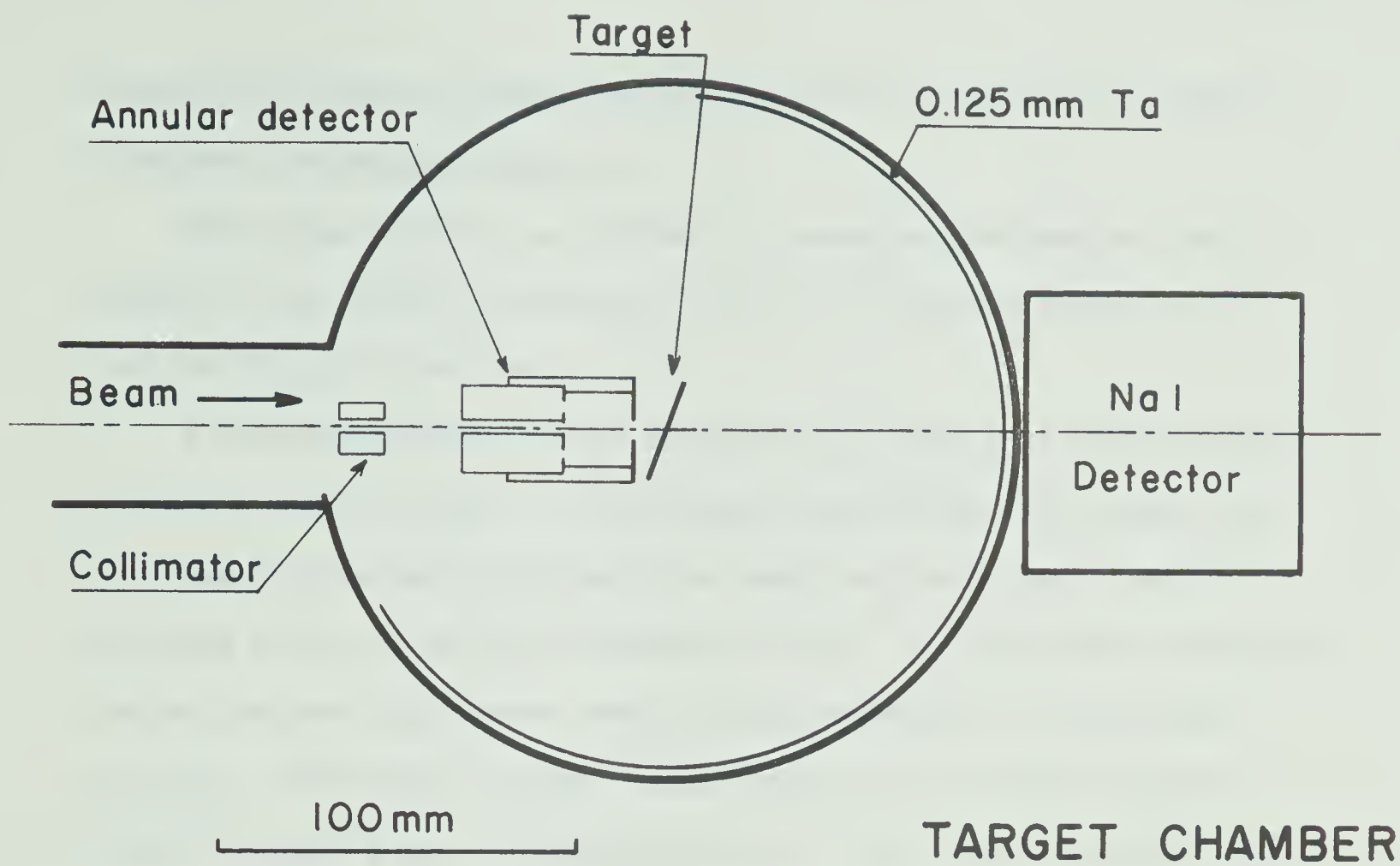
The gamma rays were detected by a 7.5 cm x 7.5 cm NaI(Tl) detector<sup>††</sup>

---

<sup>†</sup> Nuclear Diode Inc. ND PHG-35-14

<sup>††</sup> Harshaw "Integral line assembly" type 12S 12/3

Figure 1 Schematic diagram of target chamber and detector assembly





placed 10 cm from the target and shielded by 2 mm thickness of lead to eliminate low energy background.

The system isotropy was checked by measuring the angular distribution of the 3.09 MeV transition ( $1/2^+$  to  $1/2^-$  ground state) in  $^{13}\text{C}$  via the  $^{13}\text{C}(p,p')$  reaction.

A schematic diagram of the fast-slow coincidence of the electronic system is shown in fig. 2. Fast timing signals provided by fast zero crossing discriminators for both the gamma and the proton lines were fed into a time-to-amplitude converter (TAC). The time peak corresponding to the true coincidence events was approximately 15 nanoseconds f.w.h.m. Two windows of equal widths were set on the time spectrum, one of the time peaks corresponding to the "trues" plus "randoms" (T+R), the other on an adjacent region corresponding to the "randoms" (R). Both gamma and proton lines were self-gated in order to eliminate the low energy part of the spectra and thus, reduce the counting rates and their undesirable effects. The general coincidence gate was generated each time proton and gamma-ray pulses were in coincidence with either the "trues + randoms" or the "randoms" signal. The other gate used for routing was provided by the "randoms" signal only.

The linear signals, from the gamma and proton detectors, were fed into two analog-to-digital converters (ADC's)<sup>†</sup>. These two ADC's were

---

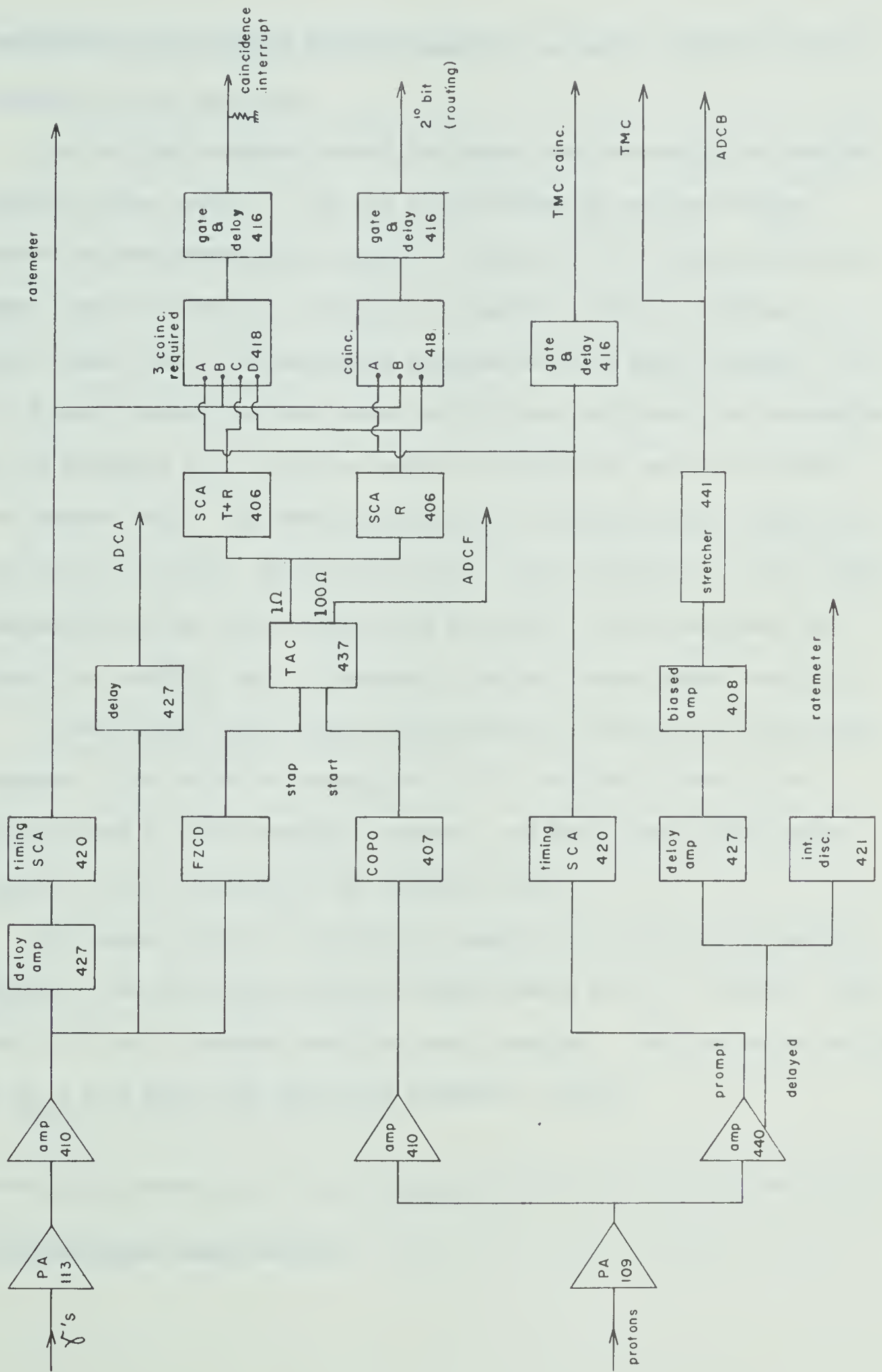
<sup>†</sup> TMC model 217 A

Figure 2 Block diagram of coincidence electronics used in the correlation measurements. Abbreviations are explained in the text. Most of the electronic equipment was obtained from Ortec <sup>†)</sup>. Ortec model numbers are used.

---

<sup>†)</sup> Oak Ridge Technical Enterprises Corp., Oak Ridge, Tennessee







connected to the on-line SDS 920 computer, as was a third ADC<sup>†</sup> which recorded the TAC spectrum.

The on-line computer sorted the gamma rays according to charged-particle pulse height. This was accomplished by setting windows around the charged-particle peaks of interest and routing coincident gamma rays into separate regions of computer memory, according to which window their corresponding charged particle pulse belonged. Up to 16 such charged particle bins could be set with each bin consisting of 256 channels for true plus random coincidences, and 256 channels for randoms only. The sorting routine also provided 1024 channels for the total coincident charged particles, 1024 channels for total random charged particles, 256 channels for the total coincident gamma ray trues plus randoms, and 256 channels for the random gamma rays only.

A self-gated proton single spectrum was recorded for monitoring purposes. The relative intensities of the excited states to the ground state of  $^{53}\text{Cr}$  remained constant, and hence the latter proton peak was used to normalize the different runs.

The gamma rays were detected at angles of 0, 30, 45, 60 and 90 degrees. For the first series of measurements at  $E_d = 4.85$  MeV, only the 0, 45 and 90 degree positions were repeated. For the second series at  $E_d = 4.11$  MeV, each angle was repeated 3 times.

---

<sup>†</sup> Nuclear Data Model ND 161 F



## 2.2. Analysis of the Gamma Ray Spectra

A slight gain shift was experienced in the gamma ray system during the course of this experiment. This was overcome by using a computer program that normalized all the spectra to a standard gain. This program, called LYNE, (Ca 69) fits two well-defined peaks with a gaussian shape, determines accurately the peak positions, then renormalizes the complete spectrum to any given gain. The different runs were then weighted by  $\sin \theta$  and added to give good statistics for the determination of branching ratios.

The intensities of the different gamma transitions were determined using a gamma line-shape analysis program GAMRAY (Sy 68). This program generates the full shape: photopeak, escape peaks and Compton distribution for each gamma ray. Peaks and Compton distribution are smeared by a near-gaussian function and allowance is made for absorption in the crystal of Compton scattered gamma rays. The parameters governing the peak widths, photopeak-to-escape peak ratio and photopeak-to-Compton ratio were reevaluated using the 3.564 and 3.48 MeV gamma rays from the  $^{26}\text{Mg}(d,p\gamma)^{27}\text{Mg}$  reaction. The absorption and efficiency parameters were checked against the decay of  $^{24}\text{Na}$ .

## 2.3. Angular Distribution Analysis

The gamma ray angular distributions were fitted according to the theory described in section 1.1 using a  $\chi^2$  computer program (Hu 68).



The distributions are fitted to:

$$W(\theta) = a_0 + a_2 P_2(\cos\theta) + a_4 P_4(\cos\theta)$$

in order to get the best fit for the Legendre Polynomial coefficients  $a_k$ .

These coefficients are also fitted using equation (II.6) [according to the method described in section 1]. Angular distributions for several transitions involved in the decay of the initial state  $|J_1\rangle$  can be fitted simultaneously.

Finally, when limitations on the population parameters were introduced (as described in section 1.4.), a modified version of a grid search program (So 68) was used. This program is basically equivalent to the  $\chi^2$  program already described, and is based on the same formalism (Ro 67). However, it was found easier to modify for that purpose.







### 3. LIFETIME MEASUREMENTS IN $^{53}\text{Cr}$

The  $^{53}\text{Cr}(p,p'\gamma)^{53}\text{Cr}$  reaction was used together with Doppler shift measurements in order to determine the lifetimes of the low-lying states of  $^{53}\text{Cr}$ . The Doppler shift attenuation method (DSAM) will just be outlined here. It has been used extensively in the last few years and is thoroughly described in many papers [see e.g. (Li 64) and references therein].

The Doppler shift in the energy of a gamma ray emitted by a nucleus moving with velocity  $v(t)$  is, to the first order in  $v(t)/c$ :

$$E = E_0 \left(1 + \frac{v(t)}{c} \cos\theta\right) \quad (\text{II.8})$$

where  $E_0$  is the unshifted gamma-ray energy and  $\theta$  is the angle of emission of the gamma ray relative to  $\vec{v}(t)$ .

Since the nuclei are slowed down in the target or in the target backing, the velocity is a function of time, and the Doppler shift is smaller than the maximum shift  $(v(0)/c \cos\theta)E_0$ . Assuming exponential law, equation (II.8) becomes:

$$E = E_0 \left\{1 + \frac{v(0)}{c} F(\tau) \cos\theta\right\}$$

where  $F(\tau)$  is called the attenuation factor and is measured for a given



stopping material.  $\tau$  is the lifetime of the excited nuclei.

The attenuation factor  $F(\tau)$  is given by:

$$F(\tau) = \frac{\text{Observed average Doppler Shift}}{\text{Full shift}} = \frac{1}{v(0)\tau} \int_0^{\infty} v(t) e^{-t/\tau} dt$$

One can see that:

$F(\tau) = 1$  {or the observed average Doppler shift is equal to full shift} when the gamma emission takes place before the recoil nucleus is actually slowed down. This corresponds to either a light stopping material or a very short lifetime  $\tau$ .

$F(\tau) = 0$  {or the observed average Doppler shift is zero} when the gamma emission takes place after the recoil nucleus has been stopped. This corresponds either to a heavy stopping material or long lifetime.

The interpretation of the measured attenuation of the Doppler shift requires a knowledge of the velocity  $v(t)$  of the recoiling excited nuclei as a function of time. In this experiment, the attenuation factor  $F(\tau)$  was calculated using a program called DSAM III based on the theoretical calculations of Blaugrund (Bl 66). The experimental  $F(\tau)$  was then compared with the calculated  $F(\tau)$ .

The targets, approximately  $200 \mu\text{g}/\text{cm}^{-2}$  thick, consisted of chromium enriched to 96.4% in  $^{53}\text{Cr}$  which has been evaporated onto a tantalum backing 0.005 cm thick. The gamma rays were detected in a  $45 \text{ cm}^3$  Ge(Li) detector which has a typical resolution of 3.5 KeV FWHM at 1.33 MeV.



Gamma rays from  $^{137}\text{Cs}$  and  $^{22}\text{Na}$  sources were recorded with the  $^{53}\text{Cr}$  spectra ensuring an accurate calibration of  $^{53}\text{Cr}$  gamma rays. Above a proton bombarding energy of 2.0 MeV, all spectra were dominated by gamma rays from the competing  $(d,n\gamma)$  reaction. However, an optimum yield for gamma rays from the first two excited states of  $^{53}\text{Cr}$  was obtained at bombarding energies of 3.2 and 3.5 MeV.



#### 4. EXPERIMENTAL RESULTS

A typical charged particle spectrum taken in coincidence with gamma rays is shown in fig. 3. This indicates the relative intensities of the excited states of  $^{53}\text{Cr}$  and also shows that two states of  $^{29}\text{Si}$  were observed via the (d,p) reaction on silicon contaminant in the target. The energies of the first two states in  $^{53}\text{Cr}$  are taken from the Ge(Li) measurements reported in section 2, but the energies listed by Rao et al. (Ra 68) are used for all the other excited states. Many of the excited states were too weakly excited to obtain angular distributions and hence only their decay modes could be established. Fig. 4 summarises all the branching ratios determined in the present work. For the multiplets near 2.7 and 3.2 MeV, only composite branching ratios are given in Table 1.

##### 4.1. The Levels Below 2.0 MeV

The isotropic angular distribution obtained for the ground state decay of the 0.564 MeV level is consistent with the previous assignment of  $1/2^-$  based on the postulated J-dependent effects in (d,p) stripping (An 64). The energy of the gamma ray to the ground state was accurately determined to be  $(564.1 \pm 0.2)$  keV from its observation in the  $^{53}\text{Cr}(p,p'\gamma)^{53}\text{Cr}$  reaction at 3.2 and 3.5 MeV bombarding energies. The observed Doppler shift obtained from measurements taken at  $0^\circ$  and

Figure 3 Charged particle spectrum in coincidence with gamma rays for the  $^{52}\text{Cr}(\text{d},\text{p}\gamma)^{53}\text{Cr}$  reaction at a bombarding energy of 4.11 MeV. The protons were detected near  $172^\circ$ . The associated random spectrum has been subtracted. Proton peaks are identified by the energies of the states in  $^{53}\text{Cr}$  to which they correspond. The peak marked by an asterisk (\*) has not been identified.



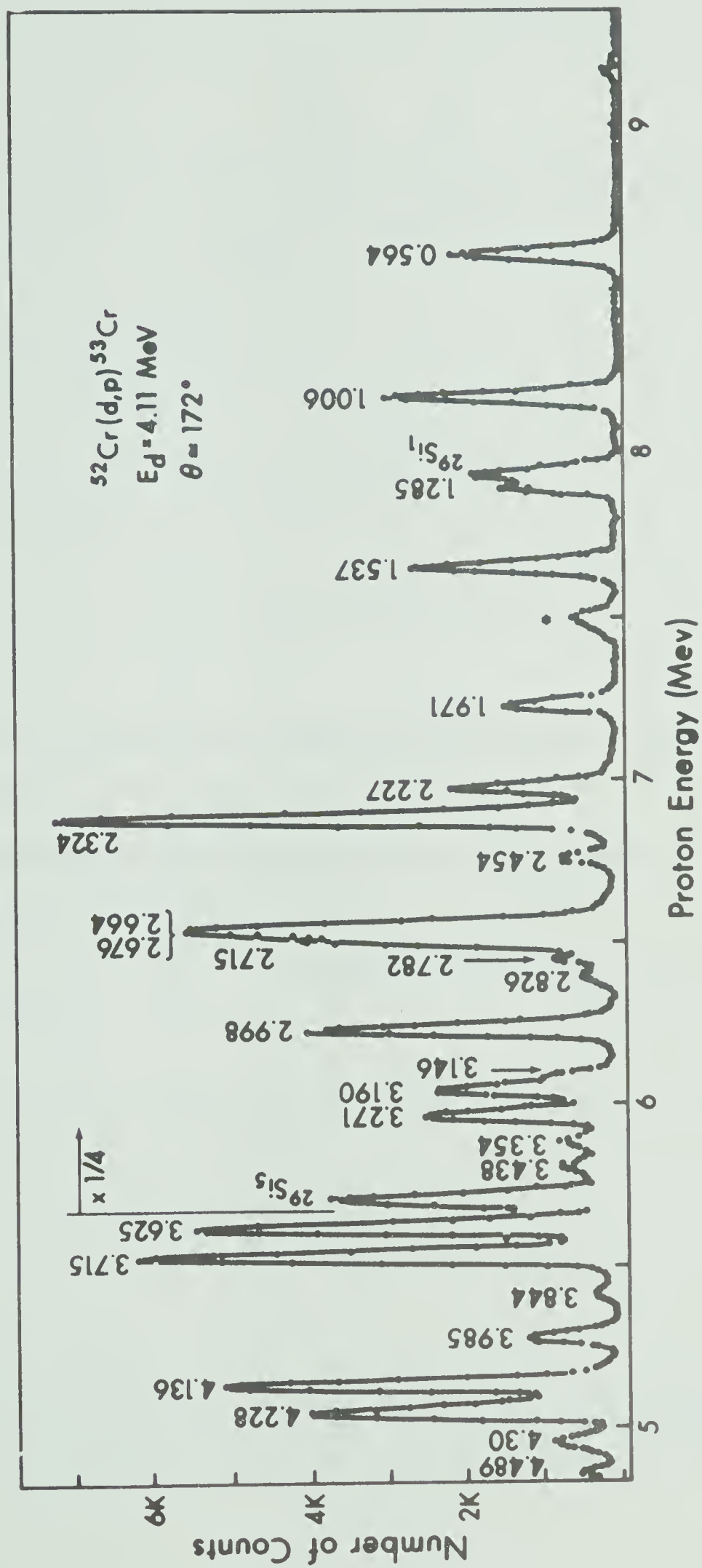
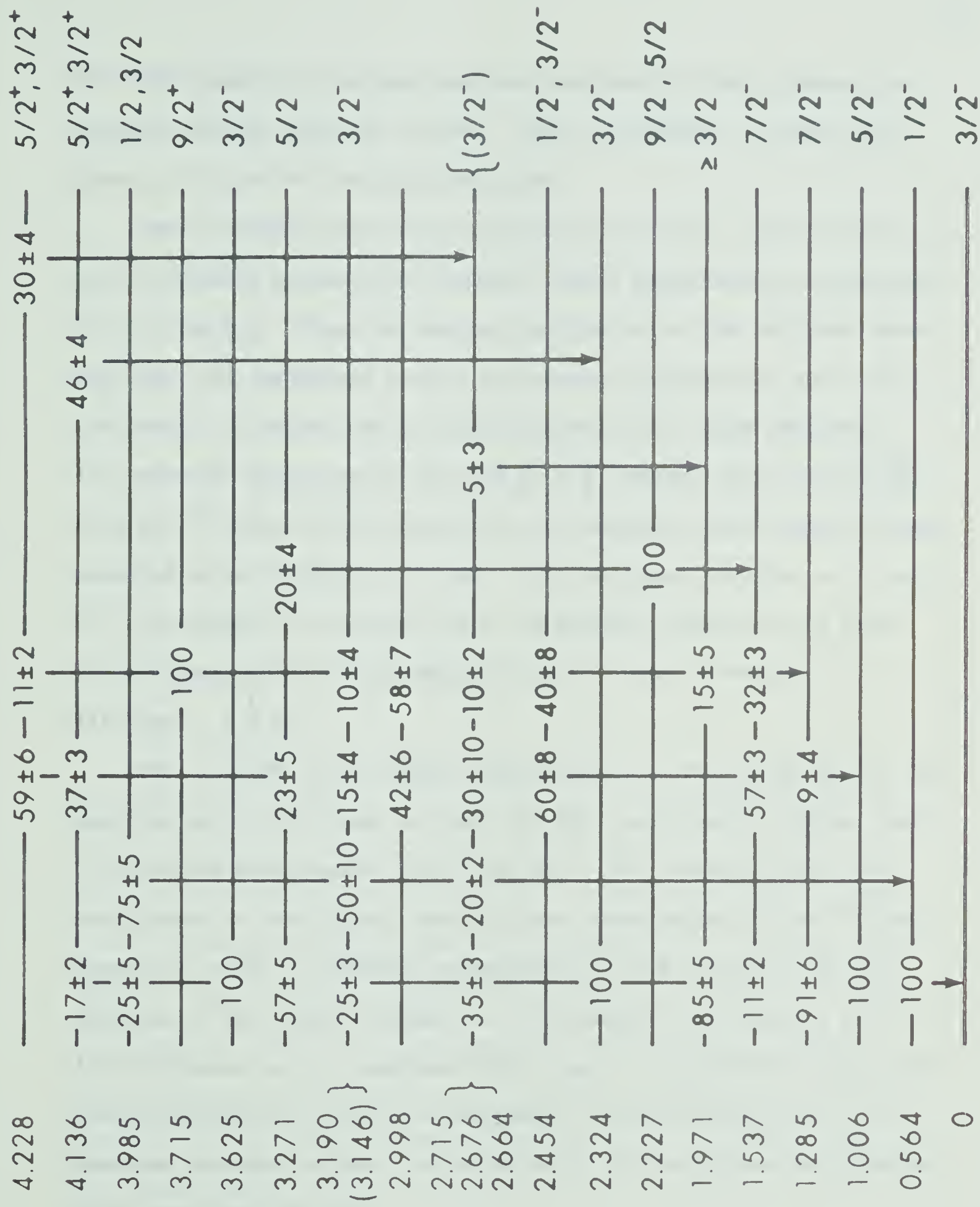


Figure 4 A summary of branching ratios and spin assignments of some of the excited states of  $^{53}\text{Cr}$  below 4.3 MeV. The branching ratios have been measured in the present experiment. The spin assignments include our measurements as well as all previously available information.





90° with respect to the beam axis was less than 0.2 keV compared to the full Doppler shift of 1.5 keV. This corresponds to a mean lifetime  $\tau \geq 0.5$  ps for the 0.564 MeV state.

The 1.006 MeV level decays entirely to ground. It is fed by an  $\ell_n = 3$  transfer in the (d,p) reaction with a spectroscopic strength of  $S \simeq 2.5$  (Bo 65). From the angular distribution of the 1006 keV gamma ray, the  $7/2^-$  assignment is just rejected on the basis of the 0.1% confidence criterion, confirming the previous  $5/2^-$  spin assignment. The extracted mixing ratio for this  $\frac{5^-}{2} \rightarrow \frac{3^-}{2}$  transition is  $-0.27^{+0.09}_{-0.31}$ . From the  $^{53}\text{Cr}(p,p'\gamma)^{53}\text{Cr}$  experiment, the energy of this transition was measured to be  $(1006.0 \pm 0.2)$  keV. With the gamma detector at 0° and 90° with respect to the beam axis, the Doppler shift was less than 0.2 keV compared to a full shift of 3 keV. This corresponds to a lifetime  $\tau \geq 1$  ps.

The 1.285 MeV state decays predominantly to the ground state. We observed only a 9% branch to the 1.006 MeV, considerably smaller than the previous measurements (Ro 65, Ra 68). The branching ratio was established in the present work by direct observation of the 278 keV gamma ray, while in previous measurements it was inferred from the presence of the 1006 keV gamma ray. The angular distribution of the 1285 keV gamma ray is consistent with a pure E2 transition from a  $7/2^-$  state confirming the previous assignment from observation of  $\ell_n = 3$  momentum transfer in both the stripping (d,p) (Ra 68), and the pick-up (p,d) reactions (Wh 67).





The gamma-ray spectrum obtained for the 1.537 MeV state is shown in fig. 5. This indicates a previously unobserved branch of 11% to the ground state. The angular distribution of the 529 keV gamma ray to the 1.006 MeV state was strongly anisotropic at both bombarding energies and indicated a probable spin of  $7/2$ . This assignment is in agreement with the work of Whitten (Wh 67) who reported that this state is the strongest excited in the pick-up (p,d) reaction with an  $\ell_n = 3$  transfer, indicating the state has a predominant  $f_{7/2}$  hole configuration.

The 1.971 MeV state decays 85% to the  $(3/2^-)$  ground state and 15% to the 1.285 MeV  $(7/2^-)$  state. This latter branch was not observed in previous work (Ro 65).

#### 4.2. The Levels Between 2.0 and 3.6 MeV

The 2.227 MeV state decays only to the 1.537 MeV  $(7/2^-)$  state. The angular distribution of the 690 keV gamma ray shown in fig. 6a can be equally well fitted by spin assignments  $5/2$ ,  $7/2$  and  $9/2$  as the  $\chi^2$  plots in fig 6b and 6c indicate. The state is weakly excited in the (d,p) reaction and exhibits no characteristic stripping pattern (Ra 68). Hence, the  $\chi^2$  analysis was repeated with limits of 0.3 and 3.0 placed on the ratio of the population parameters as discussed in section 1.4. In the region of best fit, this ratio was previously either 0 or  $\infty$ , and in the cases of  $5/2$  and  $9/2$ , the introduction of the limits has only a small effect on the  $\chi^2$  fit as shown in fig. 6b.

Figure 5 Gamma rays in coincidence with protons populating the 1.537 MeV level in  $^{53}\text{Cr}$ . The lower spectrum corresponds to the simultaneous random spectrum.



Number of Counts

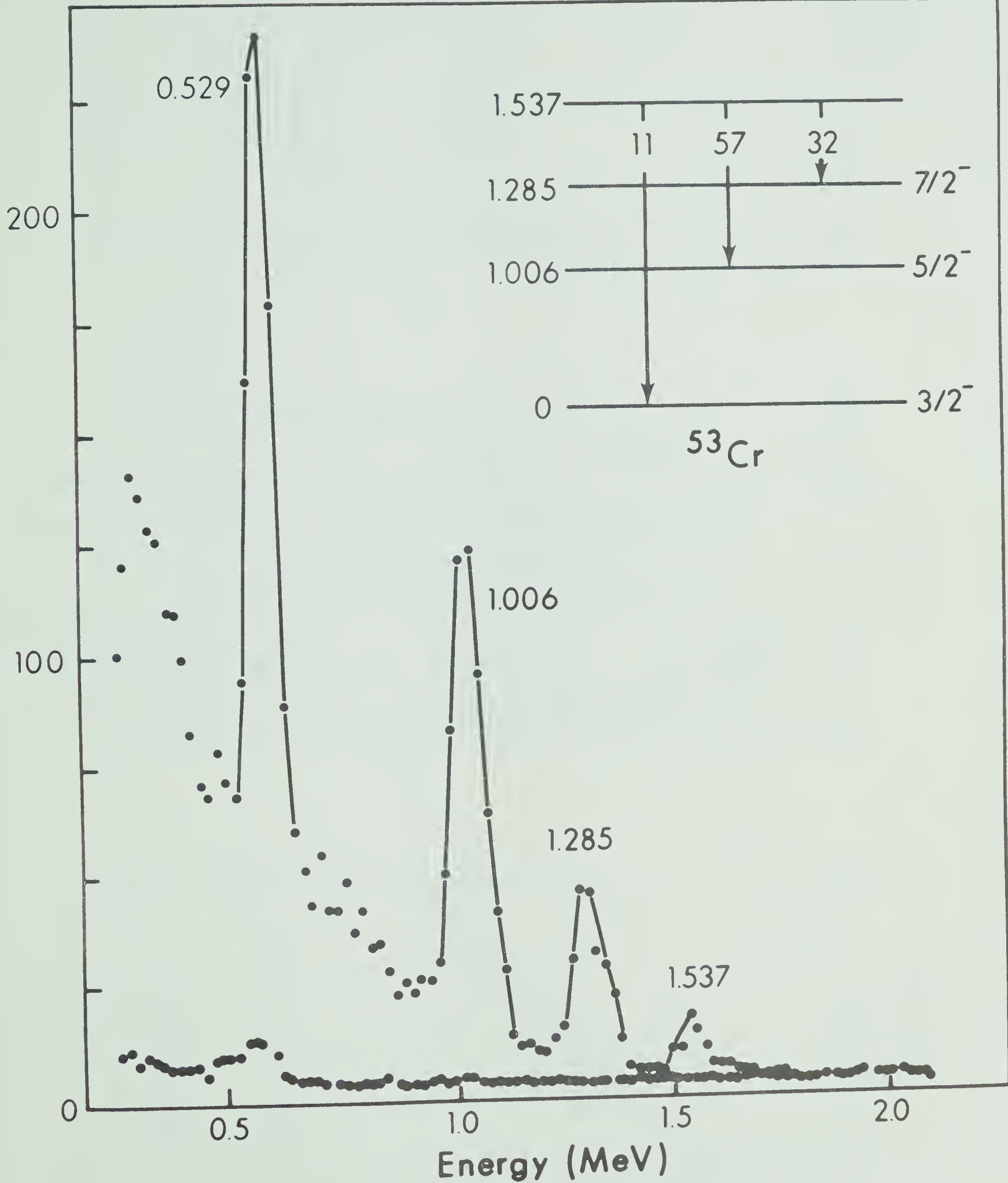
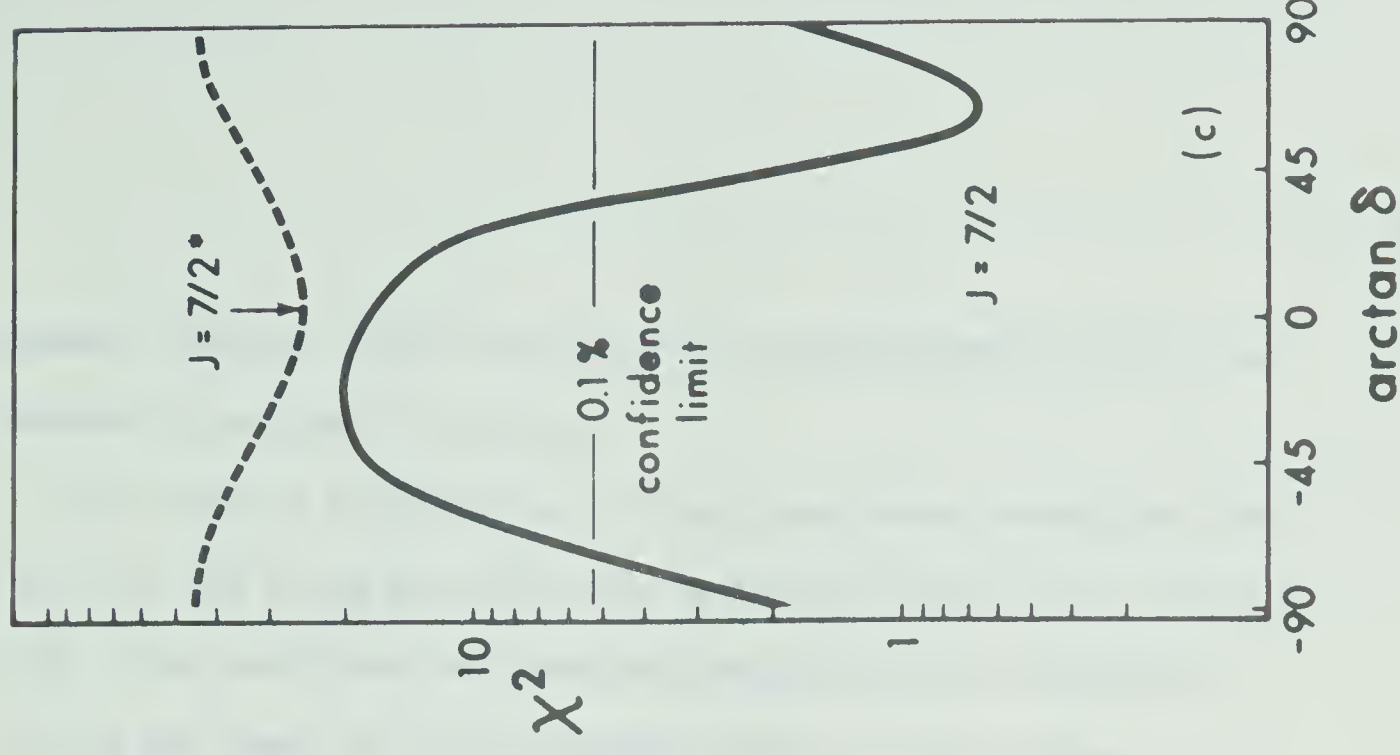
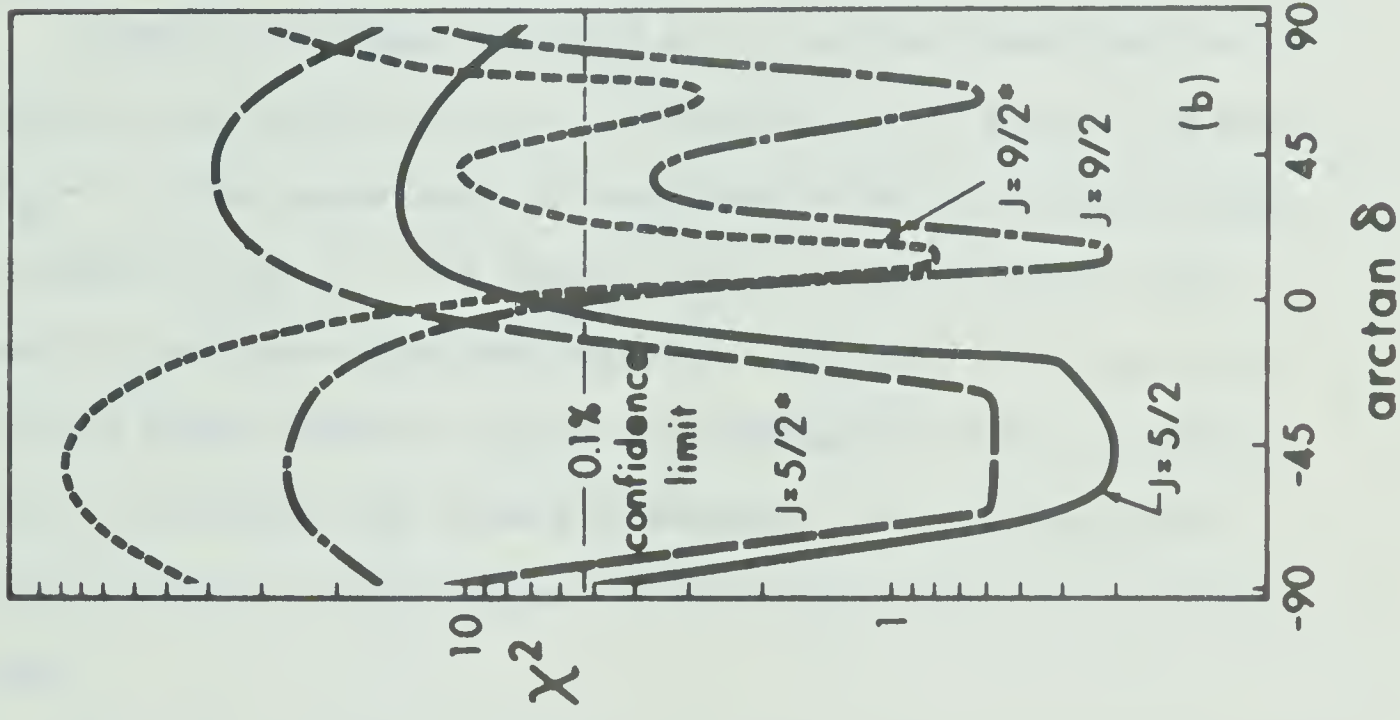
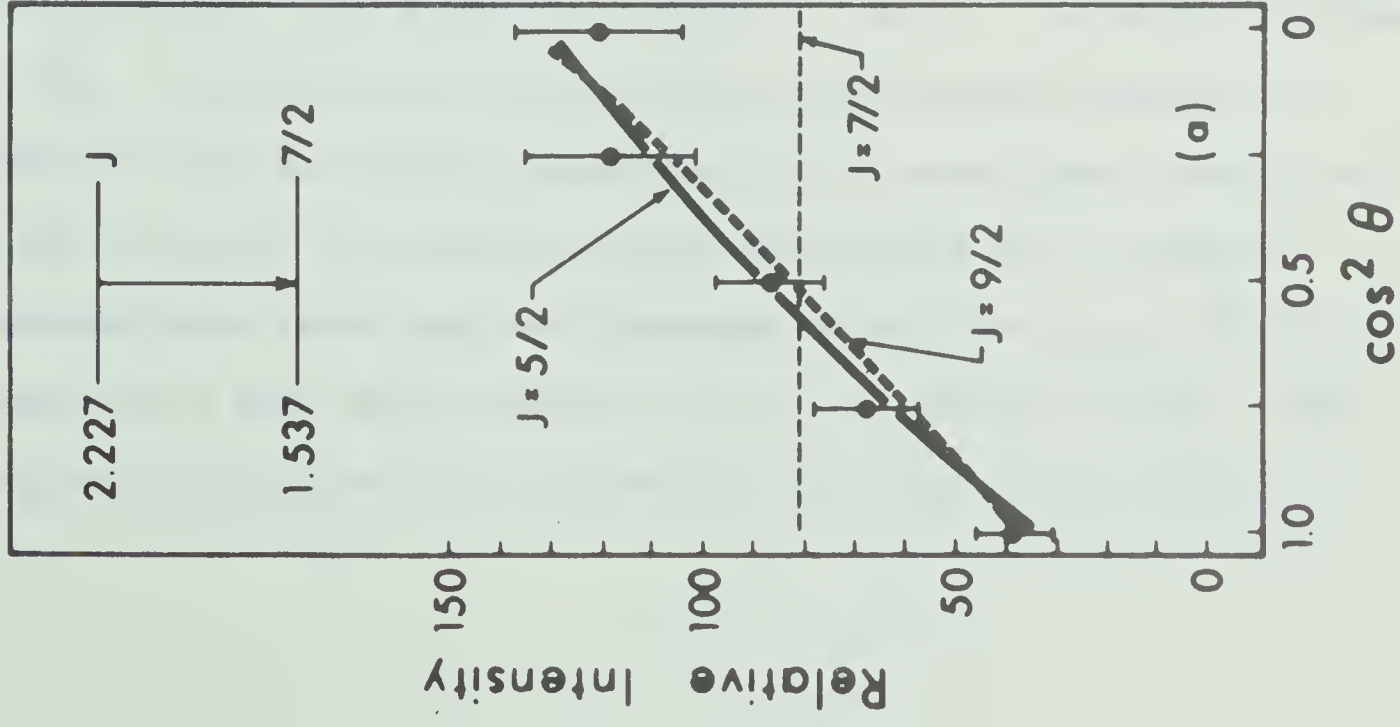


Figure 6 The 2.227 MeV state. The angular distribution (a) and  $\chi^2$  plots (b and c) for the 690 keV transition to the 1.537 MeV( $7/2^-$ ) level in  $^{53}\text{Cr}$  are shown. The  $\chi^2$  plots marked by an asterisk (\*) correspond to limits of 0.3 to 3.0 set on the ratio of population parameters (see section 1.4). The fits shown with the angular distributions correspond to the minimum  $\chi^2$  with limits on the population parameter ratio.





However, the new limits did enable the spin assignment  $7/2$  to be completely excluded (fig. 6c).

The angular distribution of the ground state transition from the 2.324 MeV state was definitely anisotropic with an  $a_2 = 0.15 \pm 0.05$ . This confirmed the previous tentative spin assignment of  $3/2^-$  on the basis of the J-dependent effect in the strong  $\ell_n = 1$  neutron stripping angular distribution (An 64).

There is a triplet of levels at  $\simeq 2.67$  MeV identified respectively as: 2.664 MeV ( $\ell_n = 3$ ), 2.676 MeV ( $\ell_n = 1$ ) and 2.715 MeV ( $\ell_n = 1$ ). The gamma decay in coincidence with the 3 proton groups is shown in fig. 7a. The angular distributions of the 2.13 MeV and 2.67 MeV gamma rays were measured. The latter was isotropic but the former enables a unique spin assignment of  $3/2$ , provided the 2.13 MeV gamma ray comes predominantly from a single level, both  $1/2$  and  $5/2$  being rejected on the basis of the 0.1% confidence test.

The gamma spectrum obtained in coincidence with the proton group corresponding to the 3.190 MeV is shown in fig. 7b. The proton spectrum in fig. 3 indicates that at most, 25% of the proton peak feeding the state at 3.190 MeV could be attributed to the proton group feeding the 3.146 MeV level. Our branching ratio measurements are in essential agreement with those previously measured by Rollefson et al. (Ro 65) except for a weak (8%) transition to the 1.285 MeV ( $7/2^-$ ) level. The angular distribution of the predominant decay mode of the 3.190 MeV

- Figure 7 a) Gamma rays in coincidence with protons populating the triplet in  $^{53}\text{Cr}$  at 2.664 MeV, 2.676 MeV and 2.715 MeV.
- b) Gamma rays in coincidence with protons populating the 3.146 MeV and 3.190 MeV levels in  $^{53}\text{Cr}$ .

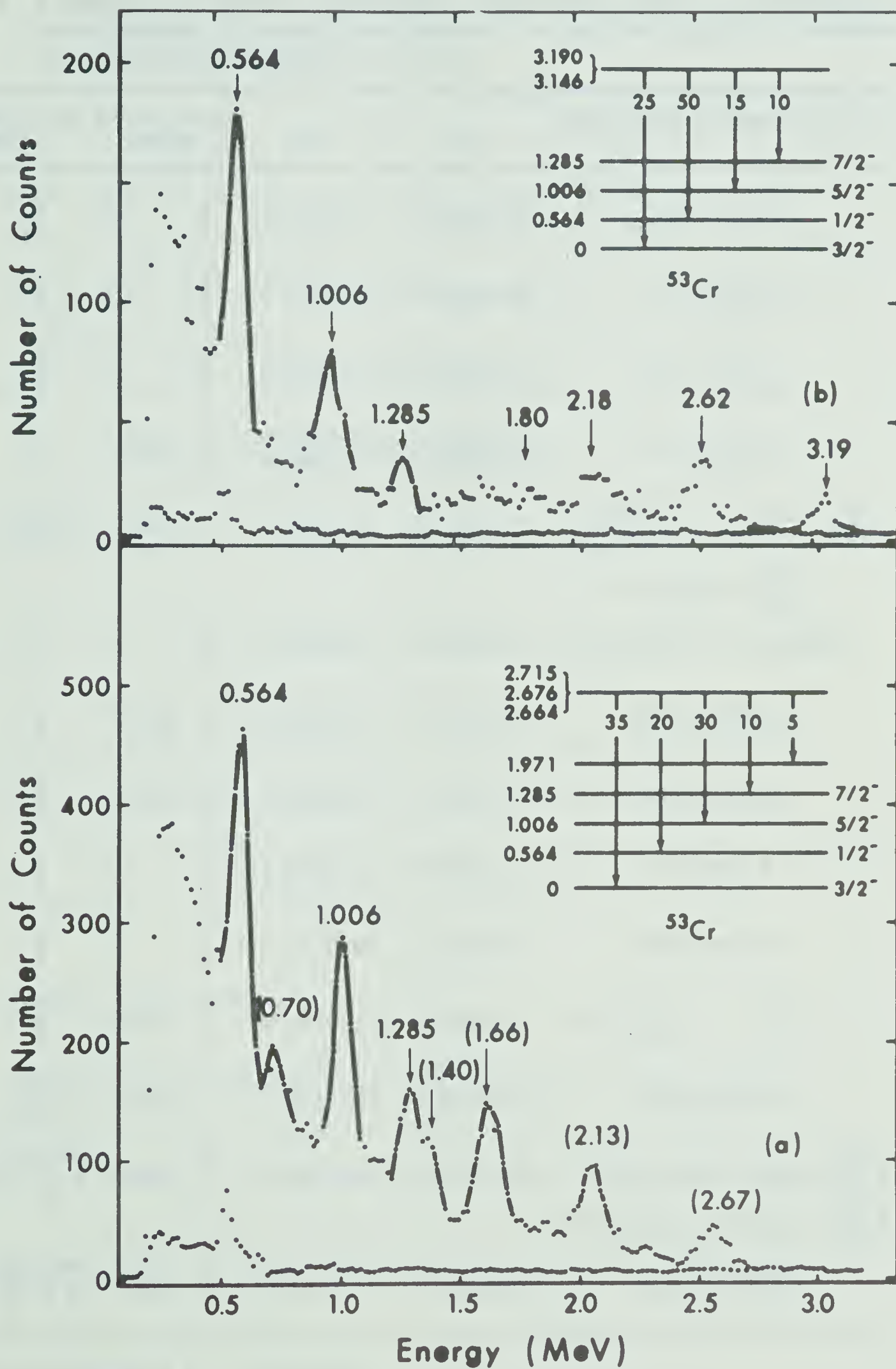








Table I A summary of Legendre polynomial coefficients fitted to the angular distributions of transitions observed in the  $^{52}\text{Cr}(d,p\gamma)^{53}\text{Cr}$  reaction at a bombarding energy of 4.11 MeV.

Initial Level (MeV)		Final Level (MeV)		$a_2$	$a_4$	Multipole Mixing Ratios
0.564	$\frac{1}{2}^-$	0.	$\frac{3}{2}^-$	$-0.12 \pm 0.09$	$0.07 \pm 0.09$	undetermined
1.006	$\frac{5}{2}^-$	0.	$\frac{3}{2}^-$	$0.15 \pm 0.06$	$-0.05 \pm 0.08$	$-0.27^{+0.09}_{-0.31}$
1.285	$\frac{7}{2}^-$	0.	$\frac{3}{2}^-$	$0.55 \pm 0.11^*$	$-0.56 \pm 0.18^*$	$0.0^{+0.18}_{-0.15}$
1.537	$\frac{7}{2}^-$	1.006	$\frac{5}{2}^-$	$\begin{pmatrix} 0.56 \pm 0.10 \\ -0.38 \pm 0.15^* \end{pmatrix}$	$\begin{pmatrix} 0.19 \pm 0.10 \\ 0.20 \pm 0.19^* \end{pmatrix}$	$0.27^{+0.33}_{-0.28}$
2.227	$\left(\frac{9}{2}, \frac{5}{2}\right)$	1.537	$\frac{7}{2}^-$	$0.58 \pm 0.15$	$-0.11 \pm 0.15$	$0.23^{+0.25}_{-0.15} ; 1.8^{+0.7}_{-0.6} \left(\frac{9}{2}\right)$ $-6.0 \leq \delta \leq 0.2 \left(\frac{5}{2}\right)$
2.324	$\frac{3}{2}^-$	0.	$\frac{3}{2}^-$	$0.15 \pm 0.05$	$0.09 \pm 0.06$	$-5.7 \leq \delta \leq 0.09 ; 0.47 \leq \delta \leq 5.7$
(2.70)	$\frac{3}{2}^-$	0.564	$\frac{1}{2}^-$	$-0.30 \pm 0.11$	$0.17 \pm 0.13$	undetermined
3.190	$\frac{3}{2}^-$	0.564	$\frac{1}{2}^-$	$0.58 \pm 0.19$	$0.21 \pm 0.20$	undetermined
3.271	$\frac{5}{2}$	0.	$\frac{3}{2}^-$	$-0.83 \pm 0.11$	$0.06 \pm 0.11$	$0.06 \leq \delta \leq 1.8$
3.625	$\frac{3}{2}^-$	0.	$\frac{3}{2}^-$	$-0.07 \pm 0.05$	$0.08 \pm 0.06$	undetermined
3.715	$\frac{9}{2}^+$	1.285	$\frac{7}{2}^-$	$-0.36 \pm 0.03$	$0.08 \pm 0.04$	$0.00^{+0.09}_{-0.04} ; 3.7^{+0.8}_{-0.6}$
3.971	$\left(\frac{1}{2}, \frac{3}{2}\right)$	0.564	$\frac{1}{2}^-$	$0.03 \pm 0.08$	$-0.04 \pm 0.09$	undetermined
4.136	$\left(\frac{3}{2}^+, \frac{5}{2}^+\right)$	2.324	$\frac{3}{2}^-$	$-0.49 \pm 0.06$	$-0.04 \pm 0.07$	$-5.4 \leq \delta \leq 0.15 ; 0.55 \leq \delta \leq 4.0 \left(\frac{3}{2}\right)$ $-0.05 \leq \delta \leq 0.7 ; 1.4 \leq \delta \leq 3.8 \left(\frac{5}{2}\right)$
4.228	$\left(\frac{3}{2}^+, \frac{5}{2}^+\right)$	1.006	$\frac{5}{2}^-$	$0.17 \pm 0.04$	$-0.03 \pm 0.05$	$-10. \leq \delta \leq 0.6 \left(\frac{5}{2}\right)$

\*Results obtained at  $E_d = 4.85$  MeV.



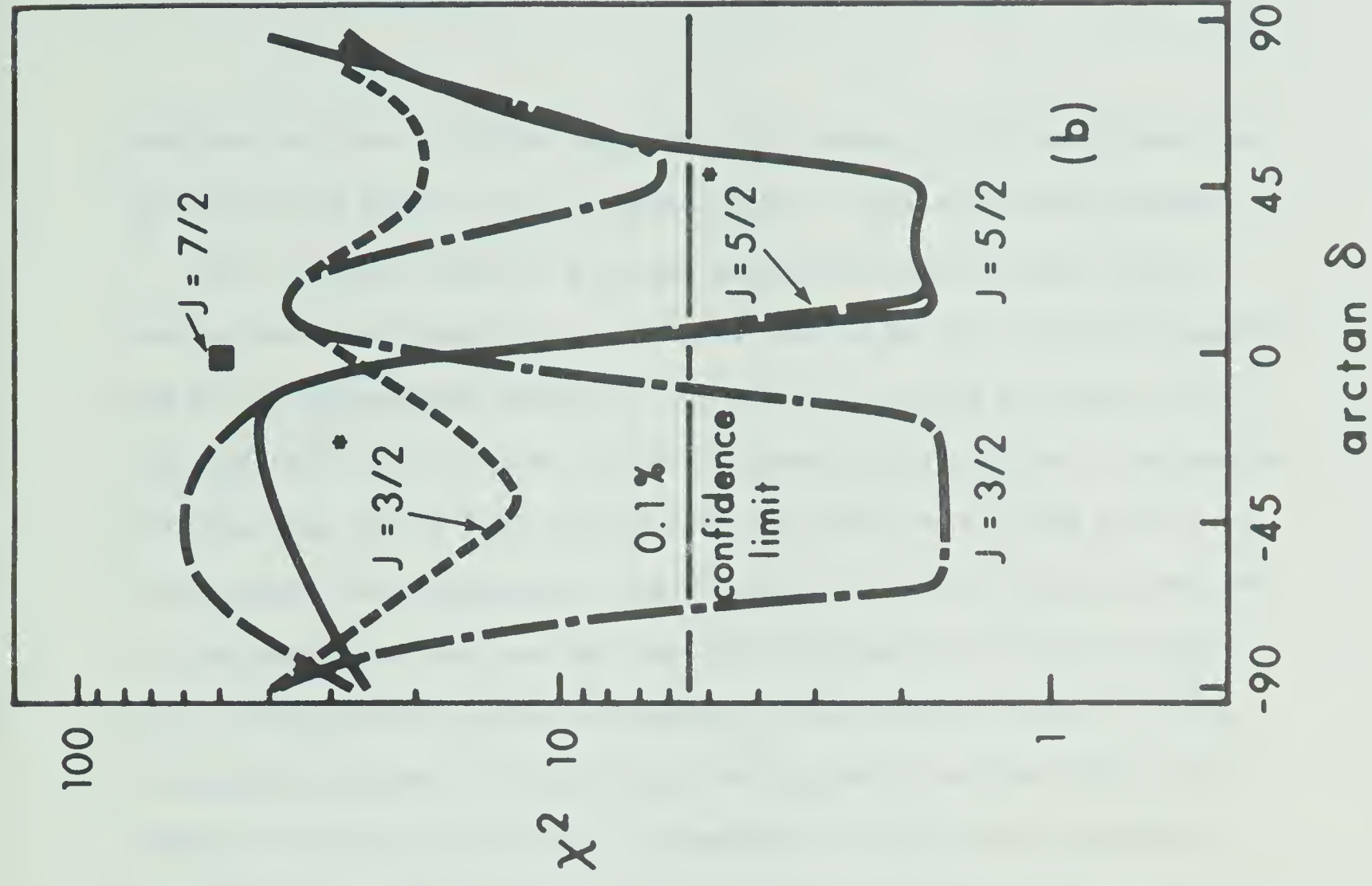
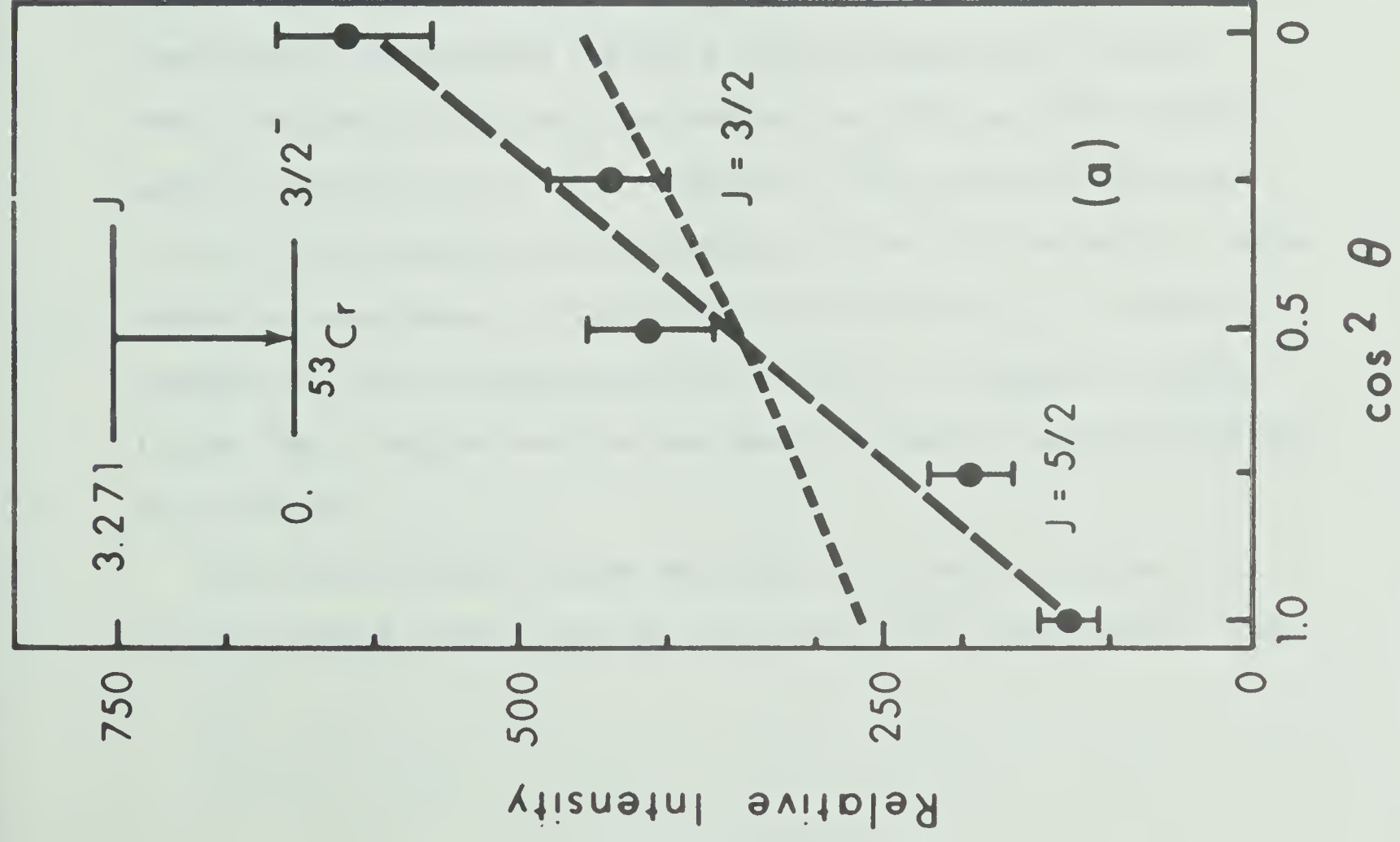
state to the 0.564 MeV ( $1/2^-$ ) state will be least affected by the presence of the 3.146 MeV level. Hence, the angular distribution of the resulting 2626 keV gamma ray enables a unique  $3/2$  spin assignment to be made to the 3.190 MeV state; all other possible spin assignments were rejected on the basis of the 0.1% confidence limit criterion. This assignment is in agreement with Rao et al. (Ra 68) who reported a possible  $\ell_n = 1$  momentum transfer to this state from the stripping (d,p) reaction.

The 3.271 MeV state decays 20% to the ( $7/2^-$ ) 1.537 MeV state, 23% to the ( $5/2^-$ ) 1.006 MeV state and 57% to the  $3/2^-$  ground state. The angular distribution of the 3271 keV gamma ray shown in fig 8a, is strongly anisotropic with  $a_2 = -0.83 \pm 0.11$ . The  $\chi^2$  plots in fig. 8b indicate that spin assignment  $3/2$  and  $5/2$  both give acceptable fits to the data. The  $\chi^2$  analysis was repeated with limits of 0.3 and 3.0 on the ratio of population parameters. The new plots shown in fig. 8b enabled a definite spin assignment of  $5/2$  to be made. A tentative  $\ell_n = 2$  transfer was assigned by Rao et al. (Ra 68) to this weak stripping state inferring the 3.271 MeV level has positive parity.

#### 4.3. Levels Above 3.6 MeV

The 3.625 MeV state which is strongly excited in the  $^{52}\text{Cr}(d,p)$  reaction with an  $\ell_n = 1$  momentum transfer decays only to ground state. The distribution of the 3625 keV gamma ray shows a very weak anisotropy  $a_2 = -0.07 \pm 0.05$  which is consistent with the previous tentative  $3/2^-$  assignment (An 64, Ba 65). Recent polarization measurements (Yu 68)

Figure 8 The 3.271 MeV state. The angular distribution (a) and  $\chi^2$  plots (b) for the 3271 keV ground state transition are shown. The  $\chi^2$  plots marked by an asterisk correspond to limits of 0.3 to 3.0 set on the ratio of population parameters (see section 1.4.). The fits shown with the angular distribution correspond to the minimum  $\chi^2$  with limits on the population parameter ratio.







indicate that the 3.625 MeV level is a  $1/2^-$  state. This would mean that our calculated error in the  $a_2$  coefficient is slightly underestimated.

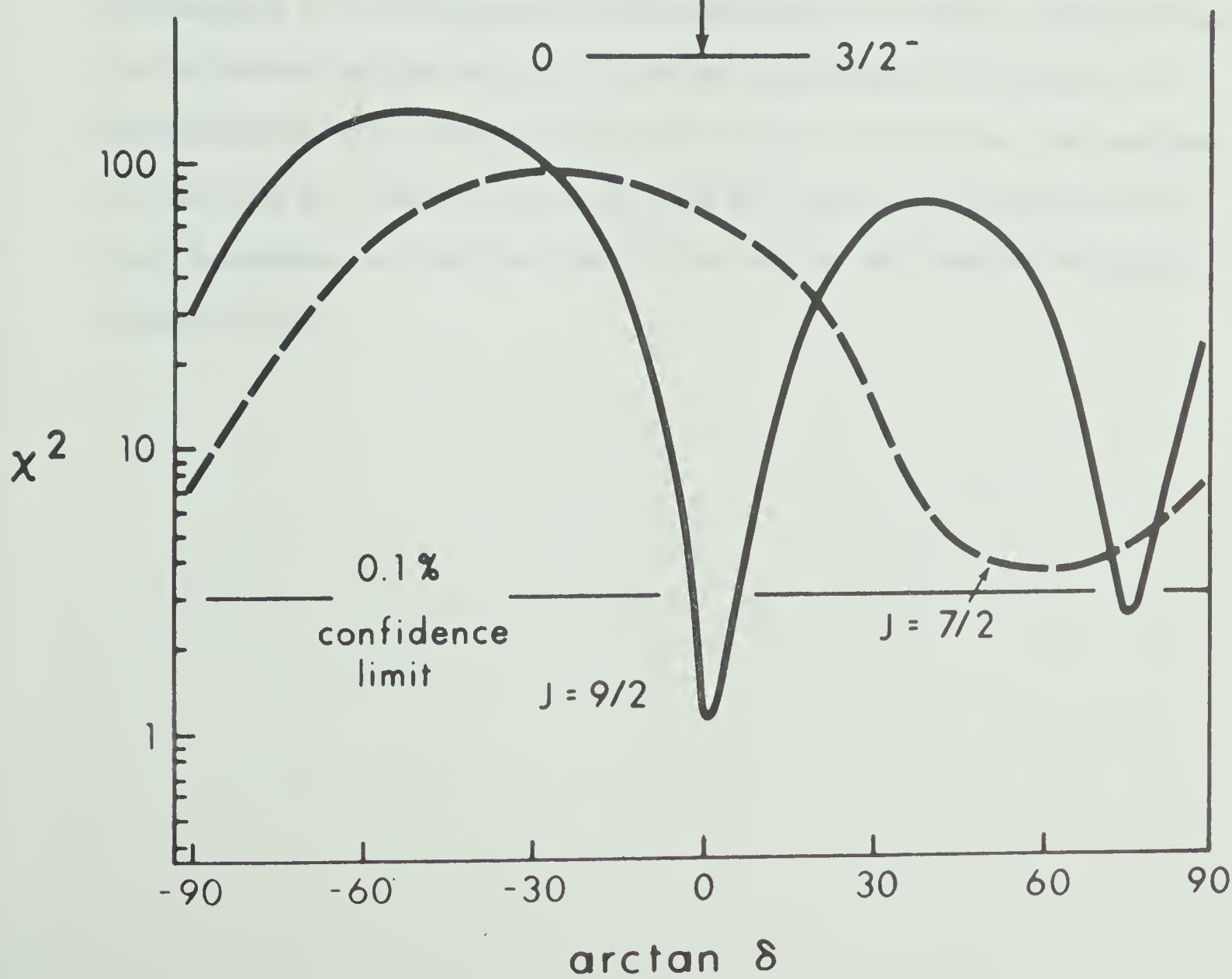
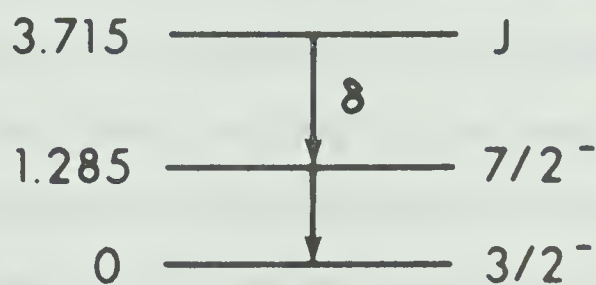
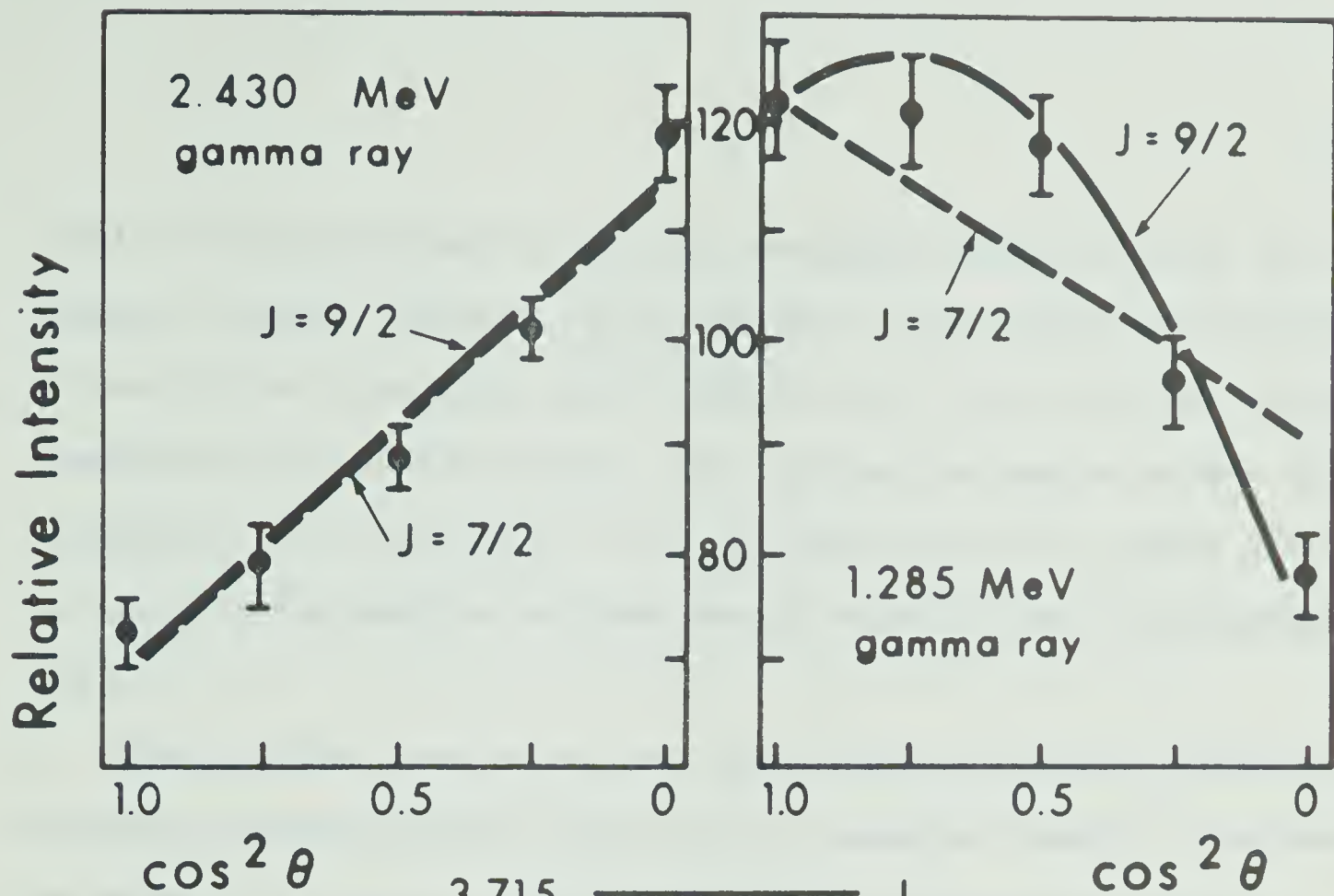
The 3.715 MeV level is a strong deuteron stripping state with a neutron momentum transfer  $\ell_n = 4$  (An 64, Ra 68, Bo 65), therefore suggesting it can be assigned either  $7/2^+$  or  $9/2^+$ . It decays entirely to the 1.285 MeV ( $7/2^-$ ) level with a 2430 keV gamma ray transition. The angular distributions of the 2430 keV and 1285 keV gamma rays, shown in fig. 9, were analysed simultaneously. The  $\chi^2$  plots, in fig 9, indicate that the  $7/2$  assignment is ruled out by the 0.1% confidence limit test leaving  $9/2^+$  as the spin and parity assignment of the 3.715 MeV level. Of the two possible values of the multipole mixing ratio for the  $9/2^+$  to  $7/2^-$  transition, the solution which corresponds to pure electric dipole is more likely than the solution corresponding to strong M2-E1 mixing.

The 3.985 MeV level decays predominantly to the 0.564 MeV ( $1/2^-$ ) level with a 75% branching and has a 25% branching ratio to ground. The  $\chi^2$  analysis of the isotropic angular distribution of the 3407 keV gamma ray enables the  $5/2$  spin assignment to be rejected leaving only  $1/2$  and  $3/2$  as possible spin assignments for the 3.971 MeV state. There exists an inconsistency in the literature as both the  $\ell_n = 2$  momentum transfer in (d,p) stripping reaction and the  $\ell_n = 1$  momentum transfer in the ( $^3\text{He},\alpha$ ) pick-up reaction have been reported for this level (Ra 68, Bo 65, DD 69).

The 4.136 MeV level decays 46% to the 2.324 MeV ( $3/2^-$ ) level, 37% to the 1.006 MeV ( $5/2^-$ ) level and 17% to the ( $3/2^-$ ) ground state. This

Figure 9 The 3.715 MeV state. The angular distributions of the 2430 keV and 1285 keV gamma rays in cascade are shown. The  $\chi^2$  plots correspond to the simultaneous analysis of the angular distributions.







level is excited strongly in the (d,p) stripping reaction with an  $\ell_n = 2$  momentum transfer. However, the  $\chi^2$  analysis of the angular distributions of the 3128 keV transition to the 1.006 MeV ( $5/2^-$ ) level and the 1812 keV transition to the 2.324 MeV ( $3/2^-$ ) level did not distinguish between spin assignments of  $3/2$  and  $5/2$  for the 4.136 MeV level but did enable limits to be put on the possible multipole mixing ratios for both spin possibilities .

The 4.228 MeV state is the next state which is strongly excited in the (d,p) stripping reaction with an  $\ell_n = 2$  momentum transfer. We found no evidence of a nearby excited state at 4.204 MeV which Rao et al. (Ra 68) report to be very weakly excited in the stripping (d,p) reaction. We measured a 59% branching to the 1.006 MeV ( $5/2^-$ ) state, 30% branching to the member of the triplet at 2.67 MeV that decays predominantly to ground and an 11% branching to the 1.285 MeV ( $7/2^-$ ) state. The analysis of the 3220 keV transition to the 1.006 MeV level was inconclusive for spin assignment but enabled limits to be put on the possible multipole mixing ratios.



## CHAPTER III

### THE $^{55}\text{Mn}(p,n\gamma)^{55}\text{Fe}$ REACTION

In Chapter II, a general expression for angular distribution of gamma rays resulting from the decay of aligned states, has been introduced. In the same chapter, a specific case of alignment, namely the triple angular correlation, was considered. This chapter deals with another way of preserving nuclear alignment, namely, by ensuring that outgoing particles are predominantly s-wave. In the following sections, the general theory describing the statistical model formalism will be outlined. Specific application of that theory to the case of the  $^{55}\text{Mn}(p,n\gamma)^{55}\text{Fe}$  will then be presented.



# 1. THE COMPOUND NUCLEAR STATISTICAL THEORY OF GAMMA-RAY ANGULAR DISTRIBUTIONS

## 1.1. Introduction

As shown in Chapter II, the angular distribution of gamma rays resulting from the decay of aligned states can be written as:

$$W(\theta) = \sum_{\text{even } k} B_k(J_1) P_k(\cos\theta) \frac{R_k(LLJ_1J_2) + 2\delta R_k(LL'J_1J_2) + \delta^2 R_k(L'L'J_1J_2)}{1 + \delta^2} \quad (\text{III.1})$$

where all the variables have been previously introduced.

This expression is the product of three terms:  $B_k(J_1)^\dagger$  which contains all the information on the alignment of the initial state  $J_1$ , the angular part,  $P_k(\cos\theta)$ , and the remaining term (hereafter labelled  $A(LL'J_1J_2\delta)$ ) which describes the interaction between the nuclear states and the electromagnetic field.

The problem now is twofold: first, to determine the conditions for alignment in a reaction such as  $^{55}\text{Mn}(p, n\gamma)$ ; second, to evaluate the term in equation (III.1) which reflects the conditions of alignment, namely,  $B_k$ . In order to achieve the latter goal, the population parameters (and consequently the  $B_k$ 's) will be evaluated after a model describing the

$$^\dagger B_k(J_1) = \sum_{m_1} P(m_1) (-)^{J_1 m_1} \sqrt{2J_1 + 1} (J_1 m_1 J_1 - m_1 | k 0)$$





reaction mechanism has been introduced.

## 1.2. Conditions for Alignment in the $A(a,b)B^*$ Experiment

Assume the reaction  $A(a,b)B^*$  takes place in two steps: first, formation, in the compound nucleus, of a state  $Y^*$ ,  $|J_1 m_1\rangle$ , with definite angular momentum and parity, then, decay by emission of a nucleon  $b$  (fig. 10).

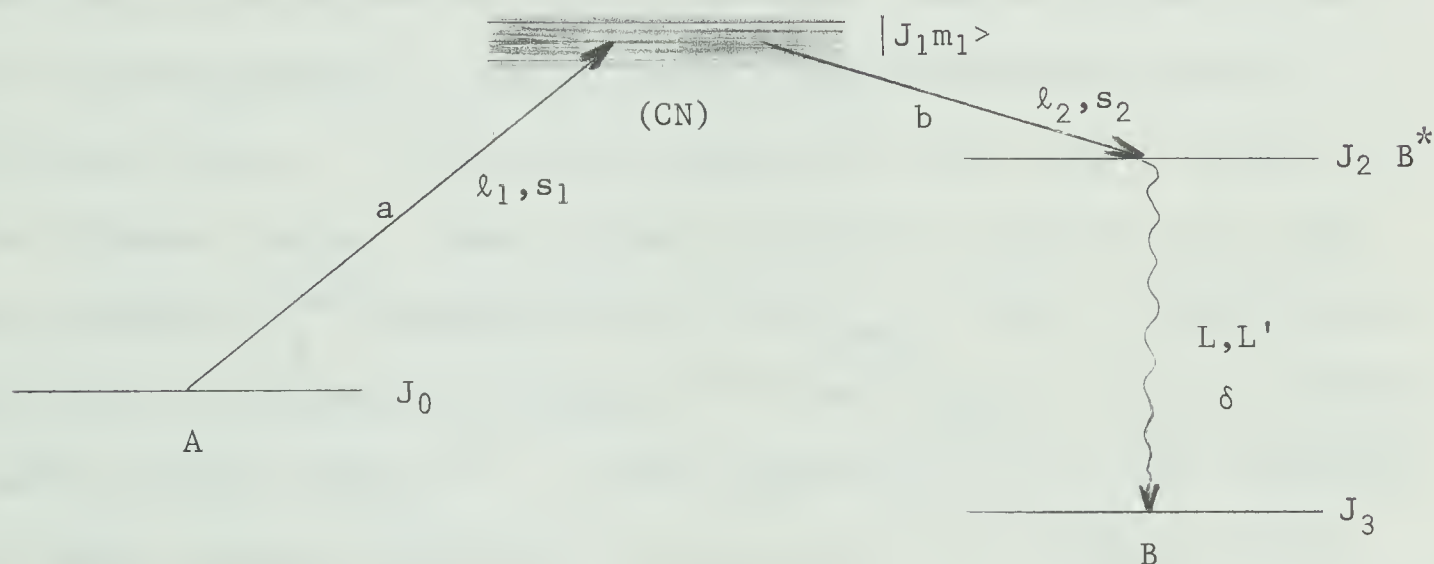


Figure 10

In the first step, the beam direction is chosen as the quantization axis ( $z$ -axis). It is moreover assumed that neither the beam of incident particles nor the target nuclei are polarized. These conditions result in alignment of the state  $|J_1 m_1\rangle$  (Ro 67 and Chapter II).



In the second step, a nucleon 'b' is emitted but not observed. The projection on the z-axis of the orbital angular momentum  $\ell_2$  of this nucleon is no longer zero as it can be emitted in any direction. One then generally expects the state  $B^*$  ( $|J_2 m_2\rangle$ ) to be de-aligned as the result of the contributions of the projection of  $\ell_2$  on the z-axis. However, if the reaction proceeds near threshold, then s-wave particles will predominate and de-alignment should be minimal.

As an example, consider the case described by fig. 10. The incoming particle, a, has an orbital angular momentum  $\ell_1$  and an intrinsic spin  $s_1$ . The outgoing particle b, has an orbital angular momentum  $\ell_2$  and an intrinsic spin  $s_2$ . J's are used to define the total angular momenta of the different levels. Since the beam direction is taken as the z-axis, the substates in  $Y^*$  are populated up to  $|m_1|_{\max} = J_0 + s_1$ . If only s-wave particles are emitted in the decay of  $Y^*$  then  $|m_2|_{\max} = (J_0 + s_1) + s_2$  for the residual nuclear state,  $B^*$ . It then follows that, in a (p,n $\gamma$ ) reaction, the largest magnetic substate to be populated in the residual nuclear state  $|J_2 m_2\rangle$  is  $|m_2|_{\max} = (J_0 + 1)$ . In this experiment, the target nucleus  $^{55}\text{Mn}$  has a spin  $J_0 = 5/2$ , therefore  $|m_2|_{\max} = 7/2$ .

Experimentally, "just above threshold" may mean as much as 30 to 50 keV, or more, above the threshold value. Therefore, contributions from higher order partial waves may be present but, the effect on the nuclear alignment of the residual state  $J_2$  is generally not very important.



### 1.3. Gamma Angular Distribution and the Statistical Model

Consider first the compound nucleus formation. In the channel spin representation, the population parameter  $P(m_1)$  is proportional to: (Li 61)

$$P(m_1) \sim (s_1 \ell_1 m_1 0 | J_1 m_1)^2 \quad (\text{III.2})$$

If more than one channel spin contributes to the formation of  $J_1$ , the different contributions are added incoherently:

$$P(m_1) \sim \sum_{s_1} (s_1 \ell_1 m_1 0 | J_1 m_1)^2 T_{s_1 \ell_1 J_1} \quad (\text{III.3})$$

If the reaction taken into consideration was simply a resonant capture, with only one partial wave contributing, one could, at this stage, introduce in the coefficient  $B_k(J_1)$  the value of  $P(m_1)$  defined in equation (III.3) to get: (Ro 67)

$$B_k(J_1) = \sum_{s_1} (-)^{s_1 - J_1} (2\ell_1 + 1) \sqrt{2J_1 + 1} (\ell_1 \ell_1 00 | k0) W(J_1 J_1 \ell_1 \ell_1; k s_1) T_{s_1 \ell_1 J_1} \quad (\text{III.4})$$

Putting this value of  $B_k$  into the expression  $W(\theta)$ , (equation III.1), would then give the equation of the distribution of gamma-rays following resonant capture.

The problem here is more complex as there are other terms to be



introduced which take into account the formation and decay of the intermediate state  $|J_2 m_2\rangle$ . Basically, one can expect another term similar to equation (III.4) which takes into account the alignment of the state  $B^*$ . As a result of the different couplings involved, there will be additional Clebsch-Gordan and Racah coefficients. Following Sheldon (Sh 63), the general expression giving  $W(\theta)$  schematically reads as:

$$\begin{aligned}
 W(\theta) \sim & \left[ \text{transition parameter for the formation of the compound nucleus} \right. \\
 & \left. \times \left( T_{s_1 \ell_1 J_1} \right) \right. \\
 & \times \left[ \text{transition parameter for the formation of the intermediate} \right. \\
 & \left. \text{state } J_2 \left( \frac{T_{s_2 \ell_2 J_2}}{\sum_{s'_2 \ell'_2} T_{s'_2 \ell'_2 J'_2}} \right) \right] \\
 & \times A_\gamma(LL'J_1J_2\delta) \times P_k(\cos\theta)
 \end{aligned} \tag{III.5}$$

In the second term, the intensity factor,  $\{...\}$ , reflects the fact that, once the compound nucleus has been formed, there are many channels open. It is a measure of the probability of decay by a particular channel.

At this stage, the only unknowns required to evaluate  $W(\theta)$  are the transition parameters,  $T$ . A knowledge of the reaction mechanism is necessary to calculate these factors. The problem is quite difficult but, under some assumptions, one can get a good estimate of the  $T$ 's. The statistical model has been extensively described in the past few years (e.g. see Sh 66,







Vo 69, Pi 69) and will be outlined in the following section.

### 1.3.1 The compound nuclear statistical model

The model assumes that the reaction proceeds dominantly through the compound nucleus formation (reactions of the type  $(p, n\gamma)$  and  $(\alpha, n\gamma)$  satisfy this condition) and that intermediate states have definite parity.

If the reaction proceeds via a large number of overlapping levels, it can be shown (Er 63) that the fluctuation in the cross section caused by interference between these levels will average out to zero. In  $(p, n\gamma)$  and  $(\alpha, n\gamma)$  reactions on medium weight nuclei, the density of levels in the compound nucleus is large. Experimentally, the use of thick targets and a broad beam energy resolution contribute to the excitation of a large number of overlapping levels. This last assumption is the basis of the statistical model. As a consequence, it is then possible to relate the mechanism of the reaction to energy averaged coefficients called transmission functions or transmission coefficients. These coefficients can be calculated using codes based on the formalism introduced by Hauser and Feshbach (Ha 52) in their theory describing the compound nucleus formation and decay. They are directly related to the  $T_{s\ell J}$  introduced earlier. The difference lies in the respective momentum space representations. The transmission coefficients are usually calculated in the  $j$ - $j$  representation whereas those used earlier are given in the  $\ell$ - $s$  representation. The relationship between the two definitions is given by:



$$T_{\ell s J} = \sum_{\sigma} (2j+1) (2\sigma+1) W^2(\ell I J s; j \sigma) T_{\ell \sigma J}$$

where  $W$  is a Racah coefficient.

For the sake of completeness, it must be pointed out that interferences between various partial waves for both incoming and outgoing waves should also be considered. These interference effects are shown to cancel out (Vo 69, Pi 69).

In conclusion, the use of the statistical model helps to describe the mechanism of the reaction. It is assumed that the reaction takes place in two separate steps: formation of a compound nucleus, then decay through many different channels. If all the conditions are met so that no resonance can occur, it is possible to calculate the transmission coefficients which in turn, yield an estimate of the population parameters of the intermediate state. The complete angular distribution formula can then be calculated. It is given by: (Pi 69)

$$\begin{aligned} W(\theta) = & \sum_{k j_1 j_2} (-)^{J_0+J_3-j_2-s_2} (2\ell_1+1) (2j_1+1) (2s_1+1)^{-1} (2J_0+1)^{-1} (2J_1+1)^{\frac{1}{2}} \\ & \times (2J_2+1)^{\frac{1}{2}} (\ell_1 \ell_1 00 | k0) W(\ell_1 \ell_1 j_1 j_1; k s_1) W(J_1 J_1 j_1 j_1; k J_0) \\ & \times W(J_1 J_1 J_2 J_2; k j_2) \times \zeta \times \frac{R_k(LLJ_1J_2) + 2\delta R_k(LL'J_1J_2) + \delta^2 R_k(L'L'J_1J_2)}{1 + \delta^2} \\ & \times P_k(\cos\theta) \end{aligned} \quad (\text{III.6})$$



in which  $\tau$  is called the penetrability term and is given by:

$$\tau = \frac{T_{\ell_1 j_1}(E_1) T_{\ell_2 j_2}(E_2)}{T_{\ell_2' j_2'}(E)}$$

The sum extends over all open channels (including elastic scattering) by which the particular compound nuclear state  $Y^* (J_1)$  can decay.



## 2. EXPERIMENTAL PROCEDURE

### 2.1. Apparatus

In this experiment, thick targets of natural Manganese (100%  $^{55}\text{Mn}$ ) were bombarded by protons. The beam was collimated to a diameter of 1.5 mm. The targets were prepared by mixing a small amount of manganese powder into a glue formed by dissolving polyurethane into benzene and smearing the mixture onto a 0.112 mm thick tantalum backing. The targets were then fixed on a holder constituted by a 2 mm thick aluminum plate placed at  $30^\circ$  with respect to the beam direction. This plate also served as charge collector.

Gamma rays were observed using a 15 cc Ge(Li) detector which could be positioned at angles ranging between  $0^\circ$  and  $90^\circ$  to the beam direction. The resolution of the Ge(Li) detector was about 3.5 keV f.w.h.m. for the 1.332 MeV peak of  $^{60}\text{Co}$ .

After amplification, the gamma-ray pulses were sent into an analog-to-digital convertor (ADC), itself connected to the on-line SDS 920 computer for live display. Self gating was used to reduce the counting rate, the cut-off being set at about 300 keV.

### 2.2. Acquisition and Analysis of Data

Following a preliminary study of the gamma-ray yield for bombarding energies ranging between 3.60 and 5.00 MeV, the decay scheme established





by Pilt (Pi 69) was slightly modified and extended up to the 3 MeV region. Two bombarding energies were chosen for the study of angular distribution, bearing in mind that some de-alignment is allowed when the spin value of the level is large ( $\geq 7/2$ ) whereas for low spin states it is necessary to excite the level as close as possible to the threshold, yield permitting.

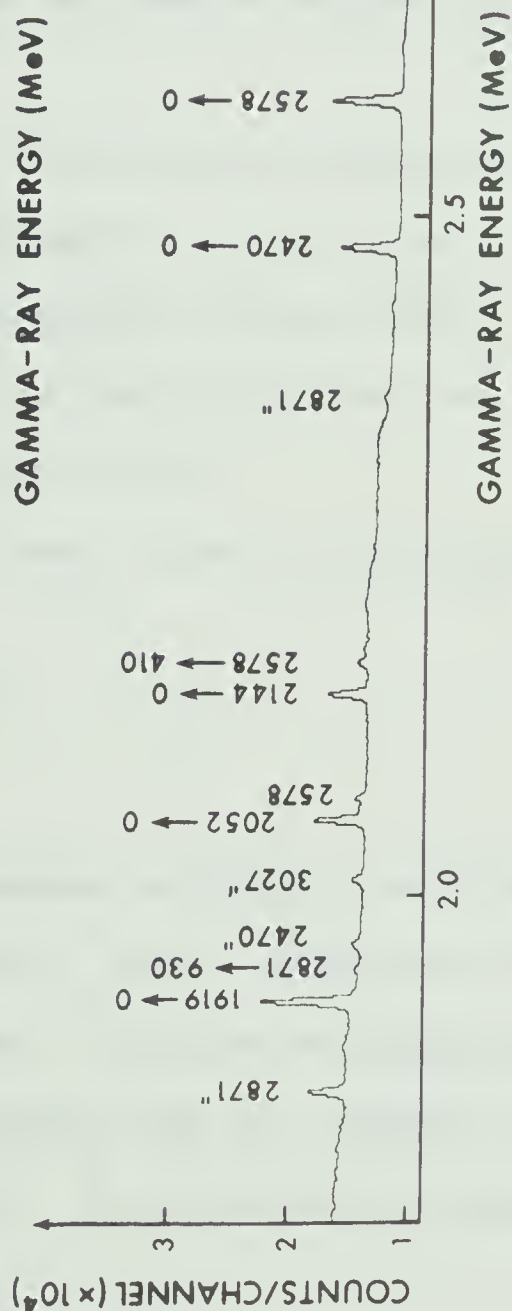
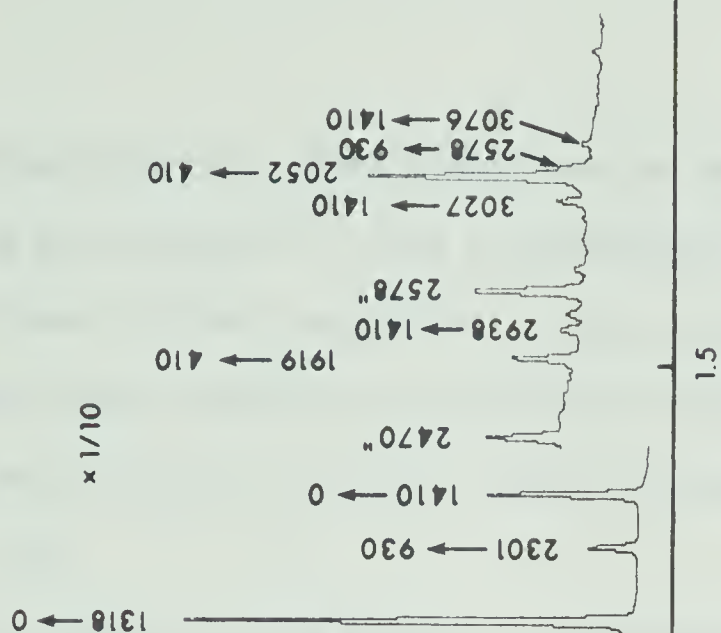
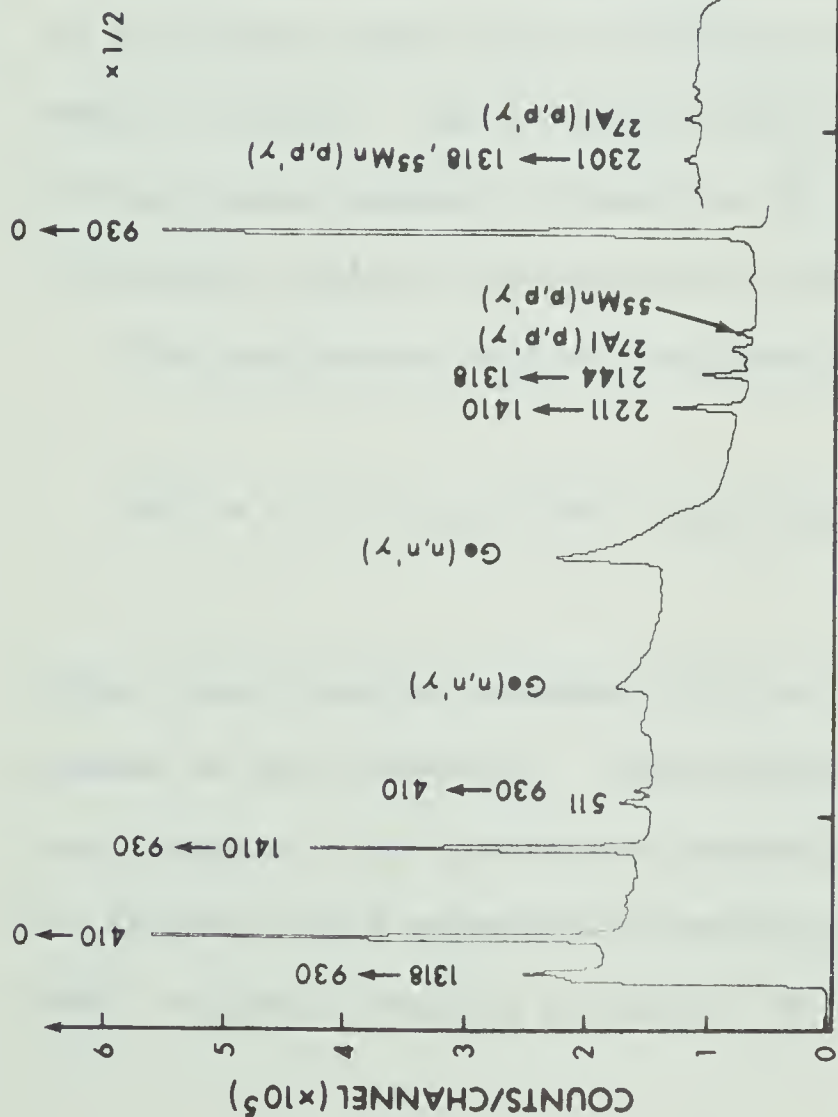
Angular distributions were taken at five angles of 0, 30, 45, 60 and 90 degrees. Measurements were repeated at least once. The beam current was kept at about 100 nA so that the counting rate remained at a reasonable value.

There was no problem caused by contamination in this experiment as the usual contaminants, oxygen, carbon and nitrogen have a very low Q-value for all reactions induced by protons. The gamma rays observed in this reaction, which were not produced by  $^{55}\text{Fe}$ , originated mainly from the decay of levels produced through the other open channels in the  $^{55}\text{Mn} + p$  reaction:  $(p, p'\gamma)$ ,  $(p, \gamma)$  and  $(p, \alpha\gamma)$ . However, only the first two or three levels of the corresponding residual nuclei were excited. Two gamma rays resulting from the  $^{27}\text{Al}(p, p'\gamma)$  reaction were also observed. The gamma rays at 598 and 693 keV resulting from the neutron inelastic scattering in Germanium were also present. A typical gamma-ray spectrum is shown on fig. 11.

The gamma-ray decay scheme of  $^{55}\text{Fe}$  was determined by observing new transitions when bombarding energy was increased and by comparison with all possible transitions from the known levels of  $^{55}\text{Fe}$  being excited.

Figure 11 A typical gamma ray spectrum taken at a bombarding energy of 4.35 MeV with the 15 cc Ge(Li) detector.

$^{55}\text{Mn}(p,n\gamma)^{55}\text{Fe}$   
 15 cc Ge(Li) DETECTOR  
 $E_p = 4.35 \text{ MeV } \theta = 55^\circ$





Branching ratios were determined from the sum of different runs weighted by  $\sin\theta$  for both sets of data corresponding to proton bombarding energies of 4.20 and 4.35 MeV respectively. The absolute intensities were obtained after correction for absorption and efficiency. The relative efficiency of the 15 cc Ge(Li) detector was measured using a  $^{56}\text{Co}$  source (fig. 12).

The strong 410 keV gamma ray corresponding to the decay of the first excited state ( $1/2^-$ ) of  $^{55}\text{Fe}$  to ground state was used as internal monitor as it has an isotropic distribution.

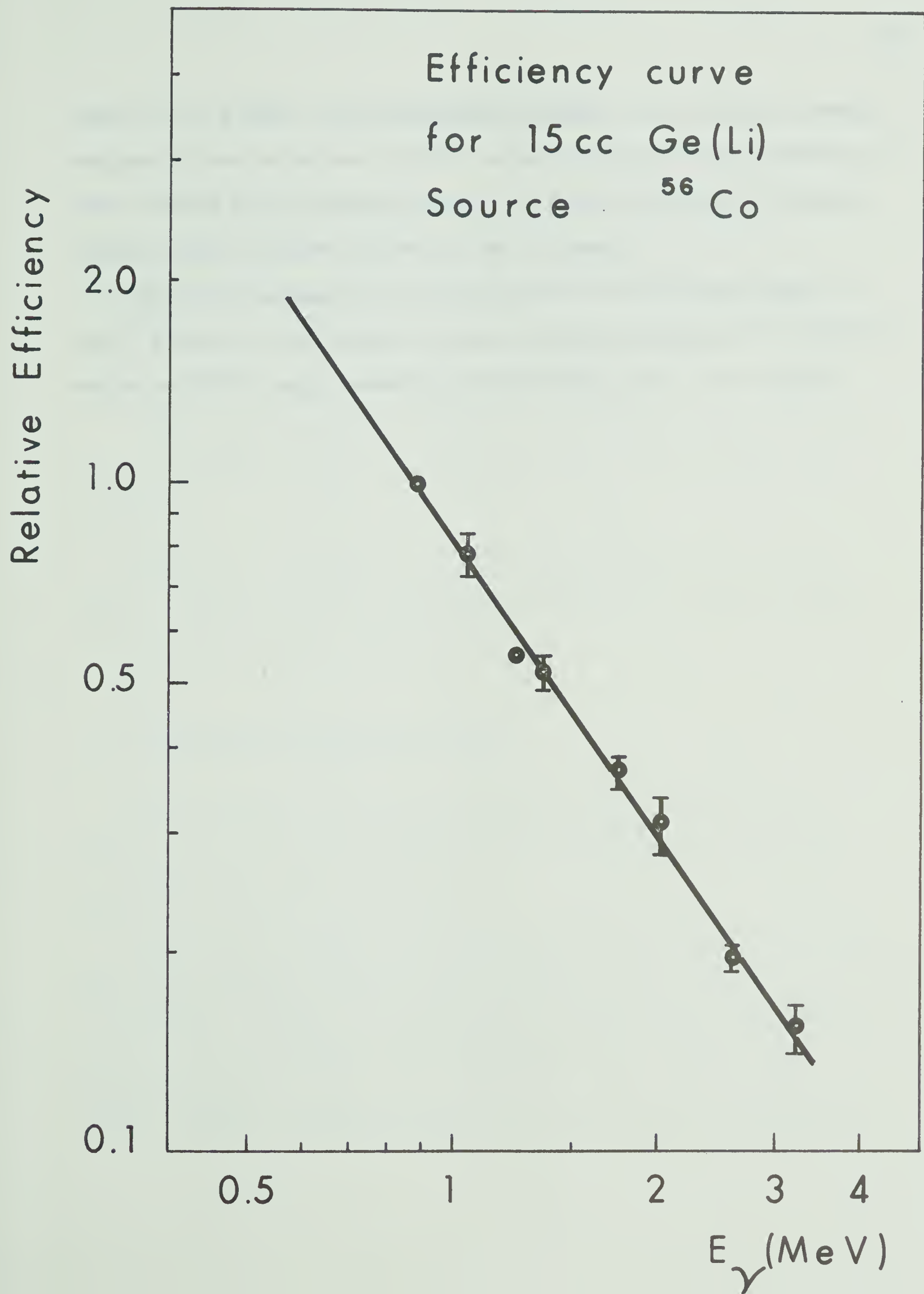
The intensities of the gamma rays were determined by summing over the full energy peaks and subtracting the background directly from computer display. Some intensities were recalculated using a peak fitting program written by Tepel (Te 66). The results obtained from both methods generally agreed within statistical error.

The experimental angular distributions were fitted to the expansion:

$$W(\theta) = a_0 [1 + a_2 P_2(\cos\theta) + a_4 P_4(\cos\theta)]$$

using a least squares procedure with the Legendre polynomial coefficients treated as free parameters. The experimental  $a_2$  and  $a_4$  coefficients were then compared to the theoretical predictions. The latter were calculated for different spin sequences and multipolarities using the computer code MANDY, originally written by Sheldon (Sh 69). The transmission coefficients

Figure 12 Relative efficiency curve for the 15 cc Ge(Li) detector. The experimental points correspond to measurements taken using a  $^{56}\text{Co}$  source.







needed for the MANDY calculations were obtained from the Hauser-Feshbach program written by Davison (Da 69), using the optical model parameters of Rosen (Ro 66) for the proton channels, of Perey (Pe 63) for the neutron channels and of Davison (Da 69) for the  $\alpha$  channel.

Spins were assigned on the basis of the 0.1% confidence limit of the  $\chi^2$  fitting. [This method has been described in Chapter II.] The Rose and Brink (Ro 67) sign convention for the mixing ratio  $\delta$  was adopted.



### 3. EXPERIMENTAL RESULTS

A typical Ge(Li) spectrum taken at 4.35 MeV bombarding energy is shown in fig. 11. The gamma ray spectra were calibrated with  $^{22}\text{Na}$ ,  $^{60}\text{Co}$  and  $^{208}\text{Tl}$ (Th C'') sources. The energy values obtained agree essentially with the more accurate energy measurements of Robertson (Ro 70), which have been adopted in this work.

Figure 13 gives a decay scheme of  $^{55}\text{Fe}$  with branching ratios and spin assignments obtained in this work as well as from previous work (Pi 69).

Tables II - IV summarize all the results obtained in this experiment: branching ratios, Legendre coefficients of the angular distributions, deduced spins and mixing ratios.

#### 3.1. Determination of Branching Ratios

The branching ratio values determined in this work are given in Table II, where they are compared with the measurements of Fischbeck et al. (Fi 66) and Pilt (Pi 69).

The 1666 keV has been totally assigned to the decay of the 3.076 MeV level reported by Sperduto and Buechner (Sp 64) to the 1.410 MeV ( $7/2^-$ ) level. However, a gamma ray of this energy could also correspond to the decay of the 2.984 MeV level to the 1.318 MeV ( $7/2^-$ ) level. Evidence of the excitation of the 2.984 MeV level was seen at



Table II

A summary of branching ratios of the excited states in  $^{55}\text{Fe}$  obtained in the present experiment with earlier investigations

Initial State (MeV)	Residual State (MeV)	This Exp.	Pilt (Pi 69)	Fischbeck <u>et al</u> (Fi 66)
2.144	0	$18 \pm 2$	$17 \pm 2$	100
	0.410	$3 \pm 1$		
	0.930	$43 \pm 4$	$58 \pm 4$	
	1.318	$36 \pm 5$	$25 \pm 3$	
2.211	1.318	(20)	(20)	not observed
	1.410	100	100	
2.301	0.930	$75 \pm 5$	$80 \pm 10$	
	1.318	$15 \pm 5$	$20 \pm 10$	not observed
	1.410	(10)	(10)	
2.542	1.318	100	not observed	not observed
2.578	0	$84 \pm 2$	(100)	100
	0.410	$7 \pm 2$		
	0.930	$6 \pm 2$		
	1.318	$3 \pm 2$		
2.871	0	$88 \pm 3$	(100)	100
	0.930	$12 \pm 3$		
2.938	0	$55 \pm 5$	100	55
	1.316	$45 \pm 4$		45
2.984	0.930	<10		not observed
	1.408	(100)		
3.027	0.	$65 \pm 6$		not observed
	0.412	$35 \pm 7$		
	1.408	<1		
3.076	1.408	(100)		not observed



bombarding energies greater than 4.25 MeV with the appearance on the gamma-ray spectrum, of the 1574 keV gamma ray corresponding to the transition to the 1.410 MeV ( $7/2^-$ ) level. Unfortunately, the bombarding energy of 4.25 MeV corresponds to an excitation of 80 keV above the threshold of the 3.076 MeV. On this basis, it was not possible to assign unambiguously the 1666 keV transition. Arguments in favor of assigning this transition to the decay of the 3.076 MeV state are the following. If the 1666 keV transition were totally assigned to the 2.984 MeV level, the measurement of the intensities of the 1666 and 1574 keV lines would indicate that the decay is 50% to the 1.410 MeV ( $7/2^-$ ) level and 50% to the 1.318 MeV ( $7/2^-$ ) level. The two  $7/2^-$  levels have configurations which are essentially different (see Chapter IV), one is predominantly a  $f_{7/2}$  hole state (G1 66), the other is the result of the coupling of the  $p_{3/2}$  neutron to the  $^{54}\text{Fe}$  core. Consequently, one would expect the 2.984 MeV level to decay predominantly to either one of the  $7/2^-$  states but not to both with equal strength. On the other hand, at 4.35 MeV bombarding energy, the analysis of the angular distribution of the 1574 keV gamma ray yields an unambiguous  $9/2$  assignment to the 2.984 MeV level, whereas the angular distribution of 1666 keV gamma ray favors strongly an  $11/2$  assignment (although  $9/2$  cannot be entirely ruled out on the basis of the 0.1% confidence limit). Therefore, the 1666 keV gamma-ray transition was entirely assigned to the 3.076 MeV state. A coincidence measurement (e.g. the  $^{54}\text{Fe}(d,p\gamma)^{55}\text{Fe}$  reaction) could confirm this assignment.

Figure 13 The  $^{55}\text{Fe}$  energy level diagram: The branching ratios for levels below 2.144 MeV were determined by Pilt (Pi 69). For levels  $\geq 2.144$  MeV, they were determined in this experiment. The  $\ell_n$  values are taken from (Fu 63) and (Ma 64).



3076	————— (100) ———					$I_n$	(11/2, 9/2)
3027	— 65 ± 6 —	— 35 ± 7 —	————— < 1 ———		1	3/2 <sup>-</sup>	
2984			< 10	(100)		9/2 <sup>-</sup>	
2938	— 55 ± 5 —			45 ± 4		< 7/2 <sup>-</sup>	
2871	— 90 ± 3 —			10 ± 3		(5/2) <sup>-</sup>	
2818	---	---	---	---			
2578	— 84 ± 2 —	— 7 ± 2 —	— 6 ± 2 —	— 3 ± 2 —	(3)	5/2 <sup>-</sup>	
2542				100		11/2 <sup>-</sup> , (9/2)	
2470	— 100 —				1	3/2 <sup>-</sup>	
2301			80	20	< 10	9/2 <sup>-</sup>	
2211				< 20	100	9/2 <sup>-</sup>	
2144	— 18 ± 2 —	— 3 ± 1 —	— 43 ± 4 —	— 36 ± 5 —	3	5/2 <sup>-</sup>	
2052	— 23 ± 2 —	— 77 ± 2 —			1	3/2 <sup>-</sup>	
1919	— 68 ± 3 —	— 32 ± 3 —			1	1/2 <sup>-</sup> , 3/2 <sup>-</sup>	
1410	— (45) —		— (55) —	< 10	3	7/2	
1318	— 96 ± 1 —		— 4 ± 1 —	↓	(3)	7/2 <sup>-</sup>	
930	— 98 ± 1 —	— 2 ± 1 —	↓		3	5/2 <sup>-</sup>	
412	— 100 —	↓			1	1/2 <sup>-</sup>	
	↓				1	3/2 <sup>-</sup>	

$^{55}\text{Fe}$



### 3.2. The 2.211 MeV Level

This level has been assigned  $J = 9/2$  by Pilt (Pi 69) using the  $^{55}\text{Mn}(p,n\gamma)^{55}\text{Fe}$  reaction, at 3.50 MeV bombarding energy (210 keV above threshold). At 4.10 MeV bombarding energy (810 keV above threshold), the distribution of the 801 keV gamma ray corresponding to the decay of the 2.211 MeV ( $9/2^-$ ) level to the 1.410 MeV ( $7/2^-$ ) level is still strongly anisotropic, ( $a_2 = -0.34 \pm 0.03$ ) as shown in fig. 14a. The  $\chi^2$  plots shown in fig. 14b indicate that, even at 810 keV above threshold, the 2.211 MeV level can be unambiguously assigned  $J = 9/2$ . The possible mixing ratio solutions ( $0.21^{+0.28}_{-0.70}$  or  $2.15^{+0.90}_{-0.85}$ ) are consistent with those obtained by Pilt (Pi 69) ( $0.19^{+0.07}_{-0.09}$  or  $2.75^{+0.75}_{-0.50}$ ).

### 3.3. The 2.301 MeV Level

This level has also been assigned  $J = 9/2$  by Pilt (Pi 69) from the study, at 3.50 MeV proton bombarding energy, of the 1371 keV transition corresponding to the decay from this level to the 0.930 MeV ( $5/2$ ) level. The angular distribution of the 1371 keV transition was measured at 4.10 and 4.35 MeV bombarding energy in this experiment. In Table III, the Legendre polynomial coefficients obtained in these measurements are given and compared with Pilt's measurements. The resulting spin assignment is also given.

Figure 14 The 2.211 MeV level: Angular distribution (a) and  $\chi^2$  plots (b) for the 801 keV gamma-ray transition to the 1.410 MeV (7/2) level.

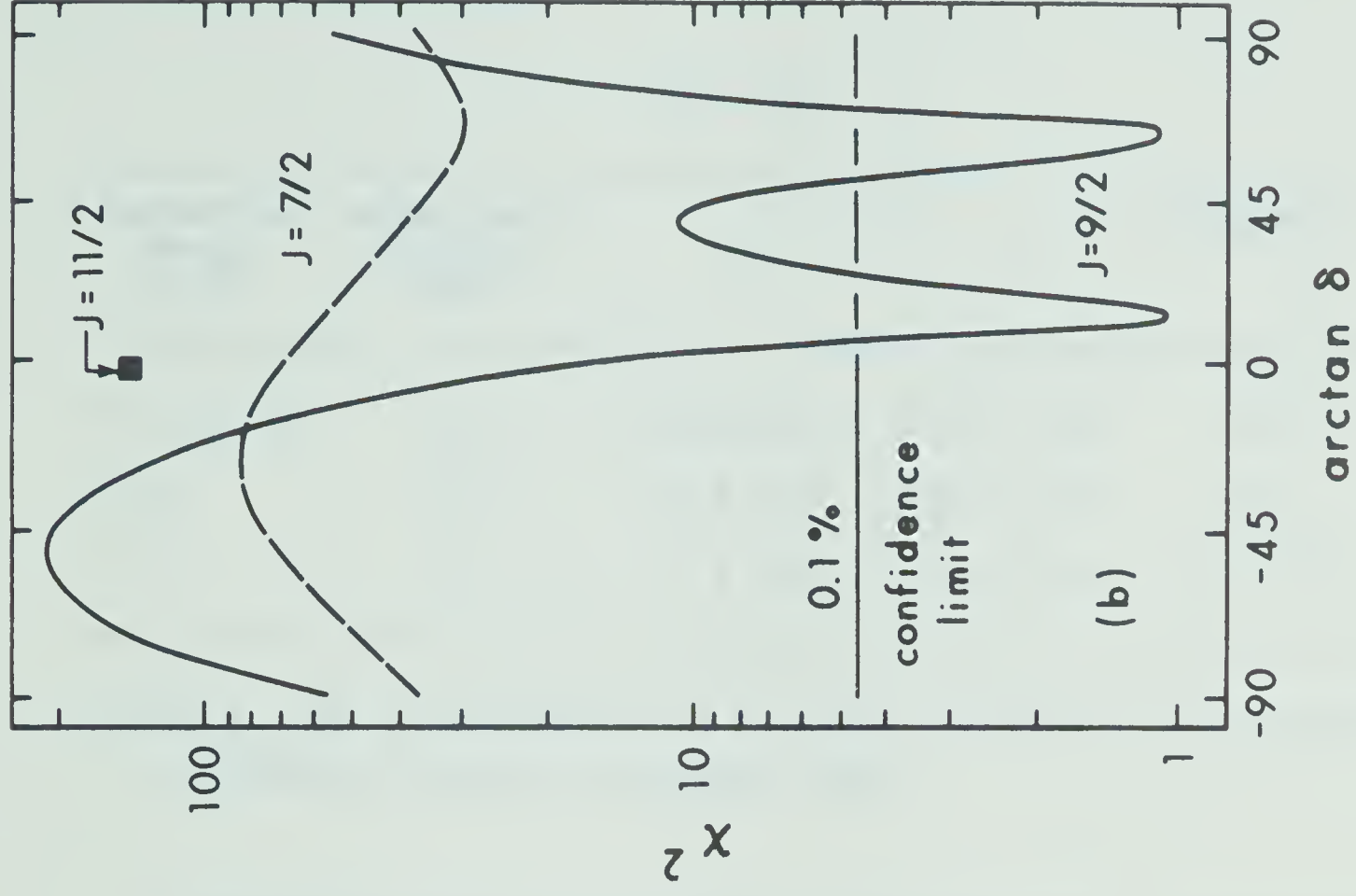
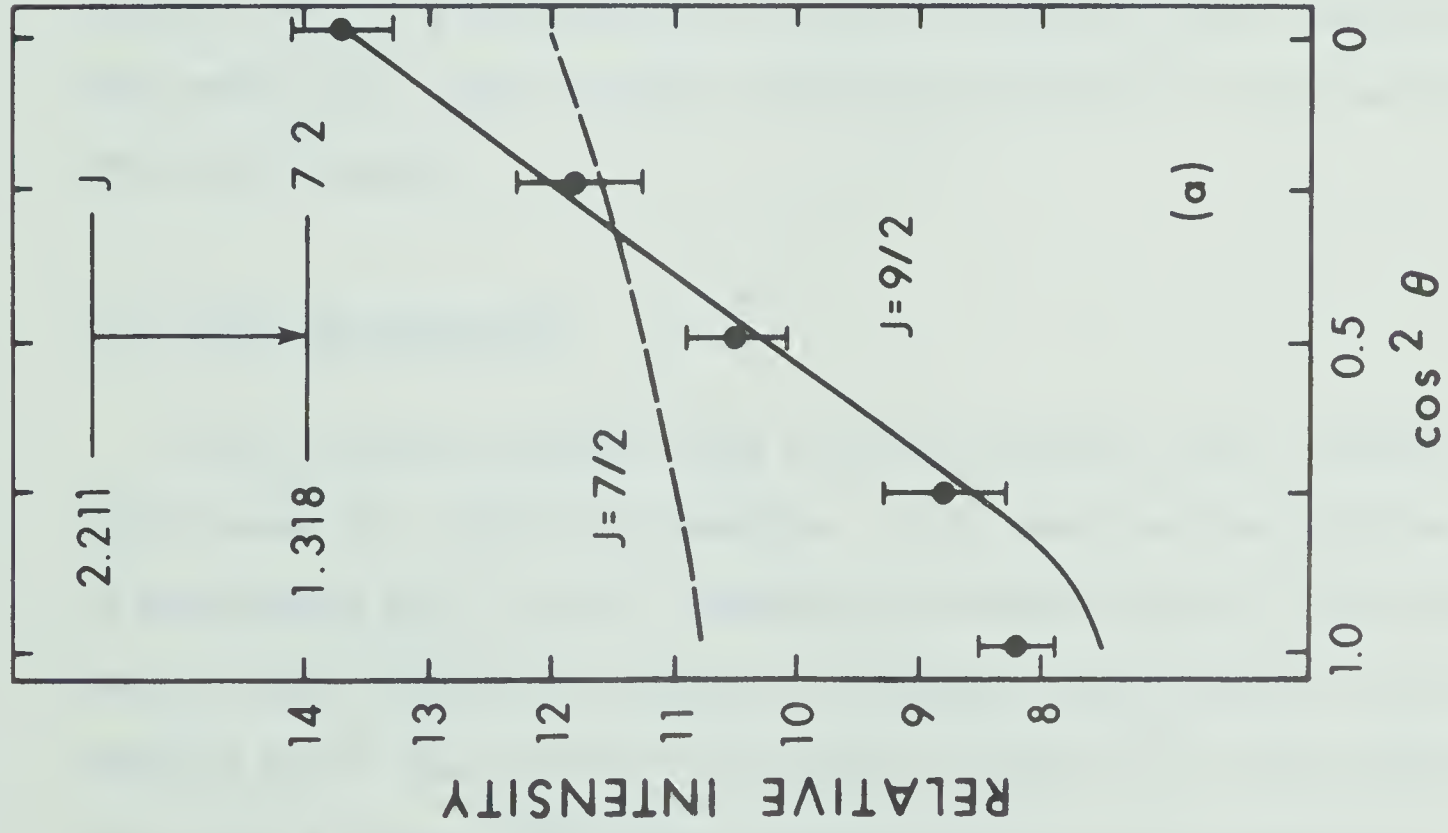




Table III

Bombarding Energy (MeV)	Energy above Threshold (MeV)	$a_2$	$a_4$	Assignment
3.50 (Pi 69)	125	$0.39 \pm 0.05$	$0.03 \pm 0.06$	9/2
4.10	725	$0.22 \pm 0.02$	$-0.01 \pm 0.02$	9/2
4.35	975	$0.19 \pm 0.03$	$-0.00 \pm 0.03$	9/2, 7/2 <sup>(*)</sup>

(\*) The  $\chi^2$  plot corresponding to  $J = 7/2$  has a minimum of 2.4; this value corresponds to about 5% confidence limit.

This table, as well as the results obtained for the 2.211 MeV level, indicate that in this experiment, levels with spin 9/2 (and consequently with spin  $\geq 9/2$ ), remain strongly aligned when excited at a few hundred keV above threshold.

#### 3.4. The 2.542 MeV Level

The 2.542 MeV level was found to decay entirely to the 1.318 MeV ( $7/2^-$ ) state via a 1224 keV transition. This level has been reported by Bjerregaard et al. (Bj 64), Sperduto and Buechner (Sp 64) from their study of the  $^{54}\text{Fe}(d,p)^{55}\text{Fe}$  reaction. Fischbeck et al. (Fe 66) in the study of the  $\beta^+$  decay of  $^{55}\text{Co}$  have found no evidence that this level is fed in the  $\beta^+$  decay. They have concluded that this level cannot be

Figure 15 The 2.542 MeV level: Angular distributions (a) and  $\chi^2$  plots (b) for the 1224 keV gamma-ray transition to the 1.318 MeV ( $7/2^-$ ) level.



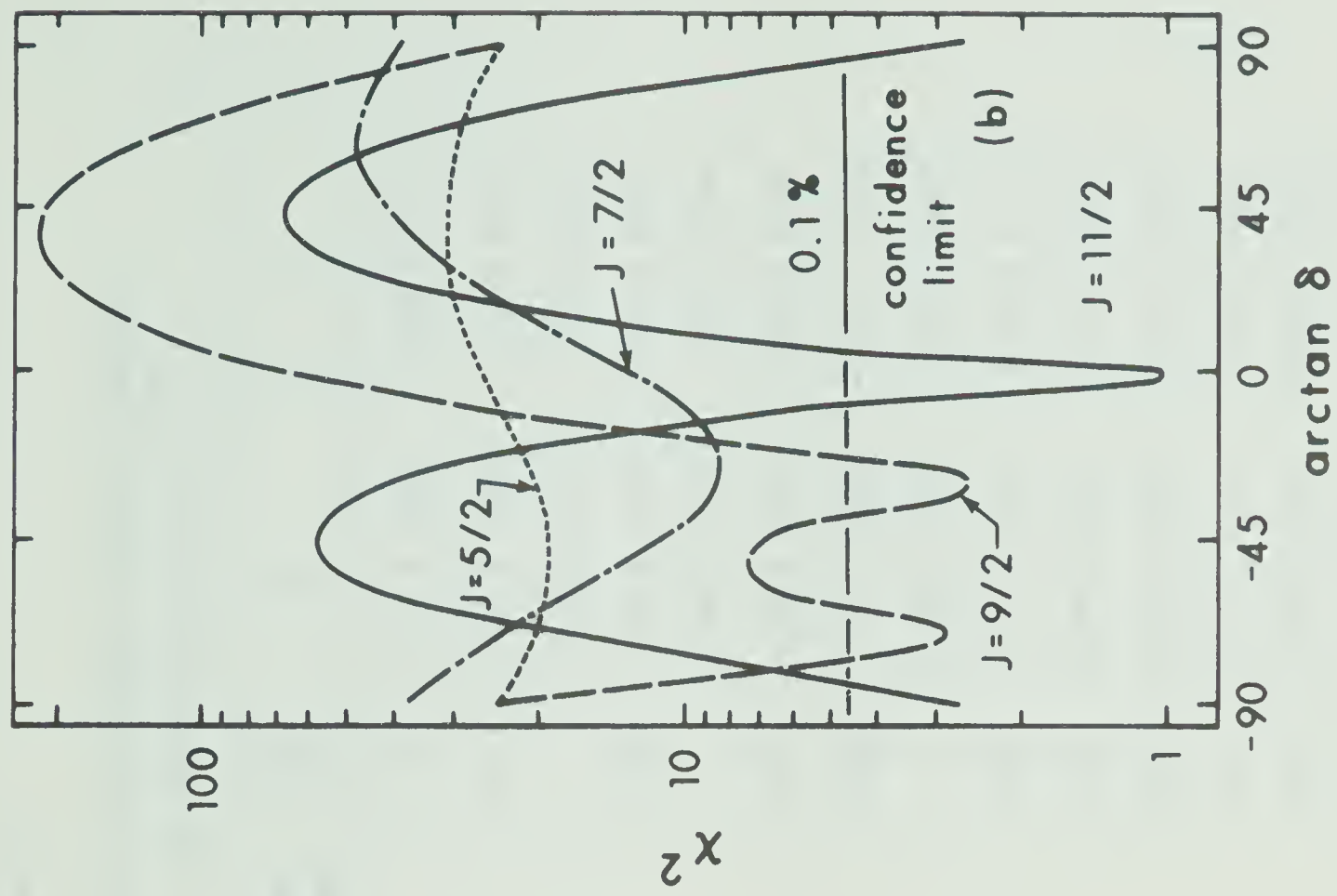
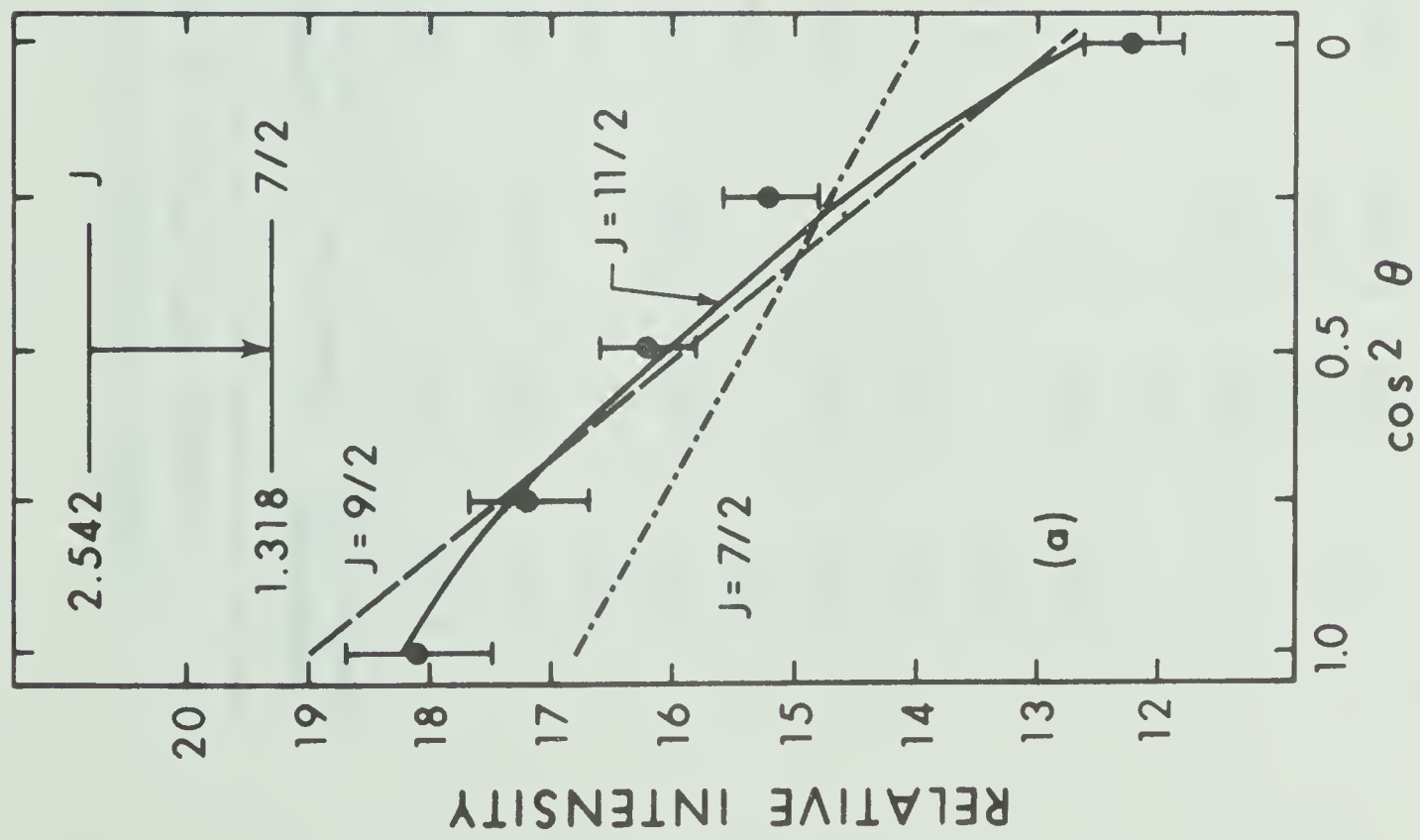




Table IV

Legendre coefficients, corrected for solid angle effects, fitted to  
angular distributions of gamma rays deexciting levels of  $^{55}\text{Fe}$

Bombarding Energy (MeV)	Transition	Energy above threshold (keV)	$E_\gamma$ keV	$a_2$	$a_4$
4.10	2.211 $\rightarrow$ 1.318	810	893	$-0.34 \pm 0.03$	$-0.05 \pm 0.03$
4.10	2.301 $\rightarrow$ 0.930	725	1371	$0.22 \pm 0.02$	$-0.01 \pm 0.02$
4.35	-	975	-	$0.19 \pm 0.03$	$-0.02 \pm 0.03$
4.10	2.542 $\rightarrow$ 1.318	450	1224	$0.30 \pm 0.03$	$-0.09 \pm 0.04$
4.35	-	700	-	$0.06 \pm 0.05$	$0.02 \pm 0.06$
4.10	2.871 $\rightarrow$ 0	100	2871	$0.00 \pm 0.08$	$0.00 \pm 0.08$
4.10	2.938 $\rightarrow$ 0	60	2938	$-0.10 \pm 0.05$	$-0.05 \pm 0.05$
4.35	-	310	-	$0.06 \pm 0.05$	$0.02 \pm 0.06$
4.35	2.984 $\rightarrow$ 0	270	2984	$-0.70 \pm 0.11$	$0.19 \pm 0.11$
	3.027 $\rightarrow$ 0	220	3027	$-0.06 \pm 0.10$	$-0.11 \pm 0.10$
	3.027 $\rightarrow$ 0.410	-	2617	$-0.53 \pm 0.19$	$0.12 \pm 0.20$
	3.027 $\rightarrow$ 1.410		1617	$-0.16 \pm 0.07$	$0.12 \pm 0.07$
	3.076 $\rightarrow$ 1.410	180	1666	$0.38 \pm 0.06$	$-0.18 \pm 0.08$



assigned  $5/2^-$ ,  $7/2^-$  or  $9/2^-$ .

The angular distribution of the 1224 keV gamma ray at 4.10 MeV bombarding energy is shown in fig. 15a. It is strongly anisotropic ( $a_2 = 0.30 \pm 0.03$ ). The  $\chi^2$  analysis (fig. 15b) yields two possible spin assignments:  $9/2$  and  $11/2$ , the former being less likely than the latter. The  $9/2^-$  assignment could be rejected on the basis of the results of Fischbeck et al. Positive parity for the  $J = 9/2$  assignment is not favored as one would rather expect the level to decay via a pure electric dipole transition in this case, assumption in disagreement with the results of the  $\chi^2$  analysis. Therefore, the  $J^\pi = 11/2^-$  assignment is more likely and corresponds to a pure E2 transition ( $\delta = 0$ ).

### 3.5. The 2.578 MeV Level

This level decays primarily to the ground state (84%). In this work, three weak transitions, not previously reported (Fi 66, Pi 69), have been observed. They correspond to decay to the 0.410 MeV ( $1/2^-$ ), 0.930 MeV ( $5/2^-$ ) and 1.318 MeV ( $7/2^-$ ) levels.

The decay of the 2.578 MeV state is consistent with the  $5/2^-$  spin assignment of Pilt (Pi 69). At 4.10 MeV bombarding energy, the distribution of the 2578 keV gamma-ray was isotropic within experimental error. No conclusions about the spin of the level could be drawn from this work.



### 3.6. The 2.818 MeV Level

No evidence was found of the existence of this level reported in the work of Sperduto and Buechner (Sp 64). Two transitions might be considered as originating from this level: a transition of 1408 keV corresponding to the decay to the 1.410 MeV ( $7/2^-$ ) level and a transition of 517 keV corresponding to the decay to the 2.211 MeV ( $9/2^-$ ) level. Because of multiple feeding of the low lying states and of the uncertainties in the branching ratios, these transitions, which would be weak were neither rejected nor confirmed.

### 3.7. The 2.871 MeV Level

This level is weakly populated in the  $^{55}\text{Mn}(p,n\gamma)$  reaction. It was found to decay 88% to the ground state and 18% to the 0.930 MeV ( $5/2^-$ ) state. This second branching, not reported by Pilt (Pi 69), was measured by Fischbeck et al. (Fi 66) to have a strength of 40%. The angular distributions of the ground state transition measured at 4.10 and 4.35 MeV proton bombarding energy were isotropic within statistical error. This limits the spin value of the 2.871 MeV level to  $J < 7/2$ . There is a level at "2.90" MeV reported by Goodman et al. (Go 62) with a neutron angular momentum transfer  $\ell_n = 3$  in the  $^{56}\text{Fe}(p,d)$  pick-up reaction. This result is confirmed by Sherr et al. (Sh 65). If this "2.90" MeV state is the 2.871 MeV level, as suggested by Auble and Rapaport (Au 70), the present results would favor a  $5/2^-$  spin assign-





ment as opposed to the  $7/2^-$  spin assignment suggested by Goodman et al. (Go 62).

### 3.8. The 2.938 MeV Level

This level is also weakly excited in this reaction. It was observed to decay 55% to the ground state and 45% to the 1.318 MeV ( $7/2^-$ ) state, in agreement with the results of Fischbeck et al. (Fi 66).

The angular distribution of the ground state transition was slightly isotropic ( $a_2 = -0.10 \pm 0.05$ ) at 4.10 MeV proton bombarding energy and nearly isotropic ( $a_2 = 0.06 \pm 0.05$ ) at 4.35 MeV bombarding energy, limiting the spin of the 2.938 MeV to  $J \leq 7/2$  in agreement with Pilt's results (Pi 69).

Auble and Rapaport (Au 70) suggest the existence of two levels around 2.94 MeV: one at 2.940 MeV which would correspond to a stripping level with a tentative neutron momentum transfer  $\ell_n = 1$  according to Sperduto et al. (Sp 64), and one level which would be the 2.948 MeV level reported by Fischbeck et al. (Fe 66), with spin value limited to  $J^\pi = 5/2^-$  or  $7/2^-$ . No evidence of a second level has been found in this study which suggests that the 2.938 MeV level may in fact be the 2.948 MeV level observed by Fischbeck et al. (Fe 66).



### 3.9. The 2.984 MeV Level

The primary decay is by a 1574 keV gamma-ray transition to the 1.410 MeV ( $7/2^-$ ) level. A weak 2054 keV gamma ray may be due to a transition to the 0.930 MeV ( $5/2^-$ ) level with a strength equal to less than 10% of the total strength. A 1666 keV gamma ray which could correspond to a transition to the 1.318 MeV ( $7/2^-$ ) has been assigned entirely to the decay of 3.076 MeV level as explained in section 3.1.

The angular distribution of the 1574 keV gamma ray (fig. 16a) is strongly anisotropic at 4.35 MeV bombarding energy ( $a_2 = -0.70 \pm 0.11$ ). The  $\chi^2$  analysis (fig. 16b) yields a unique spin assignment  $J = 9/2$  and a mixing ratio of  $-0.85^{+0.70}_{-2.30}$ . It is unlikely that this level has a positive parity as the experimental results indicate that the transition would correspond to a strong M2-E1 mixing. This assignment  $J^\pi = 9/2^-$  is in disagreement with the  $^{55}\text{Co}$   $\beta$ -decay study of Fischbeck et al. (Fi 66) who report no  $\beta$  decay to this level and consequently rule out  $5/2^-$ ,  $7/2^-$  or  $9/2^-$  as possible spin assignments. However, Haupt et al. (Ha 65) in a similar work report a 1580 keV gamma-ray transition in their Ge (Li) spectrum. Coincidence measurements indicate that this transition is fed by  $(0.09 \pm 0.05)\%$  of the total  $\beta$  decay. As they identified the 1580 keV gamma ray with a 1600 keV seen in the NaI spectrum, they concluded that this transition was the 1612 keV transition between the 2.542 MeV and the 0.930 MeV level. This 1580 keV transition is likely to be the 1574 keV transition involved here and the  $9/2^-$  assignment would

Figure 16 The 2.984 MeV level: Angular distribution (a) and  $\chi^2$  plots (b) for the 1574 keV gamma-ray transition to the 1.410 MeV ( $7/2^-$ ) level.

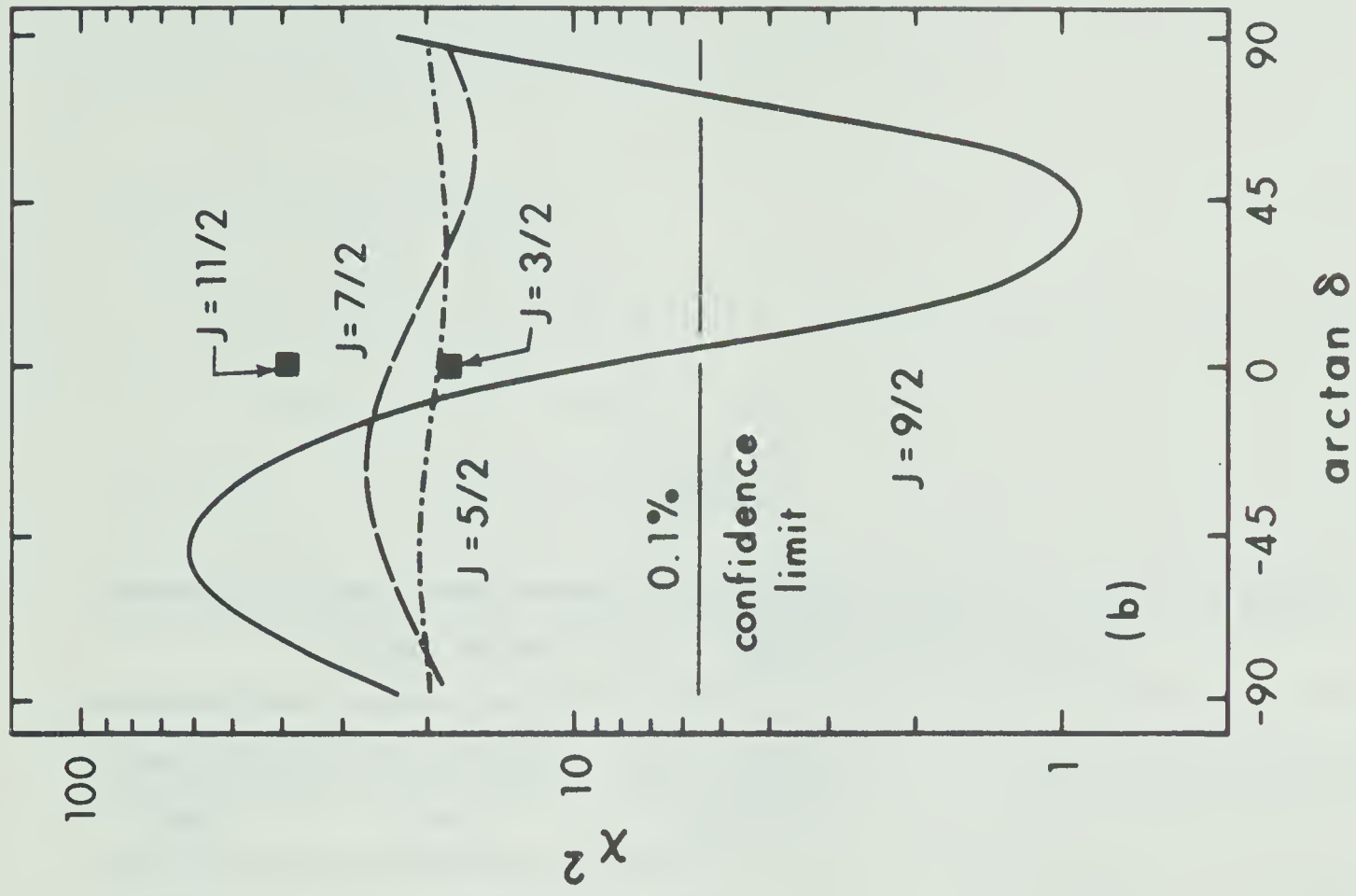
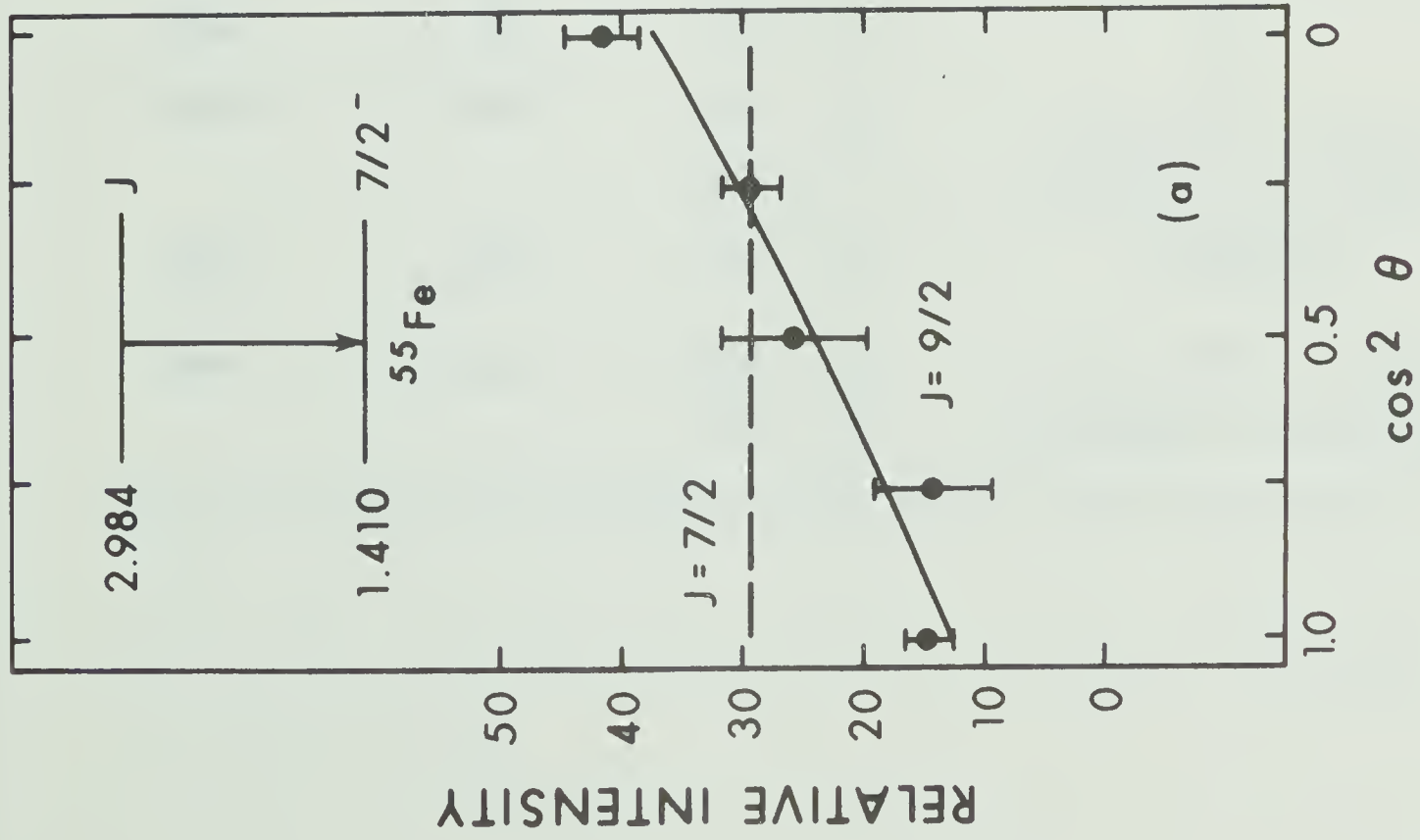




Table V

A summary of spin assignments and multipole mixing ratios determined  
in this study of the  $^{55}\text{Mn}(p,n\gamma)^{55}\text{Fe}$  Reaction

Initial State (keV)	Final State (keV)	Spin Sequence Assumed	Mixing Ratio Solution
2211	1410	9/2 - 7/2	$0.21^{+0.28}_{-0.70}$ or $2.15^{+0.90}_{-0.85}$
2301	930	9/2 - 5/2	E2
2542	1318	11/2 - 7/2	E2
.		9/2 - 7/2	$-0.60^{+0.20}_{-0.12}$ or $-2.75^{+0.75}_{-1.25}$
2984	1410	9/2 - 7/2	$0.85^{+2.30}_{-0.70}$
3076	1410	11/2 - 7/2	E2
		9/2 - 7/2	$-0.60^{+0.24}_{-2.15}$ or $-2.75^{+2.50}_{-2.90}$





then be consistent with the  $\beta^+$ -decay of  $^{55}\text{Co}$ .

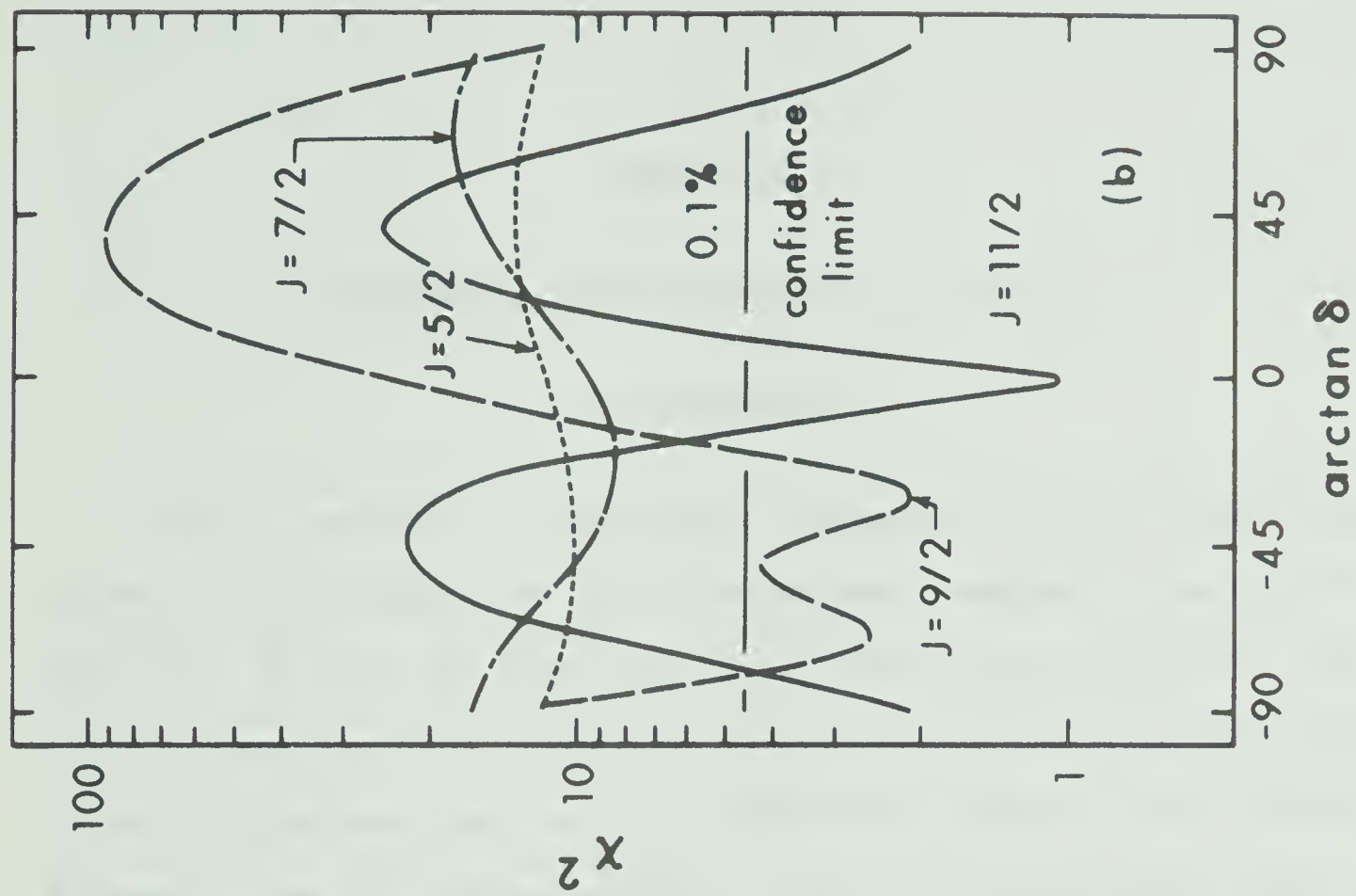
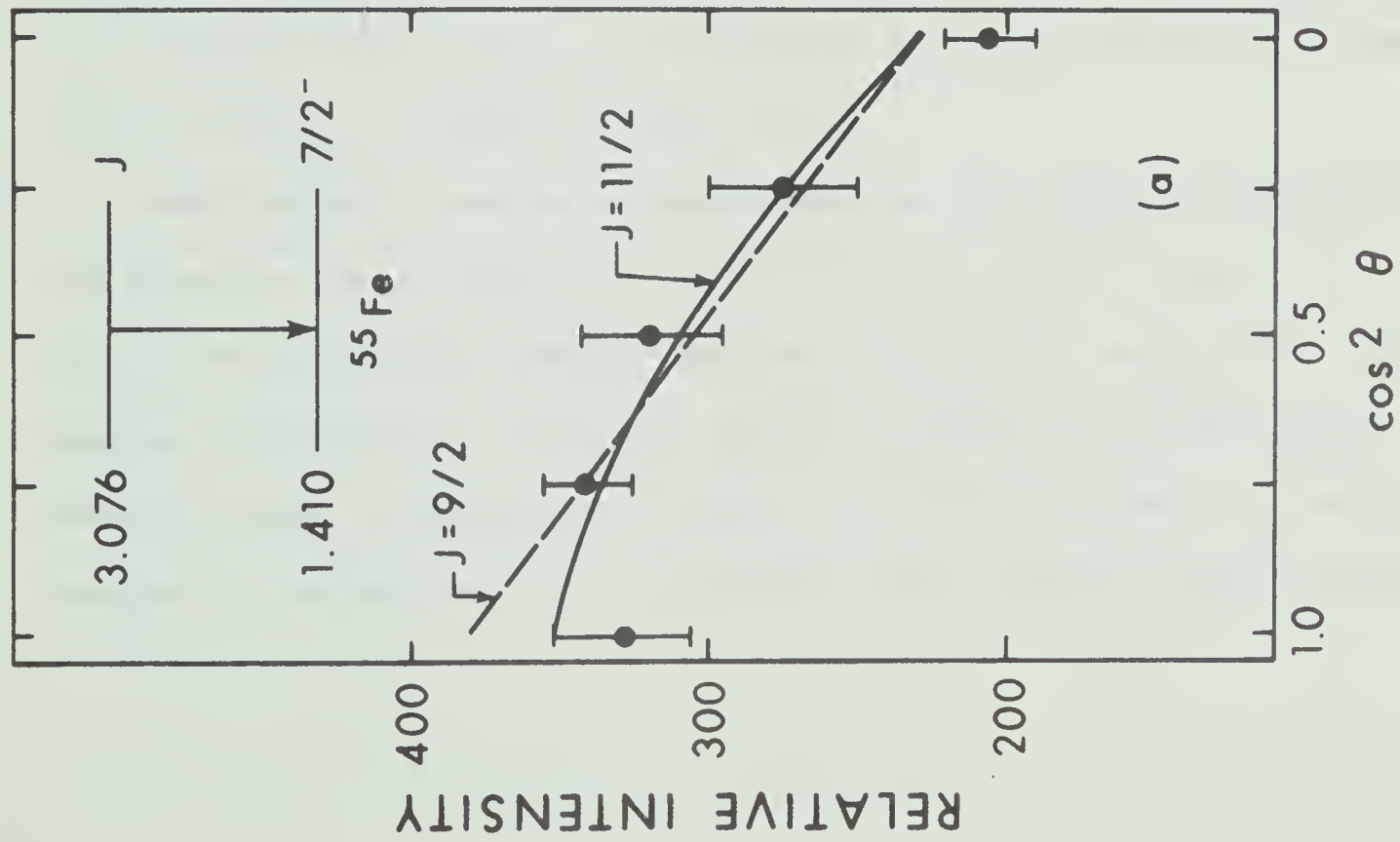
### 3.10. The 3.027 MeV Level

This level decays 65% to the ground state and 35% to the 0.410 MeV ( $1/2^-$ ) state. A weak transition ( $< 1\%$ ) to the 1.410 MeV ( $7/2^-$ ) was also observed. The angular distributions of the ground state transition and the 2617 keV transition to the 0.410 MeV were both isotropic at 4.35 MeV bombarding energy. Both the observed gamma decay and angular distributions are consistent with the  $J^\pi = 3/2$  assignment of this state, based on the radiative neutron capture measurements of Earle and Bartholomew (Ea 66) and on the  $\ell_n = 1$  momentum transfer observed in stripping reaction (Fu 63, Ma 64).

### 3.11. The 3.076 MeV Level

The 1666 keV gamma ray has been entirely assigned to the decay from the 3.076 MeV level to the 1.410 MeV ( $7/2^-$ ) state (see section 3.1.). The angular distribution of this transition is shown in fig. 17a. It is strongly anisotropic ( $a_2 = 0.38 \pm 0.06$ ) and the  $\chi^2$  analysis (fig. 17b) yields two possible assignments:  $J = 9/2$  or  $11/2$ , the former being less probable with a minimum  $\chi^2$  of 2.1. As no  $\beta^+$  decay has been observed to this level (Ha 65, Fi 66), the  $11/2^-$  assignment would be more likely.

Figure 17 The 3.076 MeV level: Angular distribution (a) and  $\chi^2$  plots (b) for the 1666 keV gamma-ray transition to the 1.410 MeV ( $7/2^-$ ) state.





## CHAPTER IV

### THEORETICAL INVESTIGATION OF $^{53}\text{Cr}$ AND $^{55}\text{Fe}$

#### 1. MOTIVATION

There is evidence of considerable fragmentation of the single particle states in the stripping and pick up experiments leading to levels in  $^{53}\text{Cr}$  and  $^{55}\text{Fe}$ . In  $^{53}\text{Cr}$ , the first three  $3/2^-$  states (the ground state, the 2.324 MeV and the 3.625 MeV states) have been assigned almost the totality of the  $2p_{3/2}$  strength, and the  $1/2^-$  (0.564 MeV) state about 40% of the  $2p_{1/2}$  strength. Four  $5/2^-$  states between 1.0 and 5.0 MeV excitation share about 50% of the  $1f_{5/2}$  strength. Most of the  $1g_{9/2}$  strength has been assigned to the 3.715 MeV state. The  $\ell_n = 2$  transfers indicate considerable fragmentation of the  $2d_{5/2}$  strength (Ra 68, Wh 67).

Many inelastic scattering experiments on  $^{53}\text{Cr}$  have been reported and all show that the 0.564 ( $1/2^-$ ), 1.006 ( $5/2^-$ ), 1.285 ( $7/2^-$ ) and 1.971 ( $\geq 3/2^-$ ) MeV states are strongly excited (Ra 68, Wh 67 and Me 66). The angular distribution of inelastic alpha scattering of the first three excited states is indicative of their description in terms of a particle coupled to the excited  $^{52}\text{Cr}$  core (Me 66). The 1.285 MeV level has been



described by a  $(2^+)$   $2p_{3/2}$  core-particle weak coupling model (BD 64, BD 65) and Whitten (Wh 67) has assigned a 20% admixture of the  $(2^+)$   $2p_{3/2}$  configuration to the  $^{53}\text{Cr}$  ground state configuration. Measurements of enhanced E2 transition probabilities for the low lying levels of  $^{53}\text{Cr}$  (Me 66, Ga 69) indicate the existence of collective effects.

In  $^{55}\text{Fe}$ , less experimental data are available but they indicate that the general features observed in  $^{53}\text{Cr}$  are present in this nucleus also. The ground state  $(3/2^-)$  has been assigned about 85% of the  $2p_{3/2}$  strength and the 0.412 MeV  $(1/2^-)$  state about 45% of the  $2p_{1/2}$  strength (Ma 64, Fu 63). Four states between 1.0 and 4.1 MeV share approximately 85% of the  $1f_{5/2}$  strength. Most of the  $\ell_n = 4$  ( $1g_{9/2}$ ) strength seems to be assignable to a level at 3.8 MeV.

The results obtained in this work have shown the probable existence of two  $11/2^-$  states in  $^{55}\text{Fe}$ . One of these at 3.076 MeV excitation energy is apparently a member of a band built on the 1.408 MeV  $(7/2^-)$  hole state, with the 2.211 MeV  $(9/2^-)$  state as second member. On the other hand, it seemed possible to describe many levels of  $^{53}\text{Cr}$  and  $^{55}\text{Fe}$  in terms of another rotational band built on a  $K = 1/2^-$  state. These remarks suggested a possible application of the Nilsson model which has been applied to  $^{57}\text{Fe}$  and  $^{59}\text{Fe}$  (So 67, So 69) with some success. However,  $^{56}\text{Fe}$  and  $^{58}\text{Fe}$  are apparently strongly deformed, whereas  $^{54}\text{Fe}$  as well as  $^{52}\text{Cr}$  exhibit vibrational properties (see e.g. Go 62, Fu 64). This means that, in both  $^{53}\text{Fe}$  and  $^{55}\text{Fe}$ , the Nilsson model has little chance of success. Nilsson model calculations will be described in section 2.







Calculations involving the intermediate coupling in the unified model have been done for  $N = 29$  odd nuclei in 1963 by Ramavataram (Ra 63). At the time, little was known about these nuclei outside the information garnered from stripping reaction studies. It was felt that this type of calculation could be used again with different parameters, and with the inclusion of more levels to be fitted as well as with the calculation of electromagnetic properties and spectroscopic factors. For this purpose, two programs were written which are described in the Appendix. The model is also fully described in the Appendix and again outlined in section 3. Calculations based on the "Thankappan and True" model and on the shell model have been done for  $^{53}\text{Cr}$  and  $^{55}\text{Fe}$ . Both models will be briefly described in sections 4 and 5. In section 6, results obtained from these models will be compared with the calculations based on the intermediate coupling in the unified model. A discussion will follow in section 7.



## 2. NILSSON MODEL CALCULATIONS

### 2.1. Theory

The Nilsson model has been extensively described elsewhere (Ni 55, Da 65) and no attempt will be made to derive the results here.

One can describe odd-A nuclei as constituted by an odd nucleon moving in the average field of the remaining nucleons which constitute the "core". In the single particle shell model, the average field is supposed to be spherically symmetric. In the Nilsson model, it is assumed that the core is permanently deformed. Any oscillations in shape which take place have sufficiently low frequency to permit the particle to follow adiabatically. In the strong coupling limit, the motion of the extra core nucleon is exactly the same in the body-fixed reference frame as that of a nucleon moving in a spatially fixed potential well. The average field is no longer spherically symmetric, but has spheroidal symmetry about the body-fixed 3-axis.

The total Hamiltonian of the system contains two terms: the Hamiltonian of the odd nucleon and the kinetic energy of the core. Consider first the single particle motion. It is described by the Nilsson Hamiltonian: (Ni 55)

$$\mathcal{H} = \overset{0}{\mathcal{H}}_0 + \mathcal{H}_\delta + C \vec{l} \cdot \vec{s} + D \vec{l}^2 \quad (\text{IV.1})$$



with  $\mathcal{H}_\delta = -\frac{4}{3} \hbar \omega_0 \delta \sqrt{\frac{r}{5}} r^2 Y_{20}$

$\mathcal{H}_0$  is the Hamiltonian for a spherically symmetric harmonic oscillator with eigenvalues  $N\hbar\omega_0$ ;  $\mathcal{H}_\delta$  represents the coupling of the particle to the axis of deformation;  $C \vec{\ell} \cdot \vec{s}$  is the spin-orbit term; the  $D \vec{\ell}^2$  - term gives a correction to the oscillator potential, especially at large distance. (It is sometimes referred to as the flattening parameter, as it serves to depress the high angular momentum states.)

Starting from this definition some new parameters are introduced which will express equation (IV.1) in a more convenient form for computation. In Nilsson's formalism, equation (IV.1) becomes:

$$\mathcal{H} - \mathcal{H}_0 = \kappa \hbar \omega_0 R \quad (\text{IV.2})$$

where  $R = \eta U - 2 \vec{\ell} \cdot \vec{s} - \mu \vec{\ell}^2$

with the new parameters defined by:

$$\kappa = \frac{1}{2} \frac{C}{\hbar \omega_0}, \quad \mu = 2 \frac{D}{C} \quad \text{and} \quad \eta = \frac{\delta}{\kappa} \frac{\omega_0(\delta)}{\omega_0}$$

The dependence of  $\omega_0$  on the deformation  $\delta$  arises from a requirement that the nucleus volume remains constant. At  $\delta = 0$ ,  $\omega_0(0) = \omega_0^0$  is related to the nuclear mass through the relation  $\hbar \omega_0^0 = 41 A^{-\frac{1}{3}}$  MeV.

The values of the parameters  $\kappa$  and  $\mu$  are chosen such that for zero deformation the shell model levels be reproduced. The total angular momentum  $\vec{j}$  of the particle is no longer a good quantum number but its projection  $\Omega$  along the symmetry axis, (the 3-axis in the body fixed



reference frame) is a good quantum number.

The calculation then consists in the diagonalization of the matrix  $R$  in a chosen representation. It is then possible to obtain the eigenfunctions of the particle Hamiltonian  $\mathcal{H}_p$ . The basis vectors chosen by Nilsson are those in which  $\mathcal{H}_0$  is diagonal together with  $\ell^2$ ,  $\ell_3$  ( $=\Lambda$ ) and  $s_3$  ( $=\Sigma$ ). The eigenvectors labelled by  $\Omega$  and another label  $\alpha$  are then expanded in terms of the basis vectors:

$$|\Omega\alpha\rangle = \sum_{\ell\Lambda} a_{\ell\Lambda}^{\alpha} |\ell\Lambda\Sigma\rangle \quad (\text{IV.3})$$

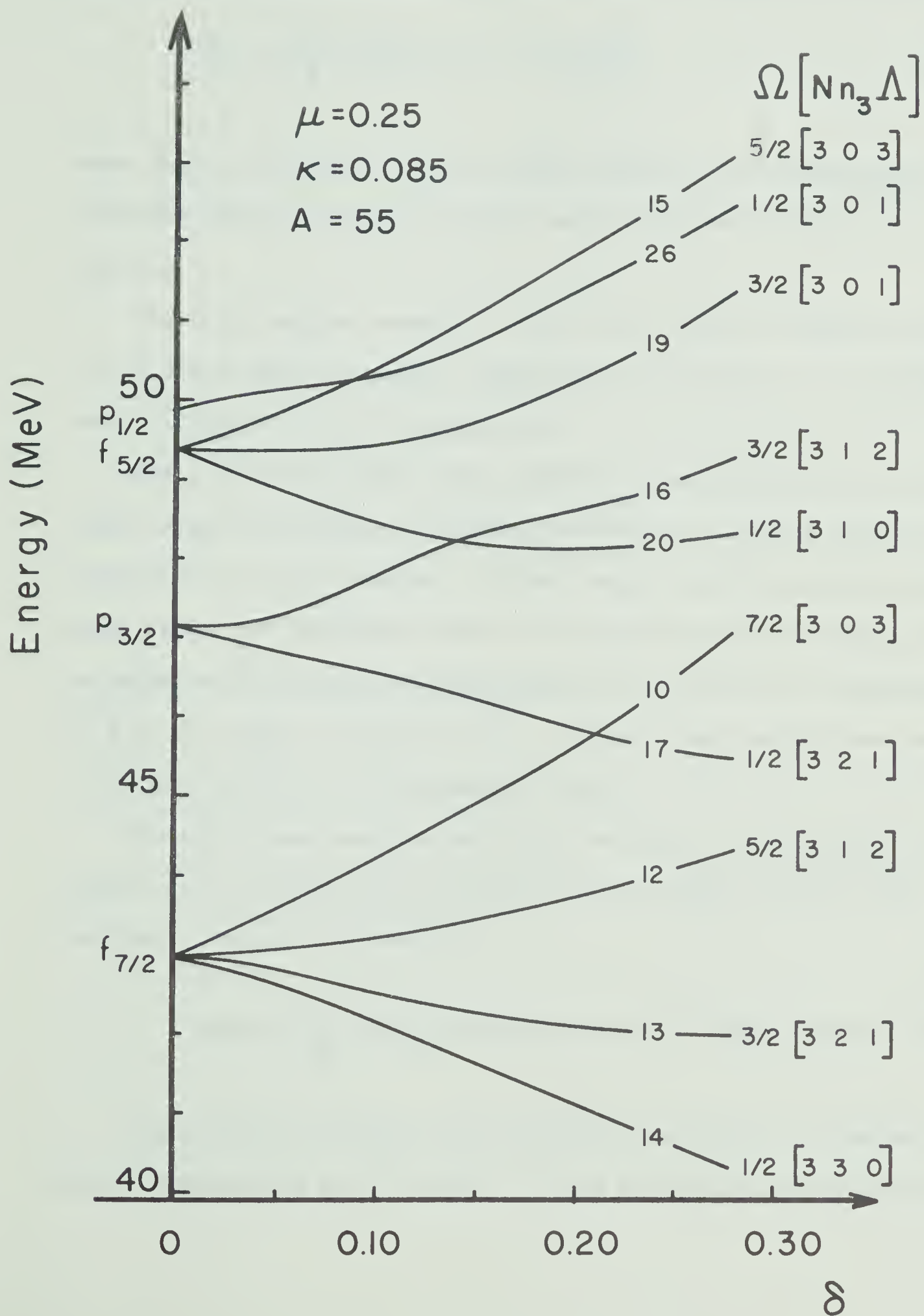
For a given set of parameters  $\mu$  and  $\kappa$ , one can calculate the energy eigenvalues  $E_{\alpha}$  of the Hamiltonian  $\mathcal{H}_p$  as functions of the deformation parameters  $\eta$  or  $\delta$ . An example of such a calculation for  $N = 3$ ,  $\mu = 0.25$  and  $\kappa = 0.085$  is given in fig. 18. It can be seen that the shell model single particle states which are reproduced for zero deformation are split into states of different  $\Omega$  for non-zero deformation. Each of these orbits is degenerate in  $\pm \Omega$ . The particles fill the orbits by pair. The curves representing each state are labelled by the value of  $\Omega$ , the parity and the triad  $[Nn_3\Lambda]$ .

In order to determine the total Hamiltonian of the nuclear system, it is now necessary to evaluate the kinetic energy of the core. As mentioned earlier, vibrations are supposed to have low frequency, consequently, the vibrational term is neglected in the core Hamiltonian. In other words, it is assumed that all the calculations correspond to the vibrational ground state. The core Hamiltonian describes only the

Figure 18 Nilsson model orbits as a function of the deformation parameter  $\delta$ , for  $\mu = 0.25$  and  $\kappa = 0.085$ .

The value of  $\Omega$  is marked on the right side of the figure as well as the Nilsson level asymptotic quantum numbers  $[Nn_3\Lambda]$ . The orbit numbers are those given by Nilsson (Ni 55). The energy scale was obtained with  $\hbar\omega_0^0 = 41(55)^{-\frac{1}{3}}$ .







rotation of the core and the total Hamiltonian can then be written as:

$$\mathcal{H}_T = \mathcal{H}_p + \frac{\hbar^2}{2\mathcal{I}} [I^2 + j^2 - 2(\vec{I} \cdot \vec{j})] \quad (\text{IV.4})$$

where  $\mathcal{H}_p$  is the single-particle Hamiltonian and the following term describes the core rotation and the coupling between rotator and particle.

The total angular momentum  $\vec{I} = \vec{R} + \vec{j}$  with  $\vec{R}$  and  $\vec{j}$  being the core and particle angular momentum, respectively. (see fig. 19).  $\mathcal{I}$  is the moment of inertia of the rotating core.

The  $(\vec{I} \cdot \vec{j})$  term, called either Coriolis or rotation-particle coupling [RPC] term, results from the coupling between the intrinsic motion of the nucleon and the core rotation. In most cases, the RPC term has a very small effect for low-lying states of an axially symmetric system and can be neglected in a first order approximation except when  $K$ , the projection of  $\vec{I}$  on the 3-axis, is equal to  $1/2$ . In this case, the RPC term does contribute directly to the energy of states.

The total wave function describing the state of the nucleus is a product of the rotation wave function and the single particle wave function. It can be written as:

$$|EIMK\rangle = \frac{1}{\sqrt{2}} \sum_j C_{j\Omega} [|IMK\rangle |j\Omega\rangle + (-)^{I-j} |IM-K\rangle |j-\Omega\rangle]. \quad (\text{IV.5})$$

The eigenvalue problem of the rotation Hamiltonian is treated in most textbooks [see e.g. (Pr 62)]. It can be shown that the total energy



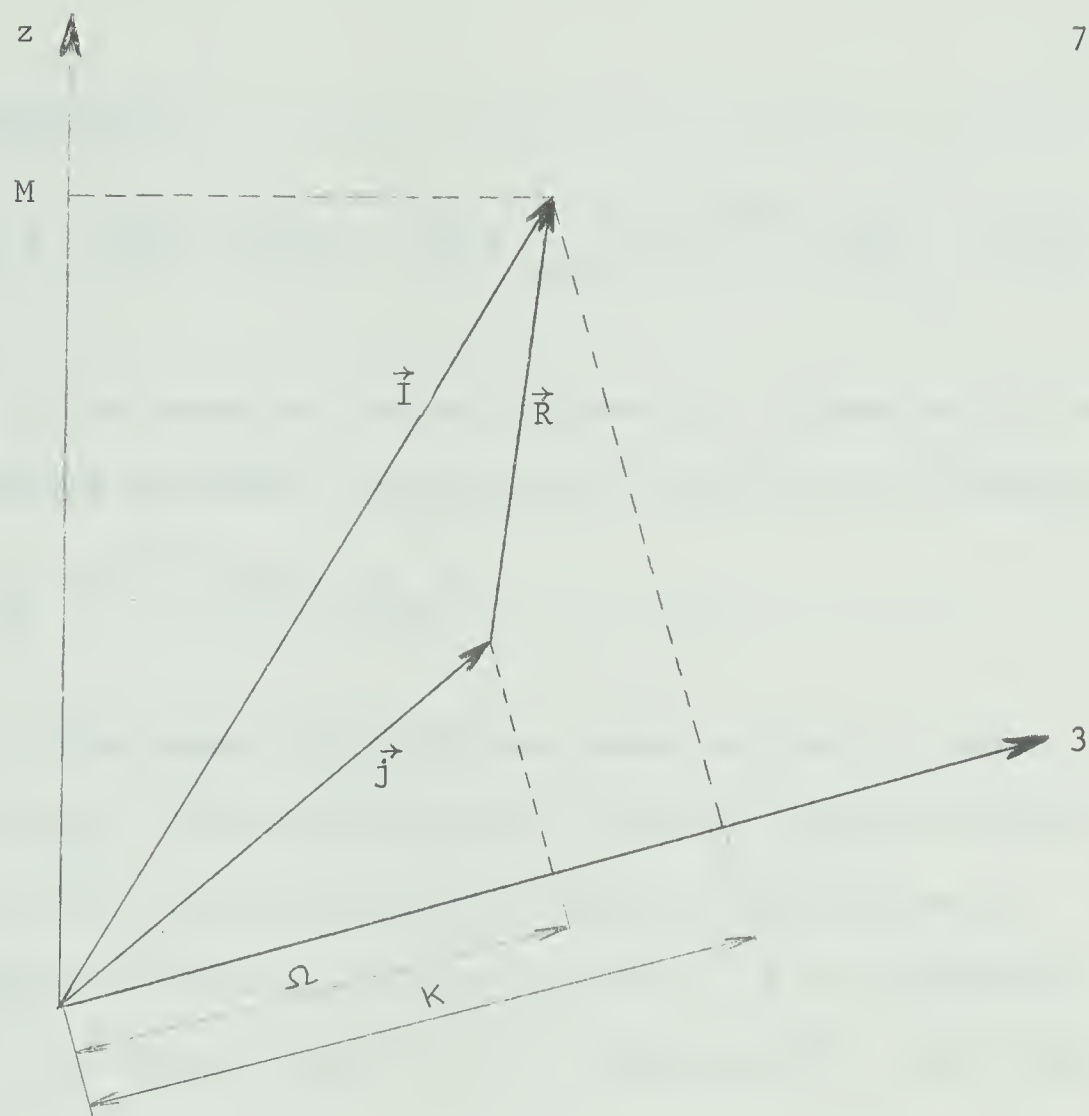


Figure 19 Angular momentum diagram

$\vec{I}$  the total angular momentum is equal to  $\vec{R} + \vec{j}$  where  $\vec{R}$  is the angular momentum generated by the collective motion of the nucleus and  $\vec{j}$  is the angular momentum of the odd-nucleon,  $z$  is the quantization axis, and  $3$  is the body-fixed symmetry axis.

In the ground state,  $\vec{R}$  is perpendicular to  $3$ , ( $\Omega = K$ ), i.e. The collective rotation takes place around an axis perpendicular to the nuclear symmetry axis.



eigenvalue is given by:

$$E_{JK} = E_K + \frac{\hbar^2}{2\mathcal{I}} [I(I+1) - 2K^2 + \delta_{K,\frac{1}{2}} a(-)^{I+\frac{1}{2}} (I + \frac{1}{2})] \quad (\text{IV.6})$$

where  $E_K = E_\Omega^\alpha$  is the energy of the odd nucleon in a Nilsson orbit, and  $a$  is the "decoupling parameter" resulting from the RPC term, defined by:

$$a = -\sum_j (-)^{j+\frac{1}{2}} (j + \frac{1}{2}) |c_{j\Omega}|^2$$

Physically, this means that rotational bands are built on each single-particle state. The core-momentum,  $R$ , has no component on the 3-axis.  $K$  is entirely due to the particle angular momentum and is constant throughout the band. All higher values  $J \geq K$  are permitted, and, when  $K \neq \frac{1}{2}$ , the lowest state has  $I = K$  and successive states have  $I = K+1, K+2, \dots$

The vibration-rotation interaction can be taken into account by adding to equation IV.6 a term which has the form: (Da 65)

$$B[I(I+1) + \delta_{K,\frac{1}{2}} a(-)^{I+\frac{1}{2}} (I + \frac{1}{2})]^2$$

The coefficient  $B$  is usually small and can be treated as an adjustable parameter.

If the particle is rather loosely bound, then the  $K$ -bands overlap strongly and the corrections due to the RPC term become important. The total Hamiltonian then includes non-negligible off-diagonal matrix elements and after diagonalization, the eigenstates are a mixture of





different K-bands. Obviously, K is no longer a good quantum number in this case. Kerman (Ke 56) has considered the problem of two-band mixing. Brockmeier et al. (Br 65) have generalized it to many bands. The band mixed states can then be written as:

$$|I\nu\rangle = \sum_K C_{\nu}(I,K) |K\rangle \quad (\text{IV.7})$$

where  $\nu$  is an additional label for states with same I. .

### 2.1.1. Electromagnetic transitions

Once the total eigenvalue problem has been solved, one can calculate the electromagnetic transition rates and static moments.

The procedure to follow is similar to the procedure described in the Appendix in the case of the intermediate coupling model. Brockmeier et al. (Br 65) have calculated the transition rates formulae in the band mixing case. For the electric quadrupole reduced transition, they obtain:

$$\begin{aligned} B(E_2, I_{\nu} \rightarrow I'_{\nu'}) &= \frac{5}{16\pi} e^2 \left\{ \sum_{\nu\nu'} C_{\nu}(I,K) C_{\nu'}(I',K') Q^{KK'} [(I2K \ K'-K | I'K') \right. \\ &\quad + (-)^{I'+K'} (I2K - K' - K | I' - K') b_{E_2} (\delta_{K,\frac{1}{2}} \delta_{K,\frac{3}{2}} \\ &\quad \left. + \delta_{K,\frac{3}{2}} \delta_{K',\frac{1}{2}}) ] \right\}^2 \end{aligned} \quad (\text{IV.8})$$

The matrix elements  $b_{E_2}$  can be calculated from the single particle wave functions (Br 65).  $Q^{KK'}$ , the matrix element of the quadrupole



operator is composed of two terms, the intrinsic quadrupole moment  $Q_0$  and a single particle term,  $Q_p$ . For nuclei with a large permanent deformation,  $Q_0 \gg Q_p$ , hence  $Q^{KK'} \simeq Q_0$ . The intrinsic quadrupole moment is given as a function of the nuclear deformality,  $\delta$ , by: (Ni 55)

$$Q_0 \simeq 0.8ZR_0^2 \delta(1 + \frac{2}{3}\delta)$$

where  $Z$  is the atomic number and  $R_0$ , the nuclear radius, is taken to be  $1.2 A^{\frac{1}{3}}$  fm.

The relation between the measured quadrupole moment,  $Q_s$ , and  $Q_0$  is given by: (Bo 57)

$$Q_s = \frac{3K^2 - I(I+1)}{(I+1)(2I+3)} Q \quad (\text{IV.9})$$

## 2.2. Application of Nilsson Model to $^{53}\text{Cr}$ and $^{55}\text{Fe}$

These calculations can be divided into two parts. First, some assumptions are made about the possible rotational bands in the nucleus under study. This allows the determination of the rotational parameter,  $A = \hbar^2/2\mathcal{J}$ , and, in the case of  $K = 1/2$  bands, of the decoupling parameter  $a$ . Then, one tests these assumptions by including the Nilsson single particle energy levels and by taking into account, if necessary, the  $K$ -band mixing. From the results thus obtained, the Nilsson-parameters are either readjusted or other bands are considered.

In the program used for these calculations, the different parameters



$\kappa$ ,  $\mu$  and  $\delta$  could be varied freely. For a given range of these parameters a  $\chi^2$  routine determined the value of each parameter yielding the best fit to a given number of experimental levels. Band mixing was also considered. As suggested by Brockmeier et al. (Br 65), the off-diagonal RPC terms were allowed to vary freely in the band mixing calculations.

The fact that in  $^{55}\text{Fe}$ , two sets of levels can apparently be described by rotational bands suggested the possibility of trying Nilsson model calculations. The first band is built on a  $K = 1/2$  ground state. With a decoupling parameter  $a = -1.86$  and a rotational parameter  $A = 159$  keV the ground state ( $3/2^-$ ), the 0.410 MeV ( $1/2^-$ ), the 1.318 MeV ( $7/2^-$ ) and the 2.144 MeV ( $5/2^-$ ) level are well reproduced. On the other hand, the 2.301 MeV ( $9/2^-$ ) and the 3.076 MeV (assumed to be  $11/2^-$ ) could be members of a second band built on  $K = 7/2^-$ . These considerations imply that the odd neutrons should be in the Nilsson orbit  $1/2^-[321]$  in its lowest configuration and that the deformation should be positive. There are other arguments favoring positive deformation: negative deformation would result in many hole-state bands built on the  $1/2[330]$ ,  $3/2[321]$ . . . Nilsson orbits in contradiction with the fact that the first strong hole state has a spin  $J^\pi = 7/2^-$ , impossibility of describing the levels of  $^{55}\text{Fe}$  with a ground state band built on the  $3/2[312]$  Nilsson level, and disagreement with the probable negative sign of the quadrupole moment.

Starting from these considerations, it was then necessary to determine the parameters  $\mu$  and  $\kappa$ . In his paper, Nilsson (Ni 55) fixes the



value of  $\mu$  at 0.35. This corresponds to a  $(f_{5/2} - p_{3/2})$  energy separation which is about half of the  $(p_{1/2} - p_{3/2})$  energy separation. [ $\kappa$  determines the absolute magnitude of these energies.] The order of these shell model levels agrees with experimental results when the odd nucleon is a proton. When the odd nucleon is a neutron, little is known when the f-shell has been filled and, in theoretical calculations, the energy separation of the single particle states is usually taken as a free parameter.

A Nilsson level diagram is shown in figure 17. It corresponds to  $^{55}\text{Fe}$  for  $\mu = 0.25$  and  $\kappa = 0.085$ . Those values are close to those obtained for the best fits of  $^{53}\text{Cr}$  and  $^{55}\text{Fe}$ .

The final sets of parameters used in the calculation of  $^{53}\text{Cr}$  and  $^{55}\text{Fe}$  are given in Table VI. The corresponding level diagrams are shown in figure 20. Band mixing was allowed in the calculations.

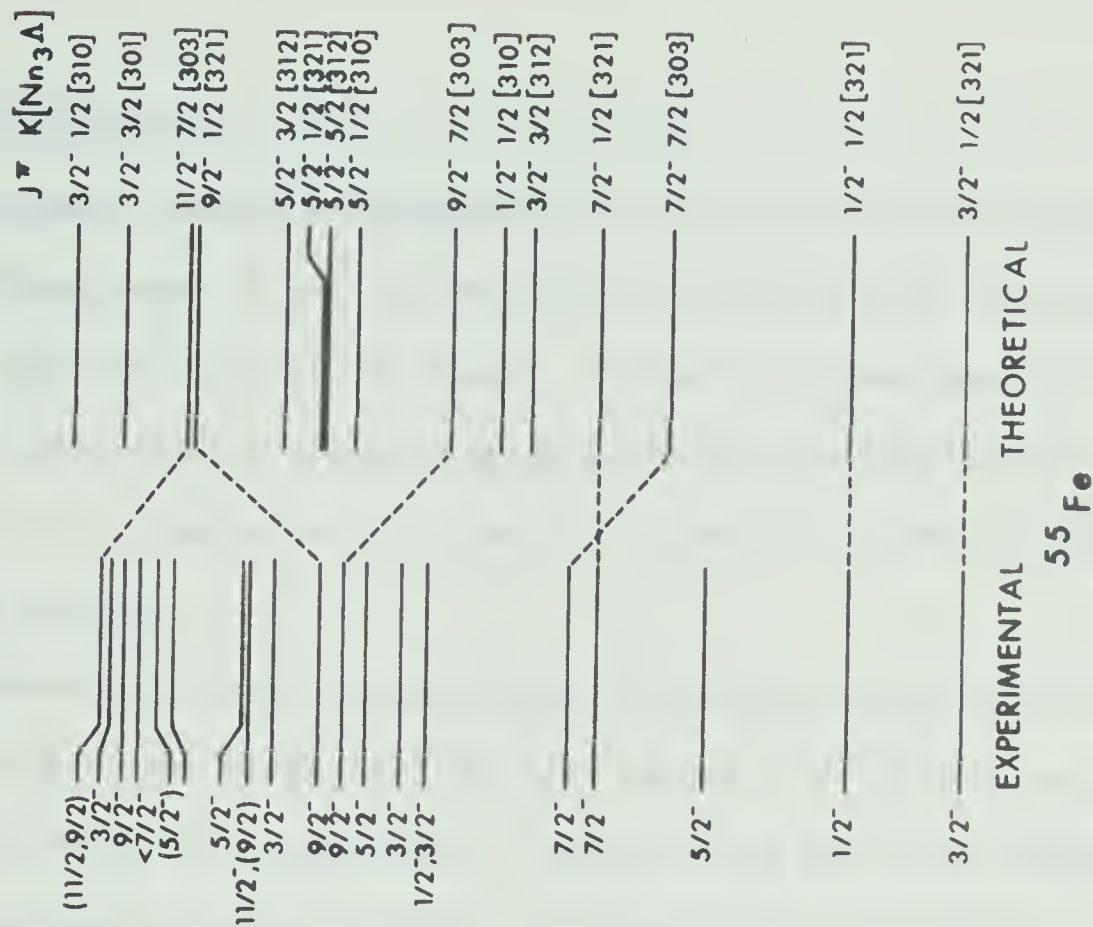
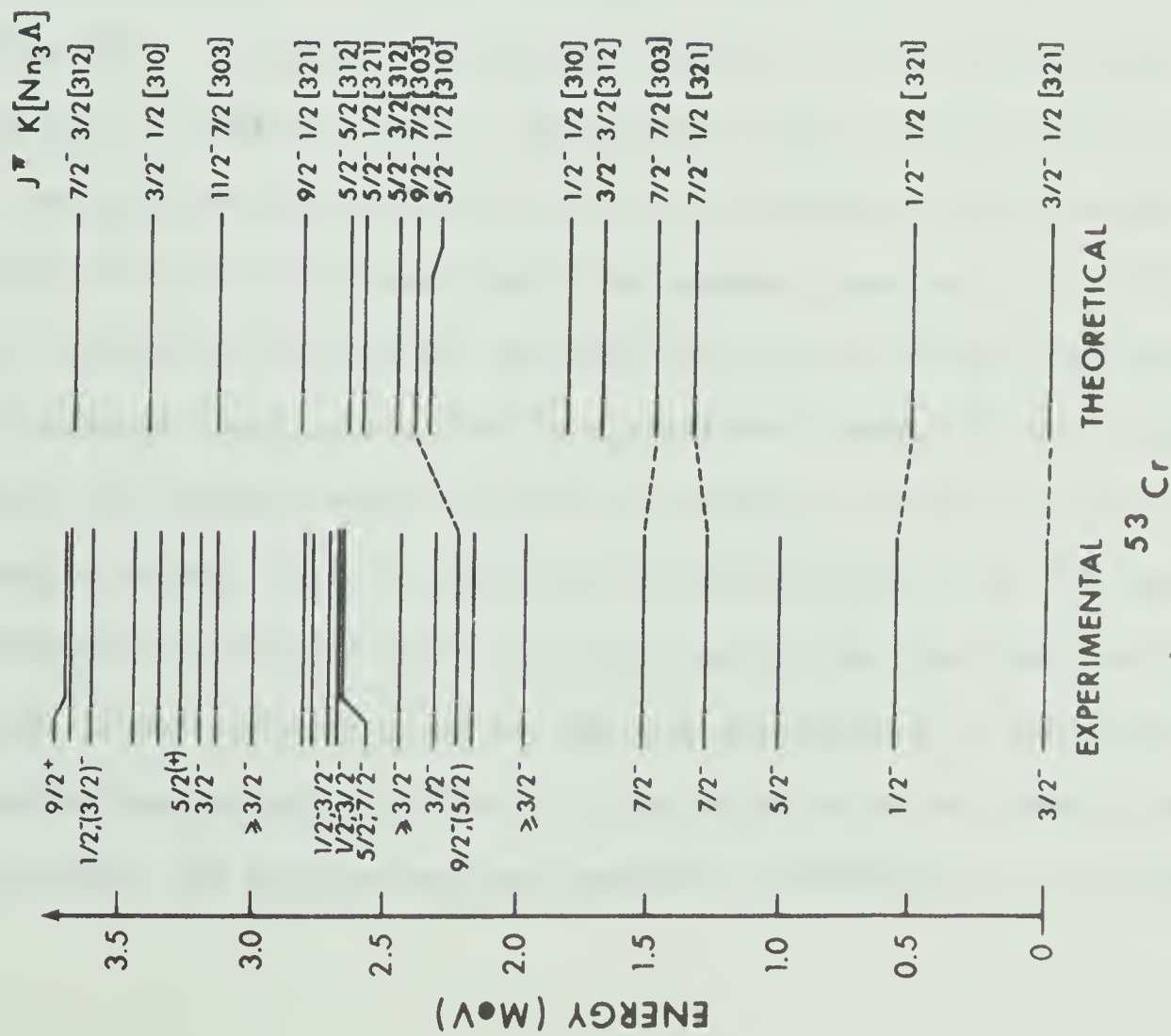
Table VI

Parameters corresponding to the best fits of the energy levels  
in  $^{53}\text{Cr}$  and  $^{55}\text{Fe}$

$^{53}\text{Cr}$	$\mu = 0.251$	$\kappa = 0.085$	$\eta = 1.35$	$\delta = 0.115$
	K = 1/2 band [g.s. band]		A = 166 keV	a = -2.0
	K = 3/2 and K = 5/2 bands		A = 166 keV	
	K = 7/2 band		A = 77 keV	
$^{55}\text{Fe}$	$\mu = 0.244$	$\kappa = 0.080$	$\eta = 1.44$	$\delta = 0.115$
	K = 1/2 band [g.s. band]		A = 159 keV	a = -1.86
	K = 3/2 and K = 5/2 bands		A = 159 keV	
	K = 7/2 band		A = 85 keV	

Figure 20 Nilsson model calculations: Theoretical and experimental spectra are shown for  $^{53}\text{Cr}$  and  $^{55}\text{Fe}$ . The parameters used for these calculations are given in Table VI. All states have negative parity.





# NILSSON MODEL CALCULATIONS



### 2.2.1. Discussion

The agreement between experimental and theoretical level schemes is not good although some slight improvement was obtained when the magnitude of the RPC term was slightly increased. The main problem lies with the  $5/2^-$  levels which cluster around 2.5 MeV for both  $^{53}\text{Cr}$  and  $^{55}\text{Fe}$  nuclei. All attempts to try to reproduce the first  $5/2^-$  state at  $\simeq 1$  MeV resulted in an overall poorer fit.

The reduced transition probabilities for electric quadrupole transitions to ground of the first  $1/2^-$  and  $7/2^-$  states of  $^{53}\text{Cr}$  were calculated to be 152 and 69  $\text{e}^2\text{-fm}^4$  respectively. These values are to be compared with the experimental values of  $(200 \pm 20)$  and  $(95 \pm 25)$   $\text{e}^2\text{-fm}^4$ , respectively, obtained from an average of the results reported in (Me 66) and (Ga 69). The electric quadrupole moment of  $^{53}\text{Cr}$  was calculated to be  $-0.12$  b to be compared with the experimental value of  $|Q| = 0.03$  b (Fu 69).

As explained earlier, (section 1), the apparent failure of describing  $^{53}\text{Cr}$  and  $^{55}\text{Fe}$  by the Nilsson model was somewhat expected. In  $^{52}\text{Cr}$  and  $^{54}\text{Fe}$ , collective features are observed but they are better described by a vibrational model rather than by a rotational model (Go 63). Consequently, the Nilsson model based on the assumption that the core is strongly deformed fails to reproduce the energy spectra of  $^{53}\text{Cr}$  and  $^{55}\text{Fe}$ . Band-mixing corrections which take into account the fact that the odd nucleon is not strongly bound to the core are expected to reproduce cases where the decoupling is partial. If the particle is too loosely bound to the core, the problem must be completely reformulated. The intermediate



coupling approach seemed to be the best alternative. It is described in the following and will yield results much more in agreement with the physical situation.



### 3. THE INTERMEDIATE COUPLING IN THE UNIFIED MODEL

#### 3.1. Introduction

In recent years, considerable attention has been given to the description of odd-A nuclei in which the levels are expected to be described by a model which considers a single nucleon moving in a potential field generated by the even core, (the remaining nucleons), which may be in its ground state or in an excited state.

There are two ways to approach the calculations in the intermediate coupling model. The first approach was outlined by Bohr and Mottelson (Bo 52, Bo 53) and later elaborated by Choudhury (Ch 54) and Ford and Levinson (Fo 55). It assumes that the interaction between core and particle is known and results from the coupling of a single particle, which has available different orbital states, to a core capable of performing quadrupole vibrations. This model is known as the intermediate coupling in the unified model and will simply be labelled as "intermediate coupling model" in the following. The second approach was suggested by Lawson and Uretsky (La 57) and de-Shalit (Sh 61), and has been developed by Thankappan and True (Th 65). It makes no assumption on the nature of the excited states of the even core and introduces a general type of interaction. This approach, now referred to as the "Thankappan and True" (T.T., hereafter) model will be briefly outlined in section 4.





### 3.2. Outline of the Intermediate Coupling Model

In this model, the odd-A nuclear system is described by the coupling of the odd nucleon to the remaining nucleons constituting a core capable of performing quadrupole oscillations. The complete formalism of this model is given in the Appendix. Only the main features will be recalled here.

The total Hamiltonian of the system consists of three terms: the even core Hamiltonian,  $\mathcal{H}_c$ , the single nucleon Hamiltonian,  $\mathcal{H}_p$ , and the interaction Hamiltonian,  $\mathcal{H}_{int}$ . That is:

$$\mathcal{H} = \mathcal{H}_c + \mathcal{H}_p + \mathcal{H}_{int} \quad (\text{IV.10})$$

The interaction Hamiltonian,  $\mathcal{H}_{int}$ , is given by:

$$\mathcal{H}_{int} = -\xi \hbar \omega \sqrt{\frac{\pi}{5}} \sum_{\mu} \{b_{2\mu} + (-)^{\mu} b_{2,-\mu}^*\} Y_{2\mu}(\theta, \phi)$$

in which  $\xi$  is the dimensionless coupling strength,  $b$  and  $b^*$  are boson creation and annihilation operators,  $Y_{2\mu}$  is the spherical harmonic operator and  $\hbar\omega$  is the phonon energy.

The representation chosen is the representation for which  $(\mathcal{H}_c + \mathcal{H}_p)$  is diagonal. The resulting basis vectors are defined by  $|j \text{ NR IM}\rangle$  and, (neglecting the zero order energy point), satisfy:

$$(\mathcal{H}_c + \mathcal{H}_p) |j \text{ NR IM}\rangle = (N\hbar\omega + E_j) |j \text{ NR IM}\rangle$$



where  $\vec{j}$  and  $\vec{R}$  are the angular momenta of the odd nucleon and the vibrating core, respectively;  $I = \vec{R} + \vec{j}$  is the total angular momentum of the nucleus,  $M$ , its  $z$ -component;  $N$  is the number of phonons of surface oscillations;  $E_j$  is the energy of the odd nucleon in a state  $j$ .

The problem is then to express the total Hamiltonian, which after diagonalization will yield eigenvalues and wave functions. Once the wave functions have been obtained, it is possible to calculate transition rates, static moments, etc. (see Appendix).

### 3.3. Application of the Intermediate Coupling Model to the Study of $^{53}\text{Cr}$ and $^{55}\text{Fe}$

In the study of  $^{53}\text{Cr}$  and  $^{55}\text{Fe}$ , the 29<sup>th</sup> neutron was considered to have available the  $2p_{3/2}$ ,  $2p_{1/2}$  and  $1f_{5/2}$  states. The single particle energies, labelled as  $\epsilon_1 = p_{1/2} - p_{3/2}$  and  $\epsilon_2 = f_{5/2} - p_{3/2}$ , were considered as free parameters; the single particle spacings in  $^{49}\text{Ca}$ , ( $p_{1/2} - p_{3/2} = 2.02$  MeV and  $f_{5/2} - p_{3/2} = 3.95$  MeV) were taken as initial values. The remaining free parameters are:  $\hbar\omega$ , which was taken as the energy of the first  $2^+$  state in the even core and later varied within reasonable range, and finally the coupling strength  $\xi$ .

It was found that an accurate determination of the different parameters is not necessary to give a good description of the first excited states of  $^{53}\text{Cr}$  and  $^{55}\text{Fe}$ . In Table VII are listed different sets of parameters which resulted in almost identical energy spectra. Figure 21 shows how the energy



Table VII

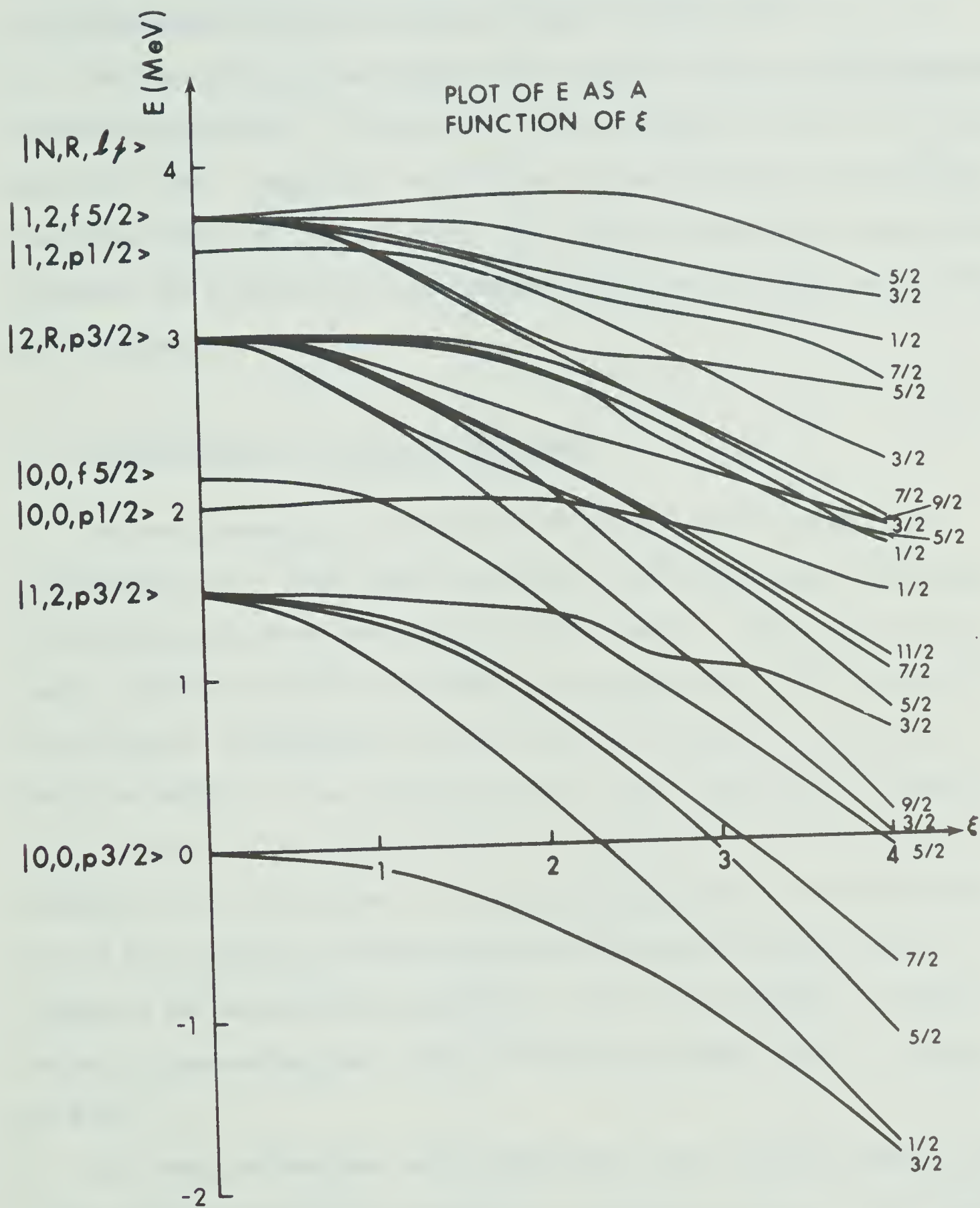
Sets of parameters used in the  
intermediate coupling model calculations

Nucleus	Set	$\epsilon_1 = p_{1/2} - p_{3/2}$ MeV	$\epsilon_2 = f_{5/2} - p_{3/2}$ MeV	$\hbar\omega$ MeV	$E(2^+_1)_{\text{exp}}^*$ MeV	$\xi$
$^{53}\text{Cr}$	A	2.0	2.2	1.5	1.43	2.5
	B	1.8	2.0	1.6	—	2.25
$^{55}\text{Fe}$	C	2.0	2.2	1.45	1.40	2.75
	D	—	—	—	—	3.00
	E	2.2	2.0	1.40	—	2.75

\* This value is the excitation energy of the first  $2^+$  level in the neighbouring even nucleus.

Figure 21 The intermediate coupling model: Energy levels of the total Hamiltonian as a function of the coupling parameter  $\xi$ .

PLOT OF E AS A  
FUNCTION OF  $\xi$







levels of the total Hamiltonian vary when the coupling parameter  $\xi$  increases. (The remaining parameters are those of set C in Table VII.)

The best fits were determined after comparison with all the experimental information available. In Table VII, they correspond to set B for  $^{53}\text{Cr}$  and to set E for  $^{55}\text{Fe}$ . Tables VIII and IX give the resulting wave functions for low-lying states of  $^{53}\text{Cr}$  and  $^{55}\text{Fe}$ . The complete theoretical results will be presented and compared with experimental data as well as with other theoretical calculations in section 6.

### 3.4. Justification of the Use of this Model

The main assumption of this model is based on the existence of a vibrational core. There seems to be great controversy in the literature on the structure of the even nuclei in the f-shell. From a strict shell model view point, most of the levels of a nucleus such as  $^{52}\text{Cr}$  result from the different configurations obtained from the coupling of 4  $f_{7/2}$  protons. With the addition of the seniority quantum number, most of the levels are in fact reproduced, but levels such as the 2.65 MeV ( $0^+$ ) in  $^{52}\text{Cr}$  cannot be explained from this picture. A second problem arises in the calculation of the electromagnetic transitions as the shell model usually fails to reproduce the enhanced E2 transitions. This problem however, is easily solved by introducing the concept of "effective charge" (see e.g. (Fe 69, Ri 69)).

The simple vibrational model introduced by Bohr (Bo 52) predicts levels which are equidistant and degenerate for each phonon group. Recent calcula-



Expansion coefficients corresponding to states  $|E(\text{keV}); J\pi\rangle$  of  $^{53}\text{Cr}$   
calculated from the intermediate coupling model (Set B of Table VIII)

Basic States $ NR; j\rangle$	$ 0; 3/2^- \rangle$	$ 536; 1/2^- \rangle$	$ 1174; 5/2^- \rangle$	$ 1358; 7/2^- \rangle$	$ 1850; 5/2^- \rangle$	$ 2011; 3/2^- \rangle$
00; 3/2	0.8582					0.4077
12; 3/2	-0.3884	0.6325	0.5743	0.8393	0.6273	0.7549
20; 3/2	0.1115					-0.3036
22; 3/2	0.0521	-0.2453	0.0593	-0.1403	0.4715	-0.076
24; 3/2			-0.3926	-0.3730	0.1046	
30; 3/2	-0.0172					0.0277
32; 3/2	-0.0324	0.0804	0.0627	0.0993	0.0499	0.1405
33; 3/2	-0.0005		-0.0157	-0.0246	0.0867	0.0839
34; 3/2			0.0946		-0.1104	
36; 3/2						
00; 1/2		0.6073				
12; 1/2	-0.2374		-0.3721		0.4030	-0.1009
20; 1/2						
22; 1/2	0.0940	0.1855	0.1575		0.0366	-0.3037
24; 1/2				-0.2875		
30; 1/2		-0.0521				
32; 1/2	-0.0307		-0.0740		0.0742	0.0516
33; 1/2			0.0434	-0.0273	0.1035	
34; 1/2				0.0420		
36; 1/2				0.0833		
00; 5/2			-0.4932	-0.0223	0.2571	
12; 5/2	0.1308	0.3284	0.2205		-0.1807	-0.0407
20; 5/2			-0.1290		0.0512	
22; 5/2	-0.0073	0.1248	-0.1135	0.0780	0.0743	-0.1046
24; 5/2	-0.1074		-0.0442	0.1081	0.2430	0.0716
30; 5/2			0.0245		-0.0327	
32; 5/2	0.0142	0.0609	0.0368	-0.0057	-0.0271	-0.0548
33; 5/2	0.0047	0.0143	0.0013	-0.0036	0.0544	-0.0761
34; 5/2	0.0324		0.0590	-0.0277	0.0164	-0.0760
36; 5/2				-0.1225		



Expansion coefficients corresponding to states  $|E(\text{keV}); J\pi\rangle$  of  $^{55}\text{Fe}$  calculated from the intermediate coupling model (Set E of Table VII)

Basic States $ NR; j\rangle$	$ 0; 3/2^-\rangle$	$ 474; 1/2^-\rangle$	$ 1013; 5/2^-\rangle$	$ 1144; 7/2^-\rangle$
00; 3/2	0.8193			
12; 3/2	-0.4336	0.6639	0.5883	0.8101
20; 3/2	0.1450			
22; 3/2	0.0630	-0.3029	0.0775	-0.1583
24; 3/2			-0.4422	-0.4072
30; 3/2	-0.0241			
32; 3/2	-0.0480	0.1096	0.0819	0.1193
33; 3/2	-0.0005		-0.0211	-0.0257
34; 3/2			0.1172	0.0483
36; 3/2				
00; 1/2		0.5156		
12; 1/2	-0.2417		-0.3444	
20; 1/2		0.2109		
22; 1/2	0.1135		0.1678	
24; 1/2				-0.2880
30; 1/2	-0.0414	-0.0679		
32; 1/2			-0.0862	
33; 1/2			0.0539	-0.0307
34; 1/2				0.0961
36; 1/2				
00; 5/2			-0.4261	
12; 5/2	0.1430	0.3343	0.2147	-0.0222
20; 5/2	-0.0063		-0.1447	
22; 5/2		-0.1485	-0.1252	0.0844
24; 5/2	-0.1302		-0.0422	0.1178
30; 5/2			0.0290	
32; 5/2	0.0205	0.0799	0.0450	-0.0062
33; 5/2	0.0066	0.0205	0.0012	-0.0064
34; 5/2	0.0455		0.0734	-0.0309
36; 5/2				-0.1411



tions where anharmonic terms are introduced remove the degeneracy (Al 69, Sh 62). Some calculations for  $^{52}\text{Cr}$  have been reported (Wi 62) and the agreement is good to the  $N = 2$  phonon states. However, the 2.37 MeV ( $4^+$ ) which has seniority  $v = 4$  is not predicted in these calculations. In  $^{54}\text{Fe}$ , the recent  $0^+$  assignment to the 2.56 MeV level gives a good support to the vibrational description (Kr 69).

Another advantage of the description in terms of vibrational model is the normal explanation of E2 enhancement through collective effects.

Without trying to enter the controversy, it can be said that the intermediate coupling model based on the coupling of a nucleon to a vibrating core should be quite applicable to the description of  $^{53}\text{Cr}$  and  $^{55}\text{Fe}$ . For more than  $N = 2$  phonon states, the resulting multiplets are probably quite spread and there is not much experimental support to the existence of most of  $N = 3$  phonon states. However, as can be seen from Tables VIII and IX,  $N = 3$  phonon state components in the resulting wave functions of calculated levels of  $^{53}\text{Cr}$  and  $^{55}\text{Fe}$  are negligible for levels with excitation below  $\simeq 3$  MeV.

#### 3.4.1. Additional remarks

In the study of inelastic scattering in the framework of the collective model, the reduced transition probability for electric quadrupole radiation,  $B(E2)$ , can be expressed as: (Sa 66, Ba 62)

$$B(E2) = \frac{3}{4\pi} ZR^2 \frac{\beta_2^2}{5} e^2 \quad (\text{IV.11})$$





where  $Z$  is the atomic number,  $R$  is the nuclear radius equal to  $1.2 A^{-\frac{1}{3}}$  fm and  $\beta_2$  is the deformation parameter introduced by Bohr (Bo 52).

In terms of the collective constants previously defined,  $\beta_2$  is given by: (equation 71 in (Bo 52))

$$\beta_2 = \sqrt{5} \sqrt{\frac{\hbar\omega}{C_2}} \quad (\text{IV.12})$$

It is interesting to compare the calculated values of  $\beta_2$  using equation (IV.12) and the parameters determined in this work, (Table VII) with the experimental values obtained from inelastic scattering experiments (Ri 69). For  $^{52}\text{Cr}$  the calculated value  $\beta_2$  is equal to  $\simeq 0.16$ , the experimental  $\beta_2$  ranges between 0.156 and 0.20. For  $^{54}\text{Fe}$  the calculated  $\beta_2$  is  $\simeq 0.17$ , compared with the experimental value of  $\simeq 0.14$ . The agreement is quite good and suggests that the parameters determined in these calculations fall in the correct range.



#### 4. THE THANKAPPAN AND TRUE MODEL

As indicated earlier, this model also considers the coupling of the odd nucleon to the neighbouring even core, but the approach is more general as no specific assumption is made on the nature of the interaction. de Shalit (Sh 61) assumed that under its most general form, the coupling between the particle and the core can be written as a sum of scalar product of tensors of rank  $k$ . That is:

$$\mathcal{H}_{int} = \sum_k T_c^{(k)} \cdot T_p^{(k)} \quad (IV.13)$$

where  $T_c^{(k)}$  operates only on the degrees of freedom of the core and  $T_p^{(k)}$  on the degrees of freedom of the particle.

On this basis, Thankappan and True write the interaction Hamiltonian as:

$$\mathcal{H}_{int} = -\xi (\vec{J}_c \cdot \vec{J}_p) - \eta (Q_c \cdot Q_p) \quad (IV.14)$$

where  $\vec{J}_c$  and  $\vec{J}_p$  are, respectively, the total angular momentum of operators for the core and particle and  $Q_c$  and  $Q_p$  are, respectively, the mass quadrupole moment operators of the core and particle.  $\xi$  and  $\eta$  are parameters describing the strength of the interaction.

The resulting matrix elements of the total Hamiltonian are functions of  $\xi$ ,  $\eta$  and two reduced matrix elements of the operators  $Q$ , namely:



$\langle J'_c || Q_c || J_c \rangle$  and  $\langle j'_p || Q_p || j_p \rangle$ . The particle reduced matrix element for  $Q_p$  is evaluated using harmonic oscillator wave functions for the radial integral part. The reduced matrix elements  $\langle J'_c || Q_c || J_c \rangle$  are considered as free parameters, as the exact nature of the core states is not supposed to be known. It must be emphasized, however, that because of the form of the operators used in the calculations, this approach is unlikely to be valid unless the core states are collective in nature (Tr 65).

In order to avoid dealing with an excessive number of free parameters, it is necessary to limit the number of core levels taken into consideration. In the calculations which will be reported in this work (section 6), only the core ground state and first excited state are taken into account. As for the intermediate particle model calculations, the particle has available three single particle states:  $1p_{3/2}$ ,  $1p_{1/2}$  and  $2f_{5/2}$ . This results in calculations with five free parameters, at least, as more free parameters (e.g. effective charge) are introduced in the calculations of transition rates.



## 5. SHELL MODEL CALCULATIONS FOR N = 29 ODD NUCLEI

In the shell model calculations reported in this work, the  $^{48}\text{Ca}$  is considered as an inert core. The Hamiltonian for the  $(\pi 1f_{7/2})^m(\nu 2p_{3/2})$  configuration outside the  $^{48}\text{Ca}$  core can be written as:

$$\mathcal{H} = \mathcal{H}_c + \sum_{\pi} \mathcal{H}_{\pi-c} + \mathcal{H}_{\nu-c} + \sum_{\text{pairs}} \mathcal{H}_{\pi-\pi} + \sum_{\text{pairs}} \mathcal{H}_{\pi-\nu} \quad (\text{IV.15})$$

where the indices  $c$ ,  $\pi$  and  $\nu$  stand, respectively, for core, proton and neutrons;  $m$  is the number of protons in the  $1f_{7/2}$  shell for the nucleus under consideration; the neutron is represented in its ground state configuration  $2p_{3/2}$ , but higher configurations are also taken into account.  $\mathcal{H}_c$  is the total interaction between the nucleons inside the core. The second and third term of equation (IV.15) represent the interactions of the extra-core protons and neutrons; the fourth and fifth terms, the residual interactions between the extra core protons and neutron-proton pairs.

The first three terms contribute to a constant energy to all the states of the  $(\pi 1f_{7/2})^m(\nu 2p_{3/2})$  configuration. The energy matrix can then be written as:

$$E(J) = \text{const.} + E_{\pi} (J_{\pi} \nu_{\pi}) \delta_{J_{\pi} J'_{\pi}} \delta_{\nu_{\pi} \nu'_{\pi}} + m E_{\pi\nu} (J_{\pi} \nu_{\pi}, J'_{\pi} \nu'_{\pi}, j_{\nu}; J)$$





This expression gives the energy of a level of total angular momentum  $J$ .  $J_\pi$  is the total angular momentum of the  $m$  protons;  $v_\pi$  is the seniority of the proton group.  $j_\nu$  is the total angular momentum of the 29<sup>th</sup> neutron.  $E_\pi$  is the contribution of the proton group and  $E_{\pi\nu}$  is the contribution of a single neutron proton pair to the matrix elements.

In order to evaluate  $E_\pi$ , it is necessary to know the effective proton-proton interaction. The two-body matrix elements of this interaction can either be evaluated from the experimental spectra of the neighbouring  $N = 28$  nuclei or calculated theoretically [see e.g. (Ku 68)].

The neutron-proton energy term is calculated by assuming some type of neutron-proton interaction. Ohnuma (Oh 66) introduces a neutron-proton interaction of the form:

$$V_{\nu\pi} = V_0 f(\vec{r}_{\nu\pi}) \{ (1-\alpha) + \alpha \vec{\sigma}_\nu \cdot \vec{\sigma}_\pi \}$$

where  $\alpha$  is an adjustable parameter and the radial function  $f(r_{\nu\pi})$  is gaussian. Vervier (Ve 66) uses the same type of interaction but his radial function is a  $\delta$ -function.

These calculations do not take into account proton configurations other than  $(\pi 1f_{7/2})^m$ , that is, configurations arising from core excitations. As a result states in  $N = 29$  nuclei, which are predominantly  $f_{7/2}$  hole states will not be reproduced.



## 6. COMPARISON BETWEEN THEORETICAL CALCULATIONS AND EXPERIMENTAL DATA

In the following, the results of the calculations based on the intermediate coupling model described in section 3 and in the Appendix are compared with the experimental results obtained in this work or elsewhere. Other calculations will also be presented for comparison purposes. They are, respectively:

i) the calculations of Ramavataram (Ra 63) also based on the intermediate coupling model, but dealing with different parameters and limited to levels with spin  $J \leq 7/2$ ;

ii) the shell model calculations of Vervier (Ve 66) and Ohnuma (Oh 66, Oh 70) described in section 5. Vervier limited his calculations to levels with spin  $J \leq 7/2$ ; in Ohnuma's calculations,  $J$  is limited to a maximum value of  $13/2$ ;

iii) the calculations of Philpott and True (Ph 70), for  $^{53}\text{Cr}$ , and of Larner (La 70), for  $^{55}\text{Fe}$ , based on the True and Thankappan (TT) model described in section 4.

In all these calculations, levels which have a predominantly hole state configuration are not predicted. In the following, calculated energy levels, branching ratios, mixing ratios, electromagnetic properties and spectroscopic factors are compared with experimental data.



## 6.1. Energy Spectra

### 6.1.1. $^{53}\text{Cr}$ spectrum

The experimental spectrum of  $^{53}\text{Cr}$  is compared with intermediate coupling and shell model calculations in fig. 22 and with the predictions of the T.T. model in fig. 24.

Agreement is very good for all the levels below 2.0 MeV except for the 1.537 MeV level which, because of its predominant hole-state configuration, is not predicted in these calculations. One common feature is the prediction of a level with spin  $J = 5/2^-$  at about 1.9 MeV. This would indicate that the 1.971 MeV level might be the corresponding level with  $J = 5/2$ . In their calculations using the T.T. model, Philpott and True have tried different fits based on the spin value of the 1.971 MeV level. They concluded that the overall results favored a  $J = 5/2$  assignment for this level. Their results presented here are those which were fitted for  $J = 5/2$ .

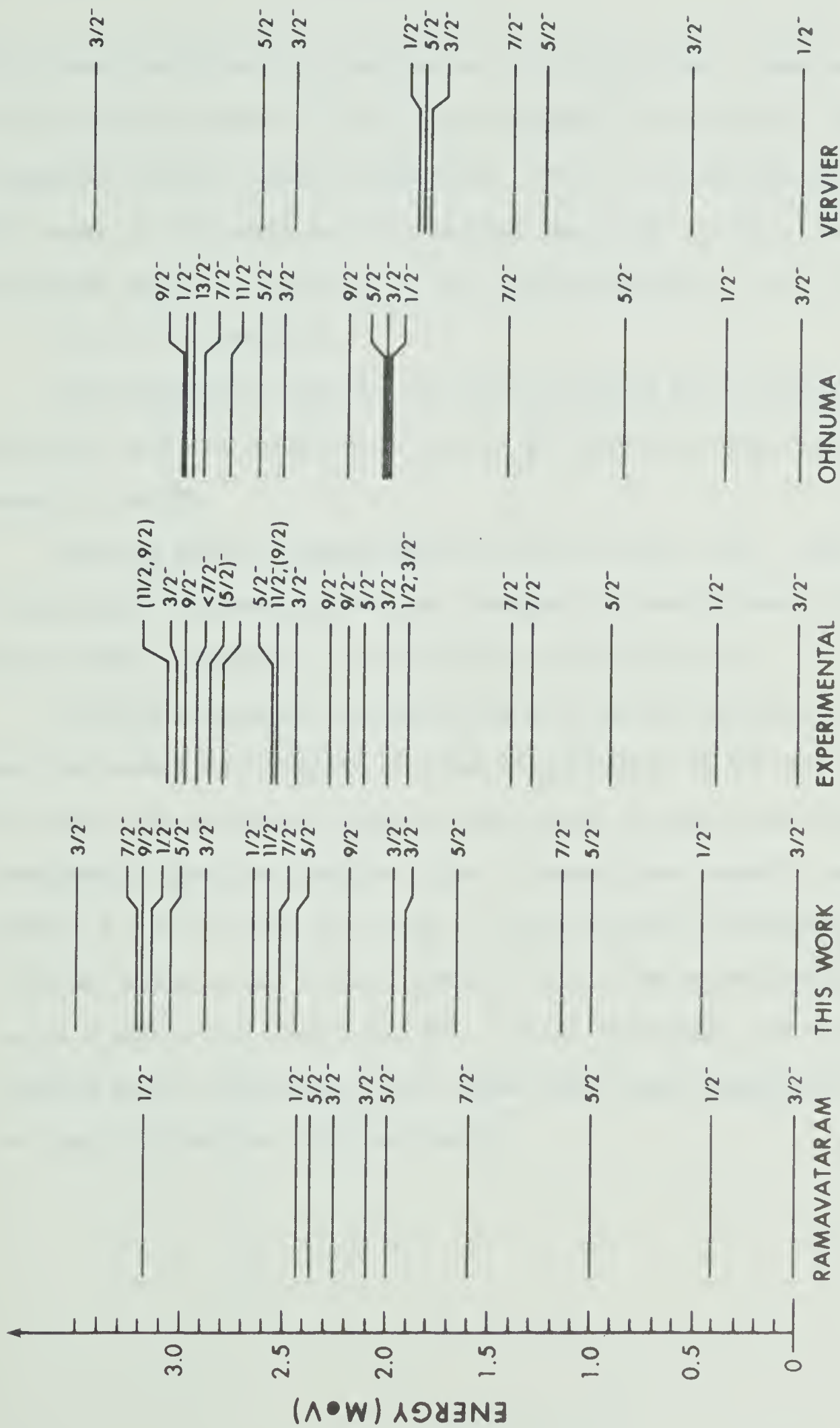
Above 2 MeV, Ohnuma's calculations and the new intermediate coupling model calculations apparently yield a better density of states than the other calculations. There are indications that the 2.169 MeV state has a spin  $J = 11/2$  (Gu 70). This level could be the level at  $\simeq 2.38$  MeV predicted by Ohnuma's shell model calculations and the level at  $\simeq 2.9$  MeV in this work. By comparing with the results of  $^{55}\text{Fe}$  (see next section), the 2.227 MeV level (which has been assigned  $J = 9/2$  or  $5/2$  in this experiment), could have the same configuration as the 2.211 MeV ( $9/2^-$ ) level of  $^{55}\text{Fe}$ , as it lies at about the same excitation energy and decays 100% to the  $7/2^-$  hole state. Therefore,

Figure 22 Energy levels and spins in  $^{53}\text{Cr}$  as predicted by intermediate coupling model and shell model calculations are compared with experimental results.



Figure 23 Energy levels and spins of  $^{55}\text{Fe}$  as predicted by intermediate coupling model and shell model calculations are compared with experimental results.





INTERMEDIATE COUPLING MODEL

SHELL MODEL

55 Fe



this level should not be predicted by the calculations. There is a  $9/2^-$  state predicted around 2.3 MeV in the different calculations. Again, by comparing with the results obtained for  $^{55}\text{Fe}$ , it can be seen that the 2.454 MeV level of  $^{53}\text{Cr}$  might be the predicted level with  $J = 9/2$ . The study of branching ratios in section 6.2. will give some weight to this assumption.

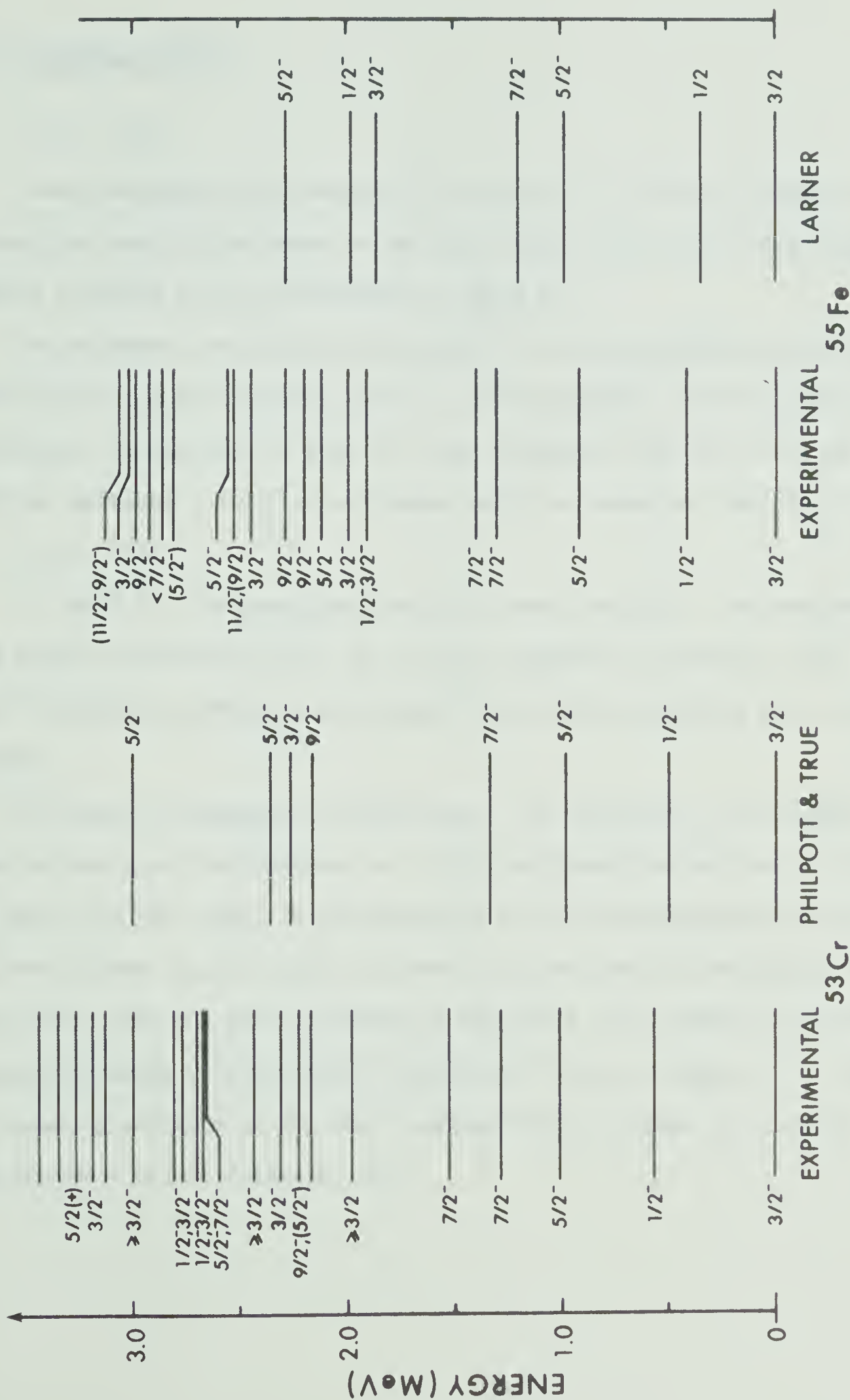
#### 6.1.2. $^{55}\text{Fe}$ spectrum

The experimental spectrum of  $^{55}\text{Fe}$  is compared with intermediate coupling and shell model calculations in fig. 23 and with the predictions of the T.T. model in fig. 24.

The same general remarks apply as in the case of  $^{53}\text{Cr}$ . Both shell model calculations of Ohnuma and the new intermediate coupling model calculations favor a spin assignment  $J = 11/2$  for the 2.542 MeV state.

In terms of density of states, the shell model calculations of Ohnuma and the present intermediate coupling calculations are the most successful. The former calculations, however, seem to give a better overall fit to the experimental spectrum than the latter. Ohnuma's and Larner's calculations predict a  $J = 1/2$  level at  $\simeq 2$  MeV. This level might correspond to the 1.919 MeV state as the neutron capture study of Earle and Bartholomew (Ea 66) favors a spin  $3/2$  for the 2.052 MeV. On the other hand, the intermediate coupling model calculations would rather favor spin assignments  $J = 3/2$  for the 1.919 MeV and 2.052 MeV levels.

Figure 24 The T.T. model: Calculations of energy levels in  $^{53}\text{Cr}$  (Ph 70) and  $^{55}\text{Fe}$  (La 70) are compared with experimental results obtained in this work.



THANKAPPAN AND TRUE MODEL



## 6.2. Branching Ratios

### 6.2.1. $^{53}\text{Cr}$

Some branching ratios measured in this work on  $^{53}\text{Cr}$  are compared with theoretical predictions based on the shell model (Oh 70) and on the intermediate coupling model calculations in Table X.

The agreement is generally good and it can be seen that the calculated branching ratios are consistent with a spin assignment  $J = 5/2$  to the 1.971 MeV state. It can also be seen that the assumption that the 2.454 MeV level might be assigned  $J = 9/2$  is consistent with the measured branching ratio.

### 6.2.2. $^{55}\text{Fe}$

In Table XI, the branching ratios for some levels of  $^{55}\text{Fe}$  measured in this work or reported by Pilt (Pi 69) are compared with Ohnuma's shell model calculations and with the present intermediate coupling model calculations.

The overall agreement is qualitative. In particular, the present calculations would rather favor a  $J = 1/2$  assignment rather than  $J = 3/2$  for the 2.052 MeV level, in contradiction with the measurements of Earle and Bartholomew (Ea 66). This contradiction may just be fortuitous, as it was noticed that the wave functions of the two  $J = 3/2$  levels at  $\simeq 2.0$  MeV excitation energy were extremely sensitive to slight changes of  $\xi$ . This is caused by exchange of the main configurations of these two  $J = 3/2$  levels when  $\xi \simeq 2.75$  (see fig. 21).







Table X

Calculated and measured branching ratios for some levels of  $^{53}\text{Cr}$   
 Calculations are based on the intermediate coupling model (this work)  
 and the shell model (Oh 70).

Initial State	Final State	Experiment (this work)	Theory	
			(this work)	Shell Model (Oh 70)
1.006 $5/2^-$	0	100	100	100
1.285 $7/2^-$	0	$91 \pm 6$	55	40
	1.006	$9 \pm 4$	45	60
1.971 ( $5/2^-$ )	0	85	87	63
	1.006		6	14
	1.285	15	7	23
2.324 $3/2^-$	0	100	50	
	0.564		25	
	1.006		23	
2.454	0			$15^+$
	0.564		$6^+$	$<1$
	1.006	60	26 $87^{++}$	64
	1.285	40	68 13	21
3.625 $1/2^-$	0	100	94	
	0.564		3	
	1.006		3	

$^+$  Assuming  $J = 5/2$  for the 2.454 MeV level

$^{++}$  Assuming  $J = 9/2$  for the same level



Table XI

Experimental and theoretical branching ratios for levels of  $^{55}\text{Fe}$  up to 2.578 MeV. The theoretical calculations are based on the intermediate coupling model (this work) and on the shell model (Oh 70)

Initial State	Residual State	Experiment (See Chapter III)	Theory	
			This work	Shell Model (Oh 70)
0.930 $5/2^-$	0.	$98 \pm 1$	~100	83
	0.410	$2 \pm 1$		17
1.318 $7/2^-$	0.	$96 \pm 1$	65	33
	0.930	$4 \pm 1$	35	67
1.919 $(1/2, 3/2)$	0.	$68 \pm 3$	$57^\dagger$	$59^{\dagger\dagger}$
	0.410	$32 \pm 3$	43	22
	0.930	-	19	60
2.052 $(1/2, 3/2)$	0.	$23 \pm 2$	$56^*$	$1^{**}$
	0.410	$77 \pm 2$	44	72
	0.930	-	-	27
2.144 $5/2^-$	0.	$18 \pm 2$	41	22
	0.410	$3 \pm 1$	4	-
	0.930	$43 \pm 4$	53	24
	1.318	$36 \pm 5$	2	54
2.301 $9/2^-$	0.930	80	86	~100
	1.318	20	14	
2.470 $3/2^-$	0.	100		
2.542 $(11/2^-)$	2.301	-	29	
	1.318	100	71	
2.578 $5/2^-$	0.	$84 \pm 2$	1	
	0.410	$7 \pm 2$	5	
	0.930	$6 \pm 2$	28	
	1.318	$3 \pm 2$	66	

$^\dagger$  assuming  $1/2^-$  for 1.919 MeV level

$^{\dagger\dagger}$  assuming  $3/2^-$  for 1.919 MeV level

$*$  assuming  $1/2^-$  for 2.052 MeV level

$**$  assuming  $3/2^-$  for 2.052 MeV level



### 6.3. Electromagnetic Properties

#### 6.3.1. Reduced transition probabilities

The calculated reduced transition probabilities and lifetimes are shown in Table XII and XIII for  $^{53}\text{Cr}$  and  $^{55}\text{Fe}$ , respectively. The  $B(E2)$ 's were calculated for neutron charge  $e_n = 0$  and  $e_n = 1$ . It can be seen that the  $B(E2)$ 's are not too sensitive to the effective charge parameter. This is to be expected as most of the contribution to the electric quadrupole transition comes from the core.

In Table XIV, the  $B(E2)$ 's for transition to ground of the lowest states of  $^{53}\text{Cr}$ , are compared with the experimental data of Meriwether (Me 66) and Galparin (Ga 69). From the weak coupling model, one would expect the  $B(E2)$  transitions in the odd-nucleus to be equal to the  $B(E2; 2^+ \rightarrow 0)$  for the decay to ground of the first  $2^+$  state of the neighbouring even nucleus. In the case of  $^{52}\text{Cr}$ , the  $B(E2; 2^+ \rightarrow 0)$  is in the order of 50 to 140  $\text{e}^2\text{-fm}^4$ , i.e. 6 to 16 w.u. (Ri 69, Me 66); in  $^{54}\text{Fe}$ , the measured  $B(E2; 2 \rightarrow 0)$  is of the order of  $\approx 100 \text{ e}^2\text{-fm}^4$ , i.e.  $\approx 11$  w.u. (Fu 64, Si 65). In the simple picture of the intermediate  $|2^+, p_{3/2}\rangle$  coupling, the ratio of  $B(E2)$  for decay to ground of levels of the  $|2^+, p_{3/2}\rangle$  quadruplet, to the  $B(E2; 2^+ \rightarrow 0)$  in the even nucleus is expected to increase from unity for those states with spin 1/2, 5/2 and 7/2 and to decrease from unity for the 3/2 state as the coupling increases. Results in Table XIV show that this simple picture does not hold for  $^{53}\text{Cr}$ . The main reason is probably because of the mixing of states in terms of single particle configurations and of



Table XII

Electromagnetic transition strengths and lifetimes in  $^{53}\text{Cr}$  calculated from the intermediate coupling model. The lifetimes, calculated for  $e_n = 0$ , are compared with experimental results when available.<sup>†</sup>

Initial State		Residual State		B(E2) $e_n = 0$	$(e^2\text{-fm}^4)$ $e_n = e$	B(M1) $(e\hbar/2Mc)^2$	Lifetime $\tau$ calc.      experiment	
0.564	1/2	0.	3/2	101	179	1.97	0.16 ps	$\geq 0.50 \text{ ps}^{\text{a)}$
1.006	5/2	0.	3/2	54.1	74.8	0.009	4.3 ps	$\geq 1 \text{ ps}^{\text{a)}$
1.285	7/2	0.	3/2	112	104	forbidden	1.1 ps	
1.971	(5/2)	0.	3/2	36.8	29	0.031	94 fs	
		1.285	7/2	44.0	81.8	0.011		
2.324	3/2	0.	3/2	50.3	32.9	0.073	24 fs	$\left\{ \begin{array}{l} (4\text{+}2) \text{ fs}^{\text{b)}} \\ (6.2\text{+}2) \text{ fs}^{\text{c)}} \end{array} \right.$
		0.564	1/2	0.002	0.024	0.085		
		1.006	5/2	19.9	35.0	0.236		
[2.190] <sup>*</sup>	3/2 <sup>**</sup>	0.	3/2	0.002	0.0001	0.0002		
2.454	(9/2)	1.006	5/2	159	215	forbidden	0.66 ps	
		1.285	7/2	17.1	25.9	0.0047		
[2.90] <sup>*</sup>	11/2	1.285	7/2	193	237	forbidden	0.25 ps	
		2.454	9/2	0.182	0.179	1.13		

<sup>†</sup> Only negative parity states have been considered

<sup>\*</sup> calculated energy

<sup>\*\*</sup> third 3/2 state in the calculations

Ref. a) This work

b) Bo 63

c) Ba 60





Electromagnetic transition strengths and lifetimes in  $^{55}\text{Fe}$  calculated from the intermediate coupling model. The lifetimes, calculated for  $e_n = 0$ , are compared with the recent measurements of Robertson (Ro 70)<sup>†</sup>

Initial State <sup>††</sup>		Residual State		B(E2) $e_n = 0$	$(e^2\text{-fm}^4)$ $e_n = e$	B(M1) $(e\hbar/2Mc)^2$	Lifetime $\tau$	
							Theory	Experiment
0.410	1/2	0.	3/2	130	210	1.89	0.43 ps	
0.930	5/2	0.	3/2	67.9	90.4	0.014	3.8 ps	
1.318	7/2	0.	3/2	129	161	forbidden	0.56 ps	
		0.930	5/2	0.287	0.40	1.10		
1.919	$(1/2)_2$	0.	3/2	17.9	1.46	0.029	110 fs	} $(25^{+9}_{-8})$ fs
		0.410	1/2	forbidden		0.051		
1.919	$(3/2)_2$	0.	3/2	44.5	27.4	0.096	44 fs	} $(25^{+9}_{-8})$ fs
		0.410	1/2	0.0078	0.0040	0.085		
2.052	$(1/2)_2$	0.	3/2	17.9	1.46	0.029	110 fs	} $(31 \pm 8)$ fs
		0.410	1/2	forbidden		0.051		
2.052	$(3/2)_3$	0.	3/2	0.020	0.043	0.0008	76 fs	} $(31 \pm 8)$ fs
		0.410	1/2	82.6	87.5	0.105		
2.144	$5/2_2$	0.	3/2	34.1	27.4	0.039		55 $^{+16}_{-12}$ fs
		0.410	1/2	46.9	59.8	forbidden	47 fs	
		0.930	5/2	21.3	35.5	0.351		
		1.318	7/2	57.1	96.5	0.040		
2.301	9/2	0.930	5/2	180	245	forbidden	0.8 ps	0.9 $^{+0.7}_{-0.23}$ ps
		1.318	7/2	21.4	30.7	0.0089		
2.470	3/2							$19 \pm 10$ fs
2.542	$(11/2)$	1.318	7/2	210	260	forbidden	1 ps	> 0.66 ps
		2.301	9/2	0.537	0.633	1.20		
2.578	$5/2_3$	0.	3/2	1.82	35.3	.0002		$(67 \pm 9)$ fs
		0.410	1/2	27.3	17.1	forbidden	31 fs	
		0.930	5/2	6.37	6.71	0.116		
		1.318	7/2	0.987	1.25	0.438		

<sup>†</sup> All states have negative parity

<sup>††</sup> The lower index i represents the i<sup>th</sup> state of the same spin as obtained from theory. It has been omitted for the first states.



Table XIV

B(E2) values in units of  $e^2\text{-fm}^4$  for decay to ground of lower states of  $^{53}\text{Cr}$ . Experimental values are based on  $(\alpha, \alpha')$  experiment (Me 68) and coulomb excitation (Ga 69)

Energy (MeV)	Experiment		Theory			
	(Me 66)	(Ga 69)	This work <sup>a)</sup>		T.T. model (Ph 70) <sup>b)</sup>	Shell model (Oh 70) <sup>c)</sup>
			$e_n=0$	$e_n=e$		
0.564	178	220	101	197	146	40
1.006	35	14	54	75	35	22
1.285	69	120	112	139	63	117
1.971			33	29	62.1	47

a) Intermediate coupling model calculation

b)  $e_n = 1.64 e$

c)  $e_p = 2e$ ;  $e_n = e$



Table XV

Calculated and measured mixing ratios in  $^{53}\text{Cr}$  and  $^{55}\text{Fe}$   
 Calculations were obtained from the intermediate coupling model

Nucleus	Transition	Experiment	Theory
$^{53}\text{Cr}$	$1.006 \rightarrow 0$	$-0.27^{+0.09}_{-0.31}$ a)	0.67
	$2.324 \rightarrow 0$	$-5.7 < \delta \leq 0.09$ a) $0.47 \leq \delta \leq 5.7$	-0.51
$^{55}\text{Fe}$	$0.930 \rightarrow 0$	$0.36 \pm 0.11$ b)	0.53
	$2.144 \rightarrow 0$	$1.0^{+\infty}_{-1.3}$ c)	0.52
	$2.470 \rightarrow 0$	$-1.0^{+1.0}_{-\infty}$ c)	0.12

a) this work

b) Ba 60

c) Pi 69



more than one phonon component. The intermediate coupling model calculations show that qualitative agreement is obtained. In the T.T. calculations, good agreement is expected as there are two free parameters to fit three pieces of data (Ph 70). In the shell model calculations of Ohnuma, the agreement is poor although an effective charge of 1e was taken for neutron and proton. This tends to reinforce the confidence in the collective description. All calculations predict a non-negligible  $B(E2)$  for the 1.971 MeV state. Although this state is well excited in inelastic scattering experiments (see e.g. (Me 66) and Wh 67)) no  $B(E2)$  measurement has been reported.

#### 6.3.2. Mixing ratios

Very few mixing ratios have been accurately measured and comparison between theory and experiment can only be semi-quantitative. Results are shown in Table XII, where the experimental mixing ratios of some transitions in  $^{53}\text{Cr}$  and  $^{55}\text{Fe}$  are compared with the predictions of the intermediate coupling model. The same phase convention is used. The overall agreement is good except for the decay to ground of the 1.006 MeV ( $5/2^-$ ) state of  $^{53}\text{Cr}$ , for which there is apparently a contradiction in sign between experimental and theoretical results. It must be noted that there is agreement between theory and experiment for the mixing ratio of the corresponding transition in the 0.930 MeV ( $5/2^-$ ) state of  $^{55}\text{Fe}$ .

#### 6.3.3. Lifetimes

Tables XII and XIII also show the calculated measured lifetimes. The overall agreement is good, mainly for the  $^{55}\text{Fe}$  results. However, for some levels like the 2.324 MeV ( $3/2^-$ ) in  $^{53}\text{Cr}$  and the 1.919 MeV ( $1/2, 3/2$ ),





2.052 MeV (1/2, 3/2) and the 2.578 MeV (5/2) in  $^{55}\text{Fe}$ , disagreement between experimental and theoretical branching ratios indicates that the corresponding theoretical lifetimes should be considered with caution. For the other levels, it can be concluded that the calculated wave functions give a good description of their configuration.

#### 6.3.4. Static moments

Static moments for  $^{53}\text{Cr}$  and  $^{55}\text{Fe}$  calculated from different models are shown in Table XVI. Only for  $^{53}\text{Cr}$  are experimental values available.

Table XVI

Calculated and experimental static moments in  $^{53}\text{Cr}$  and  $^{55}\text{Fe}$

Electric quadrupole moment  $Q$  (in barns)

Nucleus	Exp. (Fu 69)	This work	T.T. model (Ph 70)	Shell model (Oh 70)	Single neutron state <sup>††</sup>
$^{53}\text{Cr}$	$\pm 0.03$	- 0.09	- 0.15	- 0.17 <sup>†</sup>	- 0.04
$^{55}\text{Fe}$		-0.125		- 0.16 <sup>†</sup>	- 0.04

<sup>†</sup> calculated for  $e_{\text{eff}}^p = e_{\text{eff}}^n = 1$

<sup>††</sup> calculated from formula (V.1.) (Bo 53)

Magnetic dipole moment  $\mu$  (in n.m.)

Nucleus	Exp. (Al 53)	This work	Shell model unquenched	(Oh 70) quenched	Schmidt limit
$^{53}\text{Cr}$	- 0.474	- 1.83	- 1.12	- 0.47	- 1.91
$^{55}\text{Fe}$		- 1.62	- 1.03	- 0.40	- 1.91



The first published measurement of the electric quadrupole moment of  $^{53}\text{Cr}$  (Te 61) corresponded to a value  $Q = -0.03\text{b}$ . Since then, there have been many contradictory results, and at present the value adopted by Fulmer and Cohen (Fu 69) is  $|Q| = 0.03\text{b}$ . It is interesting to note that all the calculations indicate that the sign should be negative. All theoretical calculations yield a value too large in magnitude when compared with the experimental result, except for the single particle calculation. The only explanation could be either that the ground state wave function obtained from the different calculations does not give a good description of the ground state, or that for some unknown reason, some terms should cancel out. The situation is identical when one compares the experimental value of the magnetic dipole moment of  $^{53}\text{Cr}$  to the theoretical estimates. However, in this case the single particle estimate (i.e. the Schmidt limit) is about four times larger than the experimental value. It appears that the best value is obtained when "quenching" effects are taken into account. The theories which try to explain why the anomalous magnetic moment of the odd nucleon is somewhat "quenched" in the presence of other nucleons usually involve consideration of the mesonic field (see e.g. (Pr 62) p. 74, and references therein). This might explain why all the models fail to describe the magnetic dipole moment.

#### 6.4. Spectroscopic Factors

In Tables XVII and XVIII, experimental spectroscopic factors obtained in (d,p) stripping reactions are compared with values calculated from



different models, including the present intermediate coupling model calculations. From these results, it appears that most of the calculations yield a fair agreement with the experimental results. A point of interest is to compare the two intermediate coupling calculations, bearing in mind that one of Ramavataram's main goals was to check his, against the measured spectroscopic factors. For the low lying states the results are almost equivalent except for the single particle strength of the first  $5/2$  level. Ramavataram's better results for this level suggest that the  $(f_{5/2}-p_{3/2})$  single particle energy might be smaller than the value used in the present calculations. On the other hand, these calculations seem to describe better than Ramavataram's the configuration of the 2.324 MeV. In the case of the T.T. model, the results are not so good and very likely imply that, because only two core states are taken into consideration, the odd-A nuclei wave functions are too limited.



Table XVII

Sample spectroscopic factors,  $(2J+1)S$ , for the  $^{52}\text{Cr}(d,p)^{53}\text{Cr}$  reaction

The experimental values were obtained by averaging the results given in (An 64, Bo 65, SS 64 and Ra 68) and are compared with theoretical values calculated from different models.

Energy (MeV)	$\ell_n$	$J^\pi$	Experiment	Intermediate coupling model			Shell model	
				This work	(Ra 63) (*)	(Ph 70) (**)	(Oh 66)	(Ve 66)
0.0	1	$3/2^-$	$2.44 \pm 0.33$	2.83	2.44	3.3	3.17	3.06
0.564	1	$1/2^-$	$0.83 \pm 0.07$	0.62	0.61	1.22	1.0	0.88
1.008	3	$5/2^-$	$2.06 \pm 0.40$	1.03	1.83	4.2	2.92	1.763
1.971	-	$(5/2^-)$		0.31	0.18	0.65	0.97	0.39
2.324	1	$3/2^-$	$1.15 \pm 0.13$	0.75	$\begin{Bmatrix} 0.06^+ \\ 1.0^{++} \end{Bmatrix}$	0.46	0.36	0.51
2.664	3	$(5/2^-)$	$0.76 \pm 0.12$	2.11		0.86	0.53	1.54
2.676	1	(***)	$0.12 \pm 0.02$	0.19	$(3/2)$		$0.32(3/2)$	$0.66(1/2)$
2.715	1	(***)	$0.05 \pm 0.05$	0.71	$(1/2)$		$0.4(1/2)$	$0.23(3/2)$

(\*) Normalized to 2.44 for the g.s. S value

(\*\*) Assuming  $J = 5/2$  for the 1.971 MeV level

(\*\*\*) the assumed spin value is indicated after the calculated  $(2J+1)S$  value

(+) for the second  $J = 3/2$  state

(++) for the third  $J = 3/2$  state





Table XVIII

Sample spectroscopic factor (2J+1)S for the  $^{54}\text{Fe}(\text{d},\text{p})^{55}\text{Fe}$  reaction  
The experimental values were obtained by averaging the results given in (Ma 64) and (Fu 63) and are compared with theoretical values calculated from different models.

Energy (MeV)	$\ell_n$	$J^\pi$	Intermediate coupling model		T.T. model (La 70)	Shell model	
			This work	(Ra 63) (*)		(Oh 66)	(Ve 66)
0.	1	$3/2^-$	$2.55 \pm 0.70$	2.50	3.24	3.08	3.2
0.410	1	$1/2^-$	$0.9 \pm 0.3$	0.81	1.12	0.92	0.88
0.930	3	$5/2^-$	$2.85 \pm 0.75$	2.63	3.66	3.90	4.00
1.919	1		$0.15 \pm 0.10$	0.37 (3/2)	0.56 (1/2)	0.23 (1/2)	0.58 (1/2)
2.052	1	$(3/2)^-$	$0.26 \pm 0.12$	0.19 (3/2)	0.64	0.54	0.31
2.144	3	$5/2^-$	$0.71 \pm 0.14$	0.25	1.98	0.94	0.66
2.470	1	$3/2^-$	$0.52 \pm 0.16$			0.35	0.30
2.578	(3)	$5/2^-$	$0.20 \pm 0.02$	1.87		0.282	0.007
3.027		$3/2^-$	$0.07 \pm 0.02$				0.02

\*) Normalized at 2.50 for g.s.



## 7. CONCLUDING REMARKS

Considering the simplicity of the intermediate coupling model, it appears that theoretical predictions are in good agreement with experiment. The model reproduces well most of the properties of the levels below 2.5 MeV excitation, except the static moments, which all models discussed here fail to reproduce. In most cases, the contributions from coupling to 3-phonon states are negligible but contributions from 2-phonon states must be taken into account. As a result, the overall agreement obtained from these calculations is better than those based on the T.T. model in which only the coupling to ground and first excited state of the core is considered. It seems that if one wants to keep the advantages of the more general approach suggested by Thankappan and True, one should include contributions from higher excited states in the core, while trying at the same time to limit the number of free parameters by assuming that "some" collective features are the same for different states of the core. This should be a reasonable assumption in most cases.

There are many common points between intermediate coupling and shell model calculations. This suggests that the form of interaction taken in the unified model is valid. Each model, however, ignores some levels of the excited core: in shell model calculations, the  $0^+$  2-phonon vibrational state is not taken into account, in the intermediate coupling model, a level like the 2.37 MeV ( $4^+$ ) state in  $^{52}\text{Cr}$  is ignored as it is not explained by



the vibrational model. It is not possible for the time being to evaluate the importance of these neglected terms. Both models also fail to reproduce the hole-states such as the second  $7/2^-$  states in  $^{53}\text{Cr}$  and  $^{55}\text{Fe}$ . It must be pointed out, however, that these model calculations presented here can be qualified as "simple". By taking more particles into account and using the "particle-hole" formalism, undoubtedly one should get better results, but then the problem lies in prohibitive matrix sizes and computation difficulties.

For the time being the important question is to try and estimate how the overall results would be modified when hole states are included. From the study of pick-up reaction, which shows that the cross section for say, the  $7/2^-$  hole state is much larger than the pick-up cross section for the other  $7/2^-$  state, and from the measured branching ratios which show that within experimental error a level like the  $9/2^-$  state does decay to either  $7/2^-$  states but not to both, it seems to be possible to assume that mixing between such states is probably small.

If one accepts the validity of the type of interaction used in the intermediate coupling model calculations, it appears that there are possibilities of improving the calculations. Rather than considering  $\hbar\omega$  as a free parameter, it would be better to couple the odd-nucleon to the known vibrational levels of the core: for instance, in  $^{53}\text{Cr}$  the 1.434 MeV ( $2^+$ ) would be the  $N = 1$  phonon state, the 2.65 MeV ( $0^+$ ) would be the  $0^+ N = 2$  phonon state, etc. This assumes that the general theory is still valid and that the odd-particle does not appreciably affect the core properties.



The overall results might not be greatly modified but, with the elimination of one free parameter, it should then be possible to get a better estimate of the single-particle energy spacings. Another possible improvement should result from the use of effective charge and effective gyromagnetic parameters in the calculation of electromagnetic transitions. These parameters could be determined by fitting either  $B(E2)$ 's or the measured static moments but this requires that the experimental values be accurately known to make such a procedure worthwhile.

No mention has been made of the positive parity states. In  $^{53}\text{Cr}$  and  $^{55}\text{Fe}$ , there is apparently no positive parity state below 3.5 MeV excitation. This is above the excitation which has been considered as the limit of validity of the present model. Therefore, positive parity states can be ignored in these calculations.





## CHAPTER V

### CONCLUSIONS

In the study of  $^{53}\text{Cr}$ , some improvement has been brought to Litherland and Ferguson Method II, by limiting the ratio of population parameters. A better knowledge of the reaction mechanism might result in more restrictive conditions of this ratio. This would then limit the number of possible spin assignments and might also yield more accurate mixing ratios. Experimentally, this method requires rather sophisticated electronic set-ups. On the other hand, if the bombarding energy is well chosen, many levels can be studied at the same time (the only limiting factor being the number of "bins" available). As the gamma ray spectra are recorded separately by sorting according to the energy of the different proton groups, branching ratios can be accurately determined for most of the states except in the case of closely spaced multiplets. High-spin levels which are non-stripping states are weakly excited in the  $(d,p\gamma)$  reaction and another type of reaction must be used to investigate such levels.

In the study of  $^{55}\text{Fe}$  via the  $^{55}\text{Mn}(p,n\gamma)^{55}\text{Fe}$  reaction, the experimental method is quite appealing by its simplicity. This reaction also proves to be quite adequate for the investigation of high-spin states. On the other hand, levels with spin  $J \leq 5/2$  are not easily assigned with this particular reaction. As the population parameters are calculated from the statistical



model, there is one less free parameter in the  $\chi^2$ -fitting calculations and one then should expect a more accurate determination of the multipole mixing ratios. With a suitable choice of bombarding energies, many levels can be investigated at the same time. This is important, as a careless application of this method could be quite machine-time consuming. In any case, it appears that the number of levels which can be investigated by this method is limited. When too many levels are being excited, the resulting gamma spectrum becomes quite complex and some transitions are masked by other gamma rays. The determination of decay modes also becomes difficult because of multiple feeding of the lower states.

In  $^{55}\text{Fe}$ , it was hoped to find the  $13/2^-$  level predicted by the calculations of Ohnuma at 2.975 MeV. No evidence was found of the existence of such a level although one could speculate about the unobserved (?) 2.818 MeV level being such a state.

Theoretically, the failure of Nilsson model calculations confirmed that  $^{52}\text{Cr}$  and  $^{54}\text{Fe}$  cannot be regarded as strongly deformed nuclei. Thankappan and True-type calculations are quite appealing by their general approach. However, they appear to have a rather limited range of application and could only be improved by including more core excited states.

For the present state of knowledge, intermediate coupling and shell model calculations have proved to be successful in describing most of the experimental features reported. As mentioned earlier, both types of calculations could be refined and this may be necessary when higher excited states are considered. The failure to reproduce the electric quadrupole moment of  $^{53}\text{Cr}$  remains unexplained. Measurements of the electric quadrupole moment of the other  $N = 29$  nuclei may give some clue to the problem.



# REFERENCES

- Al 53 F. Alder and K. Albach, *Helv. Phys. Acta* 26 (1953) 426
- Al 69 G. Alaga, *Proc. Int. School of Physics, E. Fermi, Course 40*, Academic Press N.Y. (1969) p. 28
- An 64 P.T. Andrews, R.W. Clifft, L.L. Green and J.F. Sharpey-Schafer, *Nucl. Phys.* 56 (1964) 465
- Au 70 R.L. Auble and J. Rapaport, *Nuclear Data sheets* 3B January 1970
- Ba 60 R.W. Bauer and M. Deutsch, *Nucl. Phys.* 16 (1960) 264
- Ba 62 R.H. Bassell, G.R. Satchler, R.M. Drisko and E. Rost, *Phys. Rev.* 128 (1962) 264
- Ba 63 J.B. Ball, C.B. Fulmer and C.D. Goodman, *Phys. Rev.* 130 (1963) 2342
- Ba 64 P.D. Barnes, C.K. Bockelman, O. Hansen and A. Sperduto, *Phys. Rev.* 136 (1964) B438
- Ba 65 G.A. Bartholomew and M.R. Gunye, *Can. J. Phys.* 43 (1965) 1128
- BD 64 R. Bock, H.H. Duhm, R. Rüdél and R. Stock, *Phys. Lett.* 13 (1964) 151
- BD 65 R. Bock, H.H. Duhm, R. Jahr, R. Santo and R. Stock, *Phys. Lett.* 19 (1965) 417
- Bj 64 J.H. Bjerregaard, P.F. Dahl, O. Hansen and G. Sidenius, *Nucl. Phys.* 51 (1964) 641
- Bo 52 A. Bohr, *Mat. Fys. Medd. Dan. Vid. Selsk.* 26 (1952) #14
- Bo 53 A. Bohr and B.R. Mottelson, *Mat. Fys. Medd. Dan. Vid. Selsk.* 27 (1953) #16
- Bo 63 E.C. Booth and K.A. Wright, *Bull. Am. Phys. Soc* 8 (1963) 85
- Bo 64 E.C. Booth, B. Chasan and K.A. Wright, *Nucl. Phys.* 57 (1964) 403  
(Results for the 2.324 MeV level were obtained by reassigning spin 3/2 to this level.)
- Bo 65 R. Bock, H.H. Duhm, S. Martin, R. Rüdél and R. Stock, *Nucl. Phys.* 72 (1965) 273
- Br 65 R.T. Brockmeier, S. Wahlborn, E.J. Seppi and F. Boehm, *Nucl. Phys.* 63 (1965) 102
- Ca 69 T.P.G. Carola, University of Alberta - Nuclear Research Centre - Program Library





- Ca 70 T.P.G. Carola, W.C. Olsen, D.M. Sheppard, B.D. Sowerby and P.J. Twin,  
Nucl. Phys. A144 (1970) 53
- Ch 54 D.C. Choudhury, Dan. Mat. Fys. Medd. 28 (1954) #4
- Da 65 J.P. Davidson, Rev. Mod. Phys. 37 (1965) 105
- Da 69 N.E. Davison, University of Alberta - Internal Report (1969) unpublished
- DD 69 P. David, H.H. Duhm, R. Bock and R. Stock, Nucl. Phys. A128 (1969) 47
- Ea 66 E.D. Earle and G. A. Bartholomew, Bull. Am. Phys. Soc. 11 (1966) 98
- Er 63 T. Ericson, Ann. Phys. 23 (1963) 390
- Fe 65 A.J. Ferguson, *Angular Correlation Methods in Gamma-ray Spectroscopy*,  
North Holland Publishing Co., Amsterdam 1965
- Fe 69 P. Federman and L. Zamick, Phys. Rev. 177 (1969) 1534
- Fi 66 H.J. Fischbeck, F.T. Porter, M.S. Freedman, F. Wagner Jr. and H.H. Bolotin,  
Phys. Rev. 150 (1966) 941
- Fo 55 K.W. Ford and C. Levinson, Phys. Rev. 100 (1955) 1
- Fu 63 R.H. Fulmer and A.L. McCarthy, Phys. Rev. 131 (1963) 2133
- Fu 64 H.O. Funsten, N.R. Roberson and E. Rost, Phys. Rev. 134 (1964) 117B
- Fu 69 R.H. Fulmer and B. Cohen, Nuclear Data Tables 5 (1969) #5 & 6, and R. Auble,  
private communication
- Ga 69 L.N. Galperin, A.Z. Ilyasov, I.K. Lemberg and G.A. Firsonov, Sov. J. Nucl.  
Phys. 9 (1969) 133
- Gl 66 C. Glashausser and M.E. Rickey, Phys. Rev. 154 (1967) 1033
- Go 62 C.D. Goodman, J.B. Ball and C.B. Fulmer, Phys. Rev. 127 (1962) 574
- Go 66 L.J.B. Goldfarb and K.K. Wong, Phys. Lett. 22 (1966) 310 & private communication
- Gu 70 W. Gulholmer and Z. Sawa, Prog. Report, Research Inst. for Phys., Stockholm  
(1970)
- Ha 52 W. Hauser and H. Feshbach, Phys. Rev. 87 (1952) 366
- Ha 63 M. Harvey, Nucl. Phys. 48 (1963) 578





- Ha 65 W. Haupt, D. Langa, H.G. Eckert and A. Flammersfeld, Z. Phys. 188 (1965) 256
- Hu 68 D. Hutcheon, University of Alberta - Internal Report(1968) unpublished
- Ka 64 E. Kashy, A. Sperduto, H.A. Enge and W.W. Buechner, Phys. Rev. 135 (1964) B865
- Ke 56 A.K. Kerman, Dan. Mat. Fys. Medd. 30 (1956) #15
- Kr 69 W. Kreische, W. Lampert, G. Loos and D. Weltle, Phys. Lett. 29B (1969) 170
- Ku 68 T.T.S. Kuo and G.E. Brown, Nucl. Phys. A114 (1968) 241
- La 57 R.D. Lawson and J.L. Uretsky, Phys. Rev. 108 (1957) 1300
- La 70 D. Larner, University of Kansas, Lawrence, Internal Report COO-1120-106  
(to be published)
- Li 61 A.E. Litherland and A.J. Ferguson, Can. J. Phys. 39 (1961) 788
- Li 64 A.E. Litherland, Nucl. Struc. and e.m. int. - Scot. Univ. Summer School,  
ed. Oliver and Boyd, Edinburgh, London (1964) p. 61
- Ma 64 J.R. Maxwell and W.C. Parkinson, Phys. Rev. 135 (1964) B82
- Me 66 J.R. Meriwether, J. Gabrielli, D.L. Hendrie, J. Mahoney and B.H. Harvey,  
Phys. Rev. 146 (1966) 804
- Ni 55 S.G. Nilsson, Mat. Fys. Mett. Dan. Vid. Selsk. 29 (1965) #16
- Ni 59 G.J. Nijgh, A.H. Wapstra, and R. van Lieshout, Nuclear Spectroscopy Tables,  
North Holland Publishing Company, Amsterdam (1959)
- Oh 66 H. Ohnuma, Nucl. Phys. 88 (1966) 273
- Oh 70 H. Ohnuma, private communication
- Pe 63 F.G. Perey, Phys. Rev. 131 (1963) 745
- Ph 70 R.J. Philpott and W.W. True, to be published (private communication)
- Pi 69 A.A. Pilt, M.Sc. Thesis, University of Alberta (1969)
- Po 65 A.R. Poletti and E.K. Warburton, Phys. Rev. 137 (1965) B595
- Pr 62 M.A. Preston, *Physics of the Nucleus*, Addison-Wesley Publishing Co., Reading  
Mass., (1962)



- Ra 63 K. Ramavataram, Phys. Rev. 132 (1963) 2255
- Ra 68 M.N. Rao, J. Rapaport, A. Sperduto and D.L. Smith, Nucl. Phys. A121 (1968) 1
- Ri 69 R.A. Ricci, Proc. Int. School of Physics, E. Fermi, Course 40, Academic Press N.Y. (1969) p. 80
- Ro 65 A.A. Rollefson, R.C. Bearse, J.C. Legg, G.C. Phillips and G. Roy, Nucl. Phys. 63 (1965) 561
- Ro 66 L. Rosen, Proc 2<sup>nd</sup> Int. Symp. on Polarization Phenomena of Nucleons, Karlsruhe (1965) ed. P. Huber and H. Schopper, Birkhauser Verlag Basel (1966) p. 253
- Ro 67 H.J. Rose and D.M. Brink, Rev. Mod. Phys. 39 (1967) 306
- Ro 70 B.C. Robertson, University of Alberta, (private communication)
- Sa 66 G.R. Satchler, *Lect. in Theor. Phys.*, Vol III C, University of Colorado Press, (1966) p. 73
- Sh 61 A. de Shalit, Phys. Rev. 122 (1961) 1530
- Sh 62 Shakin and Kerman, Phys. Lett. 1 (1962) 151
- Sh 63 E. Sheldon, Revs. Mod. Phys. 35 (1963) 795
- Sh 65 R. Sherr, B.F. Bayman, E. Rost, M.E. Rickey and C.G. Hoot, Phys. Rev. 139 (1965) B1271
- Sh 66 E. Sheldon and D.M. van Patter, Revs. Mod. Phys. 38 (1966) 143
- Sh 69 E. Sheldon and R.M. Strang, Computer Phys. Comm. 1 (1969) 35
- Si 65 J.J. Simpson, J.A. Cookson, D. Eccleshall and M.J.L. Yates, Nucl. Phys. 62 (1965) 385
- So 67 P.C. Sood and D.A. Hutcheon, Nucl. Phys. A96 (1967) 159
- So 69 P.C. Sood, Phys. Rev. 179 (1969) 1100
- Sp 64 A. Sperduto and W.W. Buechner, Phys. Rev. 134 (1964) B142 and unpublished work reported in (Fu 63)
- SS 64 A. Sperduto, D.A. Smith, N.M. Rao, H.A. Enge, W.W. Buechner and H. Chen, Bull. Amer. Phys. Soc 9 (1964) 470 and unpublished results quoted in (Bo 65)
- Sy 68 D.H. Sykes, University of Alberta - Internal Report (1968) unpublished
- So 68 B.D. Sowerby, University of Alberta - Internal Report (1968) unpublished



- Te 61 R.W. Terhune, J. Lambe, C. Kikuchi and J. Baker, Phys. Rev. 163 (1961) 1265
- Te 66 J.W. Tepel, Nucl. Inst. Meth. 40 (1966) 100
- Th 65 V.K. Thankappan and W.W. True, 137 (1965) B793, Phys. Rev.
- Va 62 D.M. Van Patter, N. Nath, S.M. Shafroth, S.S. Malik and M.A. Rothman, Phys. Rev. 128 (1962) 1246
- Ve 66 J. Vervier, Nucl. Phys. 78 (1966) 497
- Vo 69 E. Vogt, *Advances in Nucl. Phys.*, Plenum Press, N.Y. (1968) p 261
- Wa 59 A.H. Wapstra, G.J. Nijgh and R. van Lieshoust, Nuclear Spectroscopy Tables, North Holland Publishing Company, Amsterdam (1959)
- Wh 67 C.A. Whitten Jr., Phys. Rev. 156 (1967) 1228
- Wi 62 R.R. Wilson, A.A. Bartlett, J.J. Kraushaar, J.D. McCullen and R.A. Ristinen, Phys. Rev. 125 (1962) 1655
- Yu 68 T.J. Yule and W. Haeberli, Nucl. Phys. A117 (1968) 1



A P P E N D I X

**C O R P A R**

A DESCRIPTION OF INTERMEDIATE COUPLING  
CALCULATIONS IN THE UNIFIED MODEL

*T.P.G. Carola*

Nuclear Research Centre  
University of Alberta  
Edmonton, Alberta, Canada

Internal Report UAE-NPL-24

June 1970





## Abstract

Two programs based on the intermediate coupling in the unified model are described. The first program, CORPAR I, calculates energy levels in the framework of this model for a single particle having up to three orbitals available, coupled to a vibrating core where up to three phonon state vibrations are considered. The second program, CORPAR II, calculates electromagnetic transitions, mixing ratios, lifetimes and nuclear static moments using the wave functions calculated by CORPAR I.



## CHAPTER I

## CORPAR I

Title: CORPAR I

Type: Main

Source Language: Fortran IV(G)

Origin: T.P.G. Carola, Nuclear Research Centre

Abstract: This program calculates the total Hamiltonian  $H_T$  in the frame of the intermediate coupling model. After diagonalization, the energy eigenvalues and wave functions are given for each value of the final spin state  $I$  and the coupling parameter  $\xi$ .

## 1. Description and theory

### 1.1 Introduction

The intermediate coupling in the unified model was first outlined by Bohr (Bo 52) and Bohr and Mottelson (Bo 53). Later, it was elaborated by Choudhury (Ch 54) and Ford and Levinson (Fo 55). This model has since been used (see e.g. Gl 60, Ro 63, Ch 67, Ru 68 and Pa 70) to describe the spectra and other relevant physical quantities such as reduced transition probabilities, lifetimes, spectroscopic factors ... in the case of odd nuclei whose even mass neighbouring nuclei exhibit a vibrational spectrum.

In this model, the odd mass nucleus is treated as a coupled system comprising: i) a doubly even core capable of performing collective quadrupole oscillations of frequency  $\omega$ ; ii) an extra core nucleon which has several single particle levels available.



In the program described here, the single particle has up to 3 orbitals available. Core excitation up to 3 phonons are considered.

The energies of the resulting states of the coupled system depend upon the following parameters:

$\hbar\omega$	phonon energy
$\epsilon_1$	energy difference between the first and ground state orbital
$\epsilon_2$	energy difference between the second and ground state orbital
$\xi$	coupling parameter.

Note:

As described extensively in (Bo 53), the limiting cases of this model correspond either to weak coupling (for nuclei near double closed shells) or strong coupling (case of deformed nuclei) and are usually treated differently.

## 1.2 Formalism

The core-particle system is described by the coupling of a single particle of angular momentum  $j$  with the quadrupole oscillations of the nuclear surface of the core.

The total Hamiltonian is the sum of three terms:

$$H_T = H_s(\alpha_{2\mu}) + H_{sp}(x) + H_{int}(\alpha_{2\mu}, x) \quad (1)$$

where:  $\alpha_{2\mu}$  are the collective coordinates as defined by Bohr and Mottelson (Bo 53)

$x$  are the single particle coordinates.

The surface Hamiltonian  $H_s$  is defined by:



$$H_s(\alpha_{2\mu}) = \sum_{\mu} \left\{ \frac{1}{2} B_2 |\dot{\alpha}_{2\mu}|^2 + \frac{1}{2} C_2 |\alpha_{2\mu}|^2 \right\} \quad (2)$$

in terms of the mass parameter  $B_2$  and the nuclear deformability  $C_2$ .

It is equivalent to a system of harmonic oscillators of frequency

$$\omega = \sqrt{\frac{C_2}{B_2}} \quad (3)$$

The particle Hamiltonian  $H_p$  is a constant. It corresponds to the motion of the odd nucleon in the effective average potential of the spherical core. The corresponding eigenvalues are then simply the single particle energy levels.

Finally, the Hamiltonian  $H_{int}$  represents the coupling of the single particle to the vibrating surface. It can be written as:

$$H_{int} = -k \sum_{\mu} \alpha_{2\mu} Y_{2\mu}(\theta, \phi) \quad (4)$$

where  $k$  is the coupling constant introduced by Bohr and Mottelson (Bo 53);<sup>\*</sup>  $Y_{2\mu}$  is the spherical harmonic;  $\theta$  and  $\phi$  are the polar angles of the particle.

It is more convenient to write the surface variable in terms of creation and annihilation operators  $b_{\mu}^*$  and  $b_{\mu}$ . The expression for  $H_{int}$  then becomes:

$$H_{int}(\alpha_{2\mu}) = -k \sum_{\mu} \sqrt{\frac{\hbar\omega}{2C_2}} (b_{\mu} - (-)^{\mu} b_{\mu}^*) Y_{2\mu}(\theta, \phi) \quad (5)$$

---

<sup>\*</sup> It is actually the radial average  $k = \langle k(r) \rangle$  and can be considered as a constant.





The representation of the system is in the angular momentum space. More specifically, the eigenvectors of the uncoupled system  $|j m\rangle$  and  $|N R m'\rangle$ , representing the single particle and the core respectively, are taken as the basis states.  $j$  is the angular momentum of the single particle,  $m$  its projection,  $N$  is the number of phonons of angular momentum  $R$ .

The basis vectors of the coupled system are then given by:

$$|j \text{ } NR \text{ } IM\rangle = \sum_{m, m'} (j \text{ } R \text{ } mm' | IM) |j \text{ } m\rangle |NR \text{ } m'\rangle \quad (6)$$

where  $(j \text{ } R \text{ } mm' | IM)$  is the Clebsch-Gordan coefficient resulting from the angular momentum coupling. The total angular momentum  $\vec{I} = \vec{j} + \vec{R}$ . From this definition, it follows that: (neglecting the zero-point energy)

$$(H_s + H_p) |j \text{ } NR \text{ } IM\rangle = (N\hbar\omega + E_j) |j \text{ } NR \text{ } IM\rangle \quad (7)$$

with  $E_j$  corresponding to the energy of the single particle with total angular momentum  $j$ . Using eq. (6), one can now evaluate the matrix elements of  $H_{int}$ :

$$\begin{aligned} \langle j' \text{ } N'R' \text{ } IM | H_{int} | j \text{ } NR \text{ } IM \rangle &= -k \sqrt{\frac{\hbar\omega}{2C}} \langle j' \text{ } N'R' \text{ } IM | \sum_{\mu} (b_{\mu} + (-)^{\mu} b_{-\mu}^*) \\ &\times Y_{2\mu}(\theta, \phi) | j \text{ } NR \text{ } IM \rangle \end{aligned} \quad (8)$$

For the time being, we will write  $-k \sqrt{\frac{\hbar\omega}{2C}}$  as  $K$  and the left hand term of equation (8) as  $\langle H_{int} \rangle$ .



$$\begin{aligned} \langle H_{int} \rangle &= K \{ \langle j' N' R' IM | \sum_{\mu} b_{\mu} Y_{2\mu} | j NR IM \rangle \\ &+ \langle j' N' R' IM | \sum_{\mu} (-)^{\mu} b_{-\mu}^* Y_{2\mu} | j NR IM \rangle \} \quad (9) \end{aligned}$$

Consider the first term of eq. (9). Using eq. (6), one gets

$$\begin{aligned} \langle \sum_{\mu} b_{\mu} Y_{2\mu} \rangle &= \sum_{mm'} \langle j' \nu | Y_{2\mu} | j m \rangle \cdot \langle N' R' \nu | b_{\mu} | NR m' \rangle (j' R' \nu \nu' | IM) \\ &\quad \times (j R mm' | IM) \quad (10) \end{aligned}$$

One can now apply the Wigner-Eckart theorem<sup>\*</sup>, bearing in mind the difference between an operator acting on the ket (like  $Y_{2\mu}$ ) and the bra (like  $b_{\mu}$ ) vectors.

$$\begin{aligned} \langle \sum_{\mu} b_{\mu} Y_{2\mu} \rangle &= \sum_{mm'} (j 2 m \mu | j' \nu) \langle j' || Y_2 || j \rangle (R' 2 \nu' \mu | R m') \langle N' R' || b || NR \rangle \\ &\quad \times (j' R' \nu \nu' | IM) (j R mm' | IM) \quad (11) \end{aligned}$$

What follows is purely Racah algebra (see e.g. Ro 57 - pages 38 and 110). In order to get a Racah coefficient out of the sum of our Clebsch-Gordan coefficients, some rearranging is necessary:

$$\begin{aligned} \langle \sum_{\mu} b_{\mu} Y_{2\mu} \rangle &= \sum_{mm'} \sum_{\mu} \langle j' || Y_2 || j \rangle \langle N' R' || b || NR \rangle (-)^{R'+2-R} (j 2 m \mu | j' \nu) \\ &\quad \times (2 R' \mu \nu' | R m') (j' R' \nu \nu' | IM) (j R mm' | IM) \quad (12) \end{aligned}$$

<sup>\*</sup>The Wigner-Eckart theorem states that:

$$\langle j' m' | T_{LM} | j m \rangle = (j L m M | j' m') \langle j' || T_2 || j \rangle$$



This can then be more simply expressed as:

$$\begin{aligned} \langle | \sum_{\mu} b_{\mu} Y_{2\mu} | \rangle &= (-)^{R'-R} \langle j' || Y_2 || j \rangle \langle N'R' || b || NR \rangle \sqrt{(2j'+1)(2R+1)} \\ &\times W(j \ 2 \ 1 \ R'; j'R) \quad (13) \end{aligned}$$

$$\begin{aligned} \langle | \sum_{\mu} b_{\mu} Y_{2\mu} | \rangle &= (-)^{R'-R+j'+R-1} \sqrt{2j'+1} \langle j' || Y_2 || j \rangle \sqrt{2R+1} \langle N'R' || b || NR \rangle \\ &\times W(jj' \ RR'; 21) \quad (14) \end{aligned}$$

The treatment of the second term of eq. (9), is equivalent to what has just been done. The  $\langle N'R' || b || NR \rangle$  terms contribute only when  $N' < N$ , whereas the  $\langle N'R' || b^* || NR \rangle$  terms contribute only when  $N' > N$ . As the total matrix is symmetric, it suffices to calculate only elements on one side of the diagonal. Limiting to the case  $N' < N$ , one gets:

$$\begin{aligned} \langle | H_{int} | \rangle &= (-)^{R'+j'-1} k \sqrt{2j'+1} \langle j' || Y_2 || j \rangle \\ &\times \sqrt{2R+1} \langle N'R' || b || NR \rangle W(jj' \ RR'; 21) \\ &\text{for } N' < N \quad (15) \end{aligned}$$

One can now introduce the dimensionless coupling parameter  $\xi$ , defined by

$$\xi = k \sqrt{5/2\pi \cdot \hbar \omega \cdot C} \quad (16)$$

(15) then becomes:



$$\begin{aligned}
\langle |H_{int}| \rangle &= (-)^{R'+j'-I+1} \sqrt{\frac{\pi}{5}} \hbar\omega \xi \sqrt{2j'+1} \langle j' || Y_2 || j \rangle \\
&\times \sqrt{2R+1} \langle N'R' || b || NR \rangle W(jj' RR'; 2I) \\
&\text{for } N' < N
\end{aligned} \tag{17}$$

Some authors write the phase factor as  $(-)^{R'+j'+I}$ . Both expressions obviously yield the same result.

The reduced matrix elements for  $Y_2$  and  $b$  are the only terms left to be explicitly defined. The former can be found in many texts (see e.g. Ro 59, page 4) and we have in the program used one of the simplest forms, namely:

$$\begin{aligned}
\sqrt{2j'+1} \langle j' || Y_2 || j \rangle &= (-)^{j'-\frac{1}{2}} \left[ \frac{(2j+1)(2j'+1)}{4\pi} \right]^{1/2} (jj' \frac{1}{2} - \frac{1}{2} | 20) \text{ if } \ell + \ell' \text{ is even} \\
&= 0 \text{ if } \ell + \ell' \text{ is odd}
\end{aligned} \tag{18}$$

Detailed calculations of the reduced matrix elements of  $b$  can be found in (Ch 54) and (Fo 55). Their values are tabulated in Choudhury's paper (Ch 54) and have been used in this program.

## 2. Description of the program

The program CORPAR I calculates the matrix elements of the total Hamiltonian  $H_T$  for given values of  $I$ ,  $\xi$ ,  $E_j$  and  $\hbar\omega$ , diagonalizes the matrix so obtained and yields energy eigenvalues. The eigenvalues are written as:





$$|E \text{ IM}\rangle = \sum_{j, \text{NR}} A_{j, \text{NR}}(E) |j \text{ NR IM}\rangle \quad (19)$$

The expansion coefficients  $A_{j, \text{NR}}(E)$  are printed out. The basis states  $|j \text{ NR IM}\rangle$  are written as  $|j \text{ N R}\rangle$  in the program output.

Fig. 1 shows a schematic flow diagram of the program. This diagram introduces the main subroutines. The remaining subroutines are used to calculate Racah coefficients, Clebsch-Gordan coefficients,  $Y_2$  reduced matrix elements, etc...

## 2.1 Input Output Data

The single particle states are defined by their total angular momentum  $j$  which can take a maximum of three values corresponding to the maximum of three orbitals available. At this point, it must be again emphasized that the orbital angular momenta,  $\ell$ , MUST have the same parity. The separation energy between the single particle states are defined by the variable EPS. The phonon energy is called EFONON (in MeV) and the coupling parameter  $XI(\xi)$  is defined by XMIN, XMAX and XSTEP for its minimum, maximum and step value respectively.

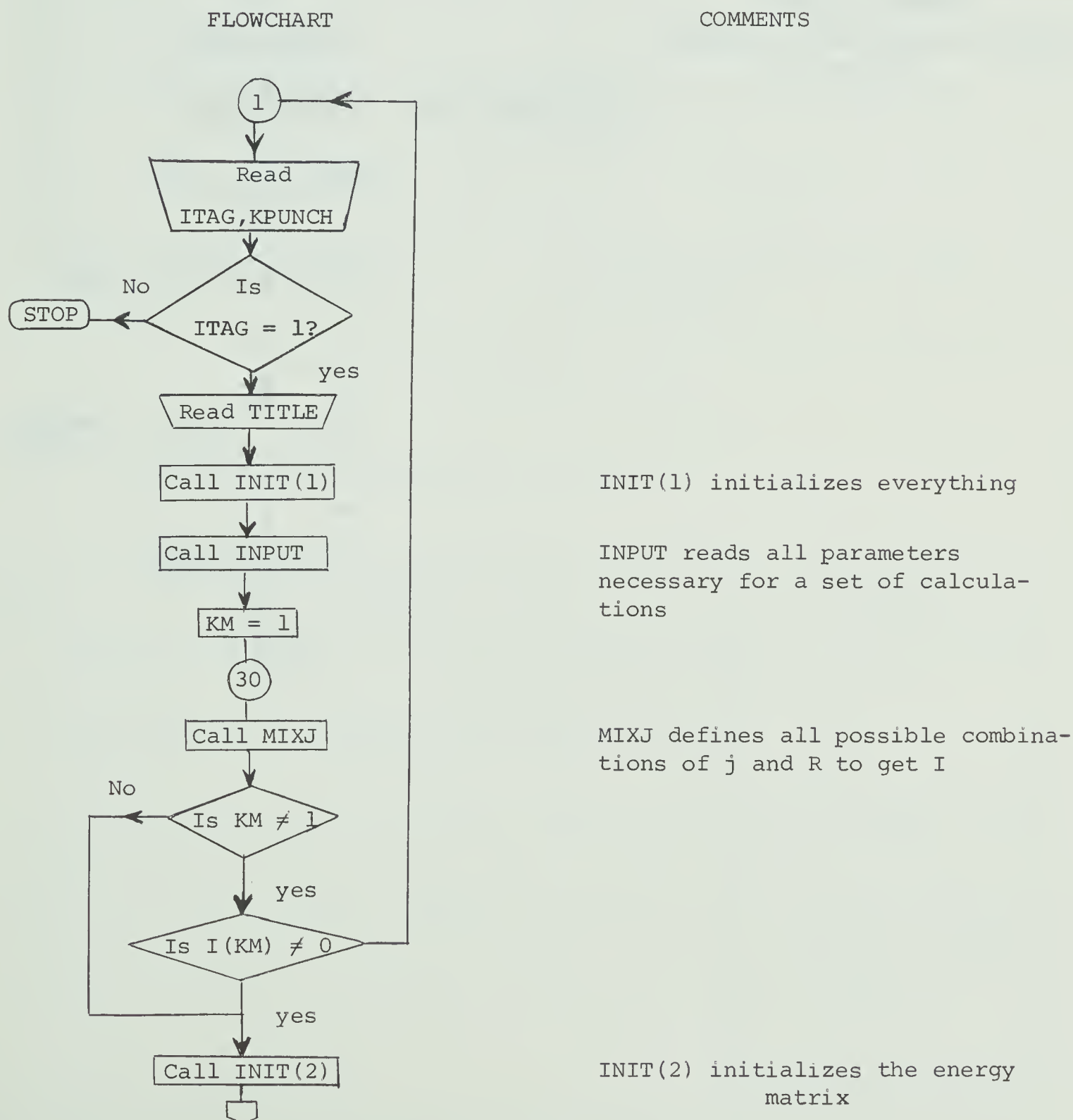
The coupling constant  $k$  has been fixed to 40 MeV, as suggested by Bohr and Mottelson. This value is commonly used by most authors (Ch 54, Pa 70). For given  $\xi$  and  $\hbar\omega$ , the value of the nuclear deformability  $C_2$  (CTWO in the program) is calculated. Finally, for comparison purposes, two other coupling variables are calculated: X0 is the  $x$  used by Choudhury (Ch 64) and HARVEY Y VALUE is the coupling parameter introduced by Harvey (Ha 63).



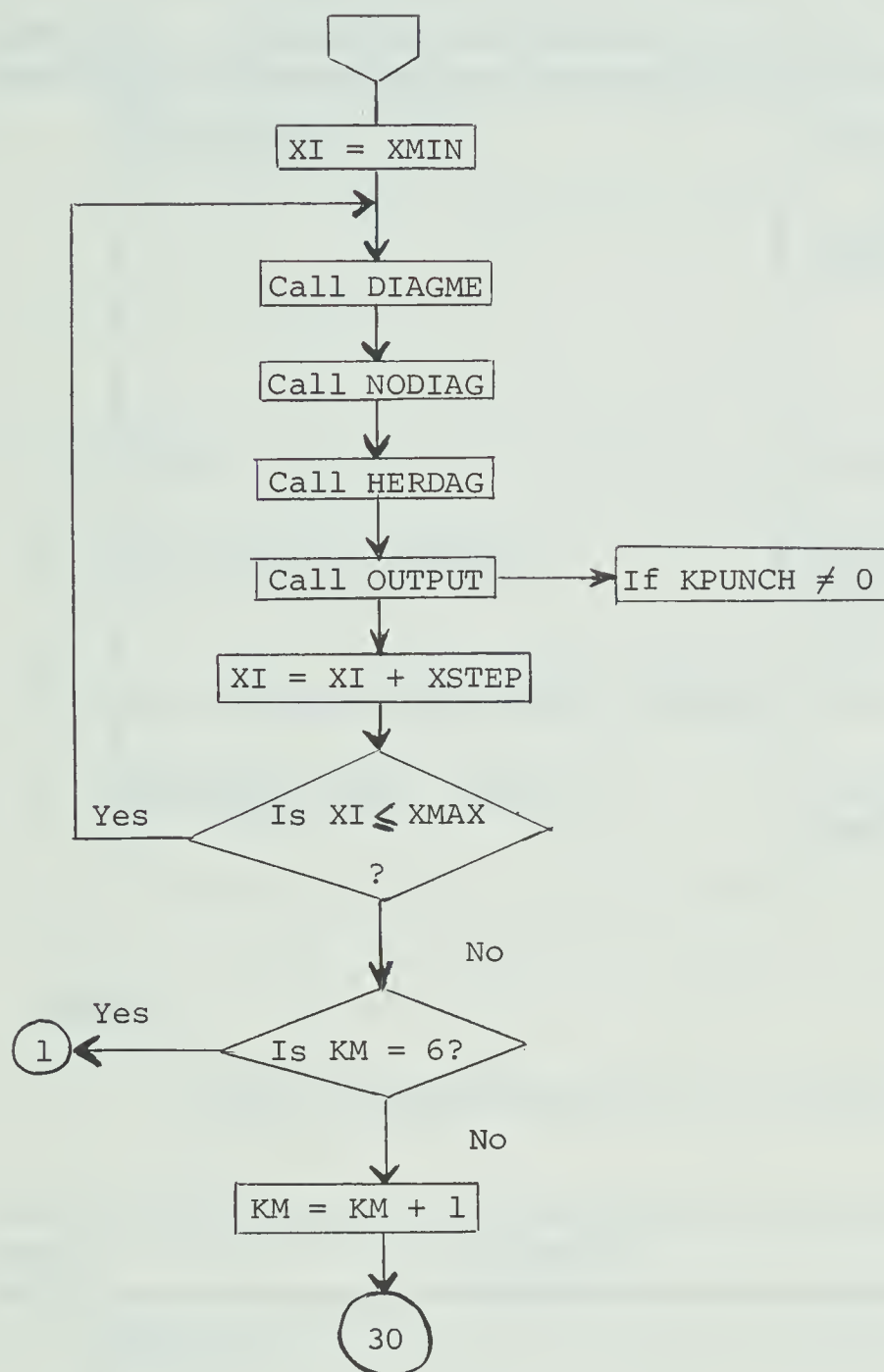
Figure 1

## Program Flowchart

In order to simplify the typing and page-setting, the use of flow-chart symbols has been greatly reduced.







DIAGME calculates diagonal  
matrix elements

NODIAG calculates off-diagonal  
matrix elements

HERDAG is the diagonalization  
subroutine



## 2.2 Input Format

Card #	Variable and Format	Comments
1	ITAG,KPUNCH (2I1)	ITAG = 1 Start a calculation ≠ 1 END KPUNCH = 1 All results for the following calculation to be punched out (see CORPAR II)
2	TITLE	80 alphameric characters
3	I(K) [K=1,6] (6F10.5)	Read spin values of the final states
4	J,J1,J2,EPS1,EPS2,EFONON (6F10.5)	Defined in the text
5	XMIN,XMAX,XSTEP (3F10.5)	For one value of $\xi$ only, make XMAX=XSTEP=0.

Example:

Set of calculations for N = 29 nuclei

Card #	Variable	Comments
1	ITAG = 1	
2	The following calculations for N=29 odd nuclei	
3	0.5      1.5      2.5      3.5      4.5      5.5	I ranging from 1/2 to 11/2
4	1.5      0.5      2.5      2.02      2.2      1.5	$\epsilon_1 = p_{\frac{1}{2}} - p_{\frac{3}{2}} = 2.02 \text{ MeV}$ $\epsilon_2 = f_{\frac{5}{2}} - p_{\frac{3}{2}} = 2.2 \text{ MeV}$ $\hbar\omega = 1.5 \text{ MeV}$
5	2.5      4.0      0.5	$\xi$ ranging from 2.0 to 4.0 by steps of 0.5





### 2.3 Corresponding Output

THE FOLLOWING CALCULATIONS FOR N=29 ODD NUCLEI  
 FIRST ORBITAL J=1.5 SECOND ORBITAL J=0.5 THIRD ORBITAL J=2.5  
 FINAL SPIN STATES: 0.5 1.5 2.5 3.5 4.5 5.5  
 EPSILON1=2.020 MeV EPSILON2=2.200 MeV PHONON ENERGY=1.500 MeV  
 XMIN=2.500 XMAX=4.000 XSTEP=0.0

(on your next page)

\*\*\*\*\*NUMBER OF BASIS STATES IS 10  
 BLOCK DATA INDEX KM 1 THIS IS FOR SPIN 0.500  
 COUPLING PARAMETER: XI=2.500 CTWO=135.8123 MeV XO=0.7217 HARVEY Y VALUE=0.4431  
 EIGENVALUES IN MeV  
 8.3230 7.3489 6.8185 5.5221 5.0847 3.9581 3.2850 2.5516 1.9603 -0.1727  
 EIGENVECTORS BUILT ON THE  $|N,R,J\rangle$  STATES  
 $|0,0,1/2\rangle$   $|1,2,3/2\rangle$   $|1,2,5/2\rangle$   $|2,0,1/2\rangle$   $|2,2,3/2\rangle$   $|2,2,5/2\rangle$   $|3,0,1/2\rangle$   $|3,2,3/2\rangle \dots$   
 -0.095 etc....  
 $\vdots$   
 0.5352 0.6673 0.3295 0.1978 -0.2871 etc....

Remarks:

- i) The index KM is to be used with the program CORPAR II.
- ii) One can see in this case that the lowest eigenvalue for spin  $I = 1/2$  has an energy -0.1727 MeV. Its wave function can be written as  

$$|-0.1727(1/2)\rangle = 0.5352|0,0,1/2\rangle + 0.6673|1,2,3/2\rangle + 0.3295|1,2,5/2\rangle + \dots$$
- iii) Some calculations of the same type sometimes include a least squares fitting procedure for the energy levels. It was felt (after using this method in conjunction with Nilsson Model calculations) that this kind of procedure is somehow uncertain or results in lengthy calculations caused by slow convergence. The former case occurs when too few levels are



being fitted. They are then heavily weighted and the overall result is usually poor. On the other hand, when too many levels are being fitted, it appears that the convergence is extremely slow when more than one free parameter is being used.

#### 2.4 Suggestions for the Use of this Program

To simplify the search, it is advised to normalize all the energy terms with respect to the phonon energy. For different values of EPS1 and EPS2 (in  $\hbar\omega$  units), one should plot the results for a reasonable span of  $\xi$ . Once the ranges of  $\xi$ , EPS1 and EPS2 are chosen, the calculations can be achieved with absolute energy units in a limited number of runs.

#### 2.5 Machine Resources

e.g. 6 spin (from  $1/2 \rightarrow 11/2$ ) and  $\xi$  stepped from 0 to 5 by  $\Delta\xi = 0.5$ :  
this corresponds to a total of 66 diagonalizations

TIME: < 2mn  
LINES: < 4K  
SPACE: 100K  
CLASS: A

If  $\xi$  is not stepped, there are only 6 diagonalizations i.e. for a 6 spin value case, one could run under class Q.



## CHAPTER II

## CORPAR II

Title: CORPAR II

Type: Main

Source Language: Fortran IV(G)

Origin: T.P.G. Carola, Nuclear Research Centre

Abstract: Using the wave functions calculated by "CORPAR I", this program calculates electromagnetic transitions, lifetimes, mixing ratios and static moments.

## 1. Description and theory

In the following, the reduced transition probabilities will be explicitly derived for magnetic dipole and electric quadrupole transition. The derivation of the static nuclear moment formulae will be omitted as it is basically equivalent to the B(M1) and B(E2) calculations.

### 1.1 Electromagnetic Transitions

The transition probability  $T(\lambda)$  for radiation of a photon of multipole order  $\lambda$  and frequency  $\omega_\lambda$  is given by (B1 52)

$$T(\lambda) = \frac{8\pi(\lambda+1)}{\lambda[(2\lambda+1)!!]^2} \frac{1}{\hbar} \left(\frac{\omega_\lambda}{c}\right)^{2\lambda+1} B(\lambda) \quad (1)$$

$B(\lambda)$  is the reduced transition probability defined by:



$$B(\lambda) = \frac{1}{2I+1} \sum_{MM',\mu} |\langle I'M' | M(\lambda,\mu) | IM \rangle|^2 \quad (2)$$

where  $M(\lambda,\mu)$  is a multipole operator of order  $\lambda$ ;  $|IM\rangle$  is the initial state and  $|I'M'\rangle$  is the final state.

The values of the multipole operators used here are those introduced by Bohr and Mottelson (Bo 53) for the system resulting of the coupling of a single particle to the quadrupole oscillations of the core surface.

The multipole operators are:

i) Electric quadrupole operators:<sup>†</sup>

$$M_e(2,\mu) = (e_p + e_{\text{eff}}) r^2 Y_{2\mu}^*(\theta,\phi) + \frac{3}{4\pi} Ze R_0^2 \alpha_{2\mu}^* \quad (3)$$

where  $e_p$  is equal to  $e$  for protons and 0 for neutrons,  $e_{\text{eff}}$  is an effective charge parameter,  $r$  the radial coordinate,  $R_0$  the nuclear radius.  $Z$ ,  $e$  have their usual meaning. All the remaining parameters have been defined in Chapter I. The effective charge parameter,  $e_{\text{eff}}$ , has been added here in place of the  $-\frac{Z}{A^2}$  term introduced by Bohr and Mottelson. This term, which corresponds to "recoil effects", is sometimes introduced in calculations but it has little theoretical support. As a matter of fact, some authors have shown that this term should cancel out in complete calculations (Fa 59).

---

<sup>†</sup>In the literature one usually finds  $Y_{2\mu}$  instead of  $Y_{2\mu}^*$ . However, for phase consistency, it is necessary to use the complex conjugate of the spherical harmonics. We recall that:  $Y_{2\mu}^*(\theta,\phi) = (-)^{\mu} Y_{2,-\mu}(\theta,\phi)$ .





ii) Magnetic dipole operators:

$$M_m(1,\mu) = \frac{e\hbar}{2Mc} \sqrt{\frac{3}{4\pi}} \left\{ g_\ell \ell_z + g_s s_z + g_R R_z \right\} \quad (4)$$

$g_\ell$  and  $g_s$  are the orbital and spin g-factors respectively. The core gyromagnetic ratio  $g_R$  is taken as  $Z/A$ , and  $\frac{e\hbar}{2Mc}$  is the nuclear magneton.

### 1.2 Calculation of the B(E2)

We write the basis vectors of the coupled system in the angular momentum space:

$$|j \text{ NR } IM\rangle = \sum_{m,m'} (j \text{ R } mm' | IM) |j \text{ m}\rangle |NR \text{ m}'\rangle \quad (5)$$

Introducing the operator (3) into equation (2) and making use of (5), it can be seen that B(E2) will have the form:

$$B(E2) \sim \frac{1}{2I+1} \left[ \sum_{j \text{ NR}} \sum_{j' \text{ N'R'}} (\alpha A + \beta B + \gamma C) \right]^2 \quad (6)$$

with  $\alpha$ ,  $\beta$  and  $\gamma$  constants to be defined later.

A, B and C are given by:

$$\begin{aligned} A &\equiv \langle j' \text{ N'R' } I'M' | Y_{2\mu}^* | j \text{ NR } IM \rangle \\ B &\equiv \langle j' \text{ N'R' } I'M' | b_\mu | j \text{ NR } IM \rangle \\ C &\equiv \langle j' \text{ N'R' } I'M' | (-)^{\mu} b_\mu^* | j \text{ NR } IM \rangle \end{aligned} \quad (7)$$



## 1.2.1 Calculation of A

$$A \equiv \langle j' N' R' I' M' | Y_{2\mu}^* | j NR IM \rangle = \langle j' N' R' I' M' | (-)^{\mu} Y_{2,-\mu} | j NR IM \rangle$$

Using (5)

$$A \equiv \sum_{\substack{\nu\nu' \\ mm'}} (j' R' \nu\nu' | I' M') (j R mm' | IM) \langle j' \nu | (-)^{\mu} Y_{2,-\mu} | j m \rangle \langle N' R' \nu' | NR m' \rangle$$

Using the orthonormality of the basis vectors  $|NR m' \rangle$  and applying the Wigner-Eckart theorem, one gets:

$$A = \sum_{\substack{\nu\nu' \\ mm'}} \delta_{NN'} \delta_{RR'} \delta_{\nu'\nu} (j' R' \nu\nu' | I' M') (j R mm' | IM) \\ \times (-)^{\mu} (j 2 m - \mu | j' \nu) \langle j' || Y_2 || j \rangle$$

All the following steps are self-explanatory. (Basically one rearranges the various Clebsch-Gordan coefficients in order to get a Racah coefficient). (see e.g. Ro 57)

$$A = \sum_{\nu mm'} (j' R' \nu m' | I' M') (j R mm' | IM) (-)^{\mu} (j 2 m \mu | j' \nu) \\ \times \langle j' || Y_2 || j \rangle \delta_{NN'} \delta_{RR'} \\ = \sum_{\nu mm'} (-)^{j'-\nu} \sqrt{\frac{2I'+1}{2R+1}} (I' j' M' - \nu | R m') (-)^{R+j-I} (R j m' m | IM) \\ \times (-)^{\mu} (-)^{j-m} \sqrt{\frac{2j'+1}{5}} (j' j \nu - m | 2 - \mu) \langle j' || Y_2 || j \rangle \delta_{NN'} \delta_{RR'}$$



$$\begin{aligned}
A &= \sqrt{\frac{(2I'+1)(2j'+1)}{5(2R+1)}} \sum_{\nu mm'} (-)^{R-j'+j-I+j+j'+j-2} \\
&\quad \times (I' j' M' -\nu | R m') (R j m' m | IM) (j' j -\nu m | 2\mu) \langle j' || Y_2 || j \rangle \delta_{NN'} \delta_{RR'} \\
&= \sqrt{(2I'+1)(2j'+1)} (-)^{R-I-j} W(I' j' I j; R 2) (I' 2 M' \mu | IM) \langle j' || Y_2 || j \rangle \delta_{NN'} \delta_{RR'} \\
&\hspace{25em} (8)
\end{aligned}$$

### 1.2.2 Calculation of B

$$B = \langle j' N' R' I' M' | b_\mu | j NR IM \rangle$$

The method is the same as in the calculation of A.

$$\begin{aligned}
&= \sum_{\nu \nu' mm'} (j' R' \nu \nu' | I' M') (j R mm' | IM) \langle j' \nu | j m \rangle \langle R' \nu' | b_\mu | R m' \rangle \\
&= \sum_{\nu \nu' mm'} \delta_{jj'} \delta_{\nu m} (j' R' \nu \nu' | I' M') (j R mm' | IM) (R' 2 \nu' \mu | R m') \langle N' R' || b || NR \rangle \\
&= \sum_{\nu' mm'} (j' R' m \nu' | I' M') (j R mm' | IM) (R' 2 \nu' \mu | R m') \langle N' R' || b || NR \rangle \delta_{jj'} \\
&= \sum_{\nu' mm'} (-)^{R'+\nu'} \sqrt{\frac{2I'+1}{2j+1}} (I' R' -M' \nu' | j -m) (j R mm' | IM) \\
&\quad \times (-)^{R'-\nu'} \sqrt{\frac{2R+1}{5}} (R' R \nu' -m' | 2 -\mu) \langle N' R' || b || NR \rangle \delta_{jj'}
\end{aligned}$$



$$\begin{aligned}
B &= \sqrt{\frac{(2I'+1)(2R+1)}{5(2j+1)}} \sum_{\nu' mm'} (-)^{R'+\nu'+j+R-I+R'-\nu'} (I' R' - M' \nu' | j - m) \\
&\quad \times (j R - m - m' | I - M) (R' R \nu' - m' | 2 - \mu) \langle N' R' || b || NR \rangle \delta_{jj'} \\
&= \sqrt{(2I'+1)(2R+1)} (-)^{2R'+j+R-I} W(I' R' IR; j 2) (I' 2 - M' - \mu | I - M) \\
&\quad \times \langle N' R' || b || NR \rangle \delta_{jj'} \\
&= \sqrt{(2I'+1)(2R+1)} (-)^{2R'+j+R-I+I'+2-I} W(I' I R' R; 2 j) (I' 2 M' \mu | IM) \\
&\quad \times \langle N' R' || b || NR \rangle \delta_{jj'}, \quad (9)
\end{aligned}$$

### 1.2.3 Calculation of C

$$\begin{aligned}
C &= \langle j' N' R' IM | (-)^{\mu} b_{-\mu}^* | j NR IM \rangle \\
&= (-)^{\mu} \sum_{mm' \nu \nu'} (j' R' \nu \nu' | I' M') (j R mm' | IM) \langle j' \nu | j m \rangle \langle R' \nu' | b_{-\mu}^* | R m' \rangle \\
&= (-)^{\mu} \sum_{mm' \nu \nu'} \delta_{jj'} \delta_{\nu m} (j' R' \nu \nu' | I' M') (j R mm' | IM) (R 2 m' - \mu | R' \nu') \langle N' R' || b^* || NR \rangle
\end{aligned}$$

The calculation is the same as for A and B. The final result is:

$$\begin{aligned}
C &= \sqrt{(2I'+1)(2R'+1)} (-)^{R'+2R+j-I+I'+2-I} W(I' I R' R; 2 j) (I' 2 M' \mu | IM) \\
&\quad \times \langle N' R' || b^* || NR \rangle \delta_{jj'}, \quad (10)
\end{aligned}$$





## 1.2.4

As seen in eq. (6), the B(E2) will be proportional to a sum of the square of (A+B+C).

$$\begin{aligned}
 (A+B+C) = & \sqrt{(2I'+1)} (I' \ 2 \ M' \ M-M' | IM) [\sqrt{2j'+1} W(jj' \ I I'; 2R) (-)^{R-I-j} \langle j' || Y_2 || j \rangle \\
 & \delta_{NN'} \delta_{RR'} + \{ \sqrt{(2R+1)} (-)^{2R'+j+R-2I+I'+2} \langle N'R' || b || NR \rangle \\
 & + \sqrt{2R'+1} (-)^{R'+2R+j-2I+I'+2} \langle N'R' || b^* || NR \rangle \} \delta_{jj'} W(R'R \ I' I; 2j) ] \\
 & (11)
 \end{aligned}$$

In order to simplify the phase factors, the COMPLETE expression can be multiplied by any phase factor, bearing in mind this expression will ultimately be squared. If the complete expression is multiplied by  $(-)^{I-I'+1}$ , one then gets: (Note that in the phase factor -R or +R is equivalent as R is integer).

$$\begin{aligned}
 (A+B+C) = & \sqrt{(2I'+1)} (I' \ 2 \ M' \ M-M' | IM) \\
 & \times [ (-)^{I'+j-R} W(jj' \ I I'; 2R) \sqrt{2j'+1} \langle j' || Y_2 || j \rangle \delta_{NN'} \delta_{RR'} \\
 & + (-)^{I-j} \left\{ (-)^{R'} \sqrt{2R'+1} \langle N'R' || b^* || NR \rangle \right. \\
 & \left. + (-)^R \sqrt{2R+1} \langle N'R' || b || NR \rangle \right\} W(R'R \ I' I; 2j) \delta_{jj'} ] \\
 & (12)
 \end{aligned}$$

To get the B(E2), one must now introduce the complete quadrupole operator (the constants have been left out) and include the complete



eigenvalues functions defined by:

$$|E \text{ IM}\rangle = \sum_{j, N, R} A_{j, N, R}(E) |j \text{ NR IM}\rangle \quad (13) \quad (\text{see equation (19) in part I})$$

The notation used by Choudhury and O'Dwyer (Ch 67) has been followed closely. Keeping with these authors, the following terms are now introduced:

$$\eta_1 = (e_p + e_{\text{eff}}) \langle r^2 \rangle = \frac{3}{5} (e_p + e_{\text{eff}}) R_0^2 \quad (14)$$

$$\eta_2 = \frac{3}{4\pi} \sqrt{\frac{\hbar\omega}{2C}} Ze R_0^2 \quad (15)$$

Using eq. (12) and the expansion (13), together with the definition of  $B(E2)$ , one finally gets:

$$B(E2)_{I \rightarrow I'} = (2I'+1) \left| \sum_{\substack{j \text{ NR} \\ j' N' R'}} A_{j \text{ NRI}}(E) A_{j' N' R' I'}(E') \times \left\{ \eta_1 (-1)^{I'+j-R} \sqrt{2j'+1} \langle j' || Y_2 || j \rangle \right. \right. \\ \left. \left. W(jj' II'; 2R) \delta_{NN'} \delta_{RR'} + \eta_2 (-1)^{I-j} [(-1)^{R'} \sqrt{2R'+1} \langle N' R' || b^* || NR \rangle \right. \right. \\ \left. \left. + (-1)^R \sqrt{2R+1} \langle N' R' || b || NR \rangle \right] W(R' R I' I; 2j) \delta_{jj'} \delta_{\ell\ell'} \right\} \right|^2 \quad (16)$$

where the relation  $\sum_{MM'} |(I' 2 M' M-M' | IM)|^2 = 2I+1$  has been used. The  $\delta_{\ell\ell'}$  term has been introduced for the sake of completeness. ( $\ell$  is the orbital angular momentum of the particle in the state  $|jm\rangle$ ).



### 1.3 Calculation of B(M1)

Following the same method as described in the case of the calculation of B(E2), it can be seen that three terms have to be calculated which can be labelled as:

$$\begin{aligned}
 A &\equiv \langle j' \ N'R' \ I'M' | \ell_z | j \ NR \ IM \rangle \\
 B &\equiv \langle j' \ N'R' \ I'M' | s_z | j \ NR \ IM \rangle \\
 C &\equiv \langle j' \ N'R' \ I'M' | R_z | j \ NR \ IM \rangle
 \end{aligned} \tag{17}$$

#### 1.3.1 Calculation of A

One starts by using the expansion of  $|j \ NR \ IM\rangle$  (eq. 5), then introduces an expansion in the  $(\ell, s)$  space in order to get the eigenvalue of the operator  $\ell_z$ . The other steps deal mainly with re-expressing the different Clebsch-Gordan coefficients in order to regroup them into Racah coefficients. The different steps read as follows:

$$\begin{aligned}
 A &= \sum_{\substack{\nu\nu' \\ mm'}} (j' \ R' \ \nu\nu' | I'M') (j \ R \ mm' | IM) \langle j' \nu | \ell_z | jm \rangle \langle N'R' \ \nu' | NR \ m' \rangle \\
 &= \sum_{\substack{\nu\nu' \\ mm'}} \delta_{NN'} \delta_{RR'} \delta_{\nu\nu'} (j' \ R' \ \nu\nu' | I'M') (j \ R \ mm' | IM) A'
 \end{aligned}$$

where  $A' = \langle j' \ \nu | \ell_z | jm \rangle$

In order to evaluate  $A'$ , let us express  $|jm\rangle$  in terms of the new subspace:



$$|jm\rangle = \sum_{m_\ell m_s} (\ell s m_\ell m_s | jm) |\ell\rangle |s\rangle$$

$$\therefore A' = \sum_{\substack{m_\ell m_s \\ m'_\ell m'_s}} (\ell s m_\ell m_s | jm) (\ell' s' m'_\ell m'_s | j'v) \langle \ell' m'_\ell | \ell_z | \ell m_\ell \rangle \delta_{ss'}$$

The last term is easily evaluated using the Wigner-Eckart theorem (see e.g. Bo 69, page 82).

$$A' = \sum_{\substack{m_\ell m_s \\ m'_\ell m'_s}} (\ell s m_\ell m_s | jm) (\ell' s' m'_\ell m'_s | j'v) (\ell 1 m_\ell \mu | \ell' m'_\ell) \langle \ell' || \ell_z || \ell \rangle \delta_{s's}$$

$$= \sum_{m_\ell m_s} (\ell s m_\ell m_s | jm) (\ell' s m_\ell m_s | j'v) (\ell 1 m_\ell \mu | \ell' m_\ell) \sqrt{\ell(\ell+1)} \delta_{\ell'\ell}$$

$$= \sum_{m_\ell m_s} (-)^{\ell+s-j} (s \ell m_s m_\ell | jm) (-)^{\ell-m_\ell} \left[ \frac{2j'+1}{2} \right]^{1/2} (j' \ell m' - m_\ell | s m_s)$$

$$\times (-)^{\ell-m_\ell+\ell+\ell-1} \left[ \frac{2\ell+1}{3} \right]^{1/2} (\ell \ell - m_\ell m_\ell | 1\mu) \sqrt{\ell(\ell+1)}$$

$$= \sum_{m_\ell m_s} (-)^{\ell-j-1/2-2m_\ell} (s \ell m_s m_\ell | jm) (j' \ell' m' - m_\ell | s m_s)$$

$$\times (\ell \ell - m_\ell m_\ell | 1\mu) \left[ \frac{(2j'+1)(2\ell+1)}{3 \times 2} \right]^{1/2} \sqrt{\ell(\ell+1)}$$

$$A' = (-)^{\ell-j+1/2} \sqrt{2j'+1} \sqrt{\ell(\ell+1)(2\ell+1)} W(j' \ell j \ell; 1/2 1) (j' 1 m_\mu | jm) \quad (18)$$





Now

$$A = \sum_{\nu m m'} (-)^{\ell-j+1/2} \sqrt{2j'+1} \sqrt{\ell(\ell+1)(2\ell+1)} W(j' j \ell \ell; 1/2 \ 1) \\ \times \{ (j' \ 1 \ m' \ \mu | jm) (j' \ R' \ \nu \nu' | I' M') (j \ R \ m m' | IM) \} \delta_{NN'} \delta_{RR'} \quad (19)$$

$$\text{where } \{ \} = \sum_{\nu m m'} (j' \ R' \ \nu \nu' | IM') (j \ R \ m m' | IM) (j' \ 1 \ \nu \ \mu | jm) \delta_{NN'} \delta_{RR'} \\ = \sum_{\nu m m'} \sqrt{\frac{2I'+1}{2R+1}} (-)^{j'-\nu} (I' \ j' \ M' -\nu | R \ m') (-)^{R+j-I} (R \ j \ m' m | IM) \\ \times (-)^{j'-\nu+j'+j-1} \sqrt{\frac{2j+1}{3}} (j' j \ -\ \nu \ m | 1 \ \mu) \delta_{NN'} \delta_{RR'} \\ = (-)^{R-I+2j+j'} W(j' j \ I' I; 1R) (I' \ 1 \ m' \ \mu | IM)$$

Finally, A becomes:

$$A = (-)^{R-I+\ell-1/2+j+j'} \sqrt{(2I'+1)} \sqrt{(2j'+1)(2j+1)} \sqrt{\ell(\ell+1)(2\ell+1)} \\ \times W(j' \ell \ j \ \ell; 1/2 \ 1) W(j' j \ I' I; 1R) (I' \ 1 \ M' \ \mu | IM) \quad (20)$$

1.3.2 The calculation of the B term is equivalent, but one uses the fact that  $s = 1/2$ ; therefore one gets:

$$B = (-)^{R-I+\ell-1/2} \sqrt{2I'+1} \sqrt{(2j'+1)(2j+1)} \sqrt{3/2} \\ \times W(j' \ 1/2 \ j \ 1/2; 1 \ \ell) W(j' j \ I' I; 1R) (I' \ 1 \ M' \ \mu | IM) \quad (21)$$



1.3.3 In order to evaluate C, one will use the relation:

$$\begin{aligned}
 \langle N'R'M' | R | NRM \rangle &= \sqrt{R(R+1)} (R \ M \ 1 \ \mu | R'M') \\
 C &= \sum_{\substack{\nu\nu' \\ mm'}} (j \ R \ mm' | IM) (j' \ R' \ \nu\nu' | I'M') (R \ 1 \ m' \ \mu | R' \ \nu') \sqrt{R(R+1)} \delta_{NN'} \delta_{RR'} \delta_{jj'} \\
 &= \sum_{\substack{\nu' \\ mm'}} (-)^{R'+\nu'} \sqrt{\frac{2I'+1}{2j+1}} (I' R' - M' \ \nu | j - m) (j \ R \ mm' | IM) \\
 &\quad \times (-)^{R+m'} \sqrt{\frac{2R'+1}{3}} (R' \ R \ \nu' - m | 1 \ \mu) \sqrt{R(R+1)} \delta_{NN'} \delta_{RR'} \\
 &= \sum_{\substack{\nu' \\ mm'}} (-)^{j+R-I} \sqrt{\frac{2I'+1}{2j+1}} \sqrt{\frac{2R+1}{3}} (I' \ R - M'm' | j - m) \\
 &\quad \times (j \ R - m - m' | I-M) (R \ R \ \nu' \ m' | 1 - \mu) \sqrt{R(R+1)} \\
 &= (-)^{j+R-I} \sqrt{2I'+1} \sqrt{2R+1} W(I' R \ IR; j 1) (I' \ 1 - M' - \mu | I-M) \sqrt{R(R+1)} \\
 &= (-)^{I'+j-R} \sqrt{2I'+1} \sqrt{R(R+1)(2R+1)} W(I' R \ IR; j 1) (I' \ 1 \ M' \ \mu | IM) \quad (22)
 \end{aligned}$$

In order to get B(M1), one now proceeds as in the calculation of B(E2) (see eq. (13) and what follows). To be able to compare the complete result with the result of Choudhury and O'Dwyer (Ch 67), it is necessary to multiply throughout (before squaring) by the phase  $(-)^{I'+I+2J}$ .<sup>\*</sup> It is then possible

---

<sup>\*</sup> This difference in phase - which does NOT affect the final result - apparently comes from another definition of the basis vectors, namely:

$$|j \ NR \ IM\rangle = \sum_{m, m'} (Rj \ m'm | IM) |jm\rangle |NR \ m'\rangle$$

Comparing with the definition used here, one sees that the Clebsch-Gordan coefficients differ by a phase:

$$(Rj \ m'm | IM) = (-)^{R+j-I} (j \ R \ mm' | IM)$$



to square and sum the square of the remaining Clebsch-Gordan coefficient. The final result reads as:

$$\begin{aligned}
 B(M1)_{I \rightarrow I'} &= \frac{3}{4\pi} (\mu_N)^2 (2I'+1) \left| \sum_{jj',NR} A_{jNR I}(E) A_{j',NR I'}(E') \right. \\
 &\times \left\{ (-)^{I'+R+\ell-1/2} [(2j+1)(2j'+1)]^{1/2} \right. \\
 &\quad \times [g_\ell (-)^{j+j'} [\ell(\ell+1)(2\ell+1)]^{1/2} W(j'j \ell \ell; 1 \ 1/2) \\
 &\quad + g_s \sqrt{3/2} W(jj' \ 1/2 \ 1/2; 1 \ell)] W(j'j \ I' I; 1 R) \delta_{\ell \ell} \\
 &\quad \left. + g_R (-)^{I+j+R} [R(R+1)(2R+1)]^{1/2} W(RR \ I' I; 1 j) \delta_{\ell \ell} \delta_{jj'} \right\}^2 \quad (23)
 \end{aligned}$$

where  $\mu_N$  is the nuclear magneton  $\frac{e\hbar}{2Mc}$

#### 1.4 Static Moments

The method used to calculate the static moments is the same method we have used in all the previous calculations. The results will now merely be stated:

##### 1.4.1 Electric quadrupole moment

The electric quadrupole moment in a given state of spin  $I$  and energy  $E$  is defined as: (Bo 53, Ch 54)

$$Q(E; I) = \langle E \ I M | \sqrt{\frac{16\pi}{5}} (e_p + e_{eff}) r^2 Y_{20}^*(\theta, \phi) + \frac{3}{\sqrt{5\pi}} Z R_0^2 \alpha_{20}^* | E \ I M \rangle_{M=I}$$



where the terms of this equation have been defined earlier.

Using the wave functions defined by eq. (5), one gets:

$$\begin{aligned}
 Q(E;I) = & \frac{3}{5} R_0^2 \sqrt{\frac{I(2I+1)(2I-1)}{(I+1)(2I+3)}} \sum_{\substack{j_{NR} \\ j'N'R'}} A_{j_{NR}I}(E) A_{j'N'R'I}(E) \\
 & \times \sqrt{\frac{16\pi}{5}} (e_p + e_{eff}) (-)^{I+j-R} \delta_{NN'} \delta_{RR'} \sqrt{2j'+1} \langle j' || Y_2 || j \rangle W(jj' II; 2R) \\
 & + Z \frac{\hbar\omega}{k} \xi (-)^{I-j} \delta_{jj'} \delta_{\ell\ell'} [(-)^{R'} \sqrt{2R'+1} \langle N'R' || b^* || NR \rangle \\
 & + (-)^R \sqrt{2R+1} \langle N'R' || b || NR \rangle] W(RR' II; 2j) \quad (25)
 \end{aligned}$$

#### 1.4.2 Magnetic dipole moment

Similarly the magnetic dipole moment  $\mu$  is defined by

$$\mu(E;I) = \langle E IM | \mu_N (g_\ell \ell_z + g_s s_z + g_R R_z) | E IM \rangle_{I=M}$$

or

$$\begin{aligned}
 \mu(EI) = & \mu_N \sqrt{\frac{I(2I+1)}{I+1}} \sum_{\substack{j_{NR} \\ j'N'R'}} A_{j_{NR}I}(E) A_{j'N'R'I}(E) \left\{ g_\ell (-)^{I+j-R} \delta_{NN'} \delta_{RR'} \delta_{jj'} \delta_{\ell\ell'} \right. \\
 & \times \sqrt{R(R+1)(2R+1)} W(RR II; 1j) + g_\ell (-)^{R-\ell+1/2+j+j'-I} \delta_{NN'} \delta_{RR'} \delta_{\ell\ell'} \\
 & \times \sqrt{(2j+1)(2j'+1)} \sqrt{\ell(\ell+1)(2\ell+1)} W(jj' II; 1R) W(\ell\ell jj'; 1 \frac{1}{2}) \\
 & + g_s (-)^{\ell+1/2+R-I} \delta_{NN'} \delta_{RR'} \delta_{\ell\ell'} \\
 & \left. \times \sqrt{3/2} \sqrt{(2j+1)(2j'+1)} W(jj' II; 1R) W(jj' 1/2 1/2; 1\ell) \right\} \quad (26)
 \end{aligned}$$





## 2. Description of the program

The program CORPAR II is basically simple. It reads in the wave functions output by CORPAR I and two main subroutines called EMTRAN and STATIC are used to calculate the B's and nuclear moments respectively. The remaining of the program is constituted by INPUT-OUTPUT subroutines and various functions to be used with EMTRAN or STATIC.

### 2.1 Input-Output Data

In order to facilitate possible expansions of this program, each set of data to be read is preceded by a card identified by an index ITAG (Format I1).

The first set of data - before reading wave functions - is preceded by ITAG=1 and contains: Z, atomic number; A, atomic mass; AM1, AM2, AM3 angular momentum of the odd particle in the respective orbits available; AN1, AN2, AN3 the corresponding orbital angular momenta of these orbits (Format 8F10.5).

Normally these values are input once and for all (unless calculations are done for different nuclei!). Then data are input at will, being identified by the control index ITAG.

Other cases:

ITAG = 0

Each BLOCK DATA output by CORPAR I (i.e. for a complete set of wave functions for given  $\xi$ ,  $\varepsilon_1$ ,  $\varepsilon_2$ ,  $\hbar\omega$  and for different final spin I) must be preceded and followed by a blank card.



ITAG = 3

Read EFF (F10.5)

If EFF=0 charge is e for proton, 0 for neutron

If EFF $\neq$ 0 and  $\neq$  10 charge is (1+EFF) e for proton, EFF x e for neutron

If EFF=10 charge is  $\left(1 - \frac{Z}{A^2}\right)$  e for proton,  $-\frac{Z}{A^2}$  e for neutron.

ITAG = 4

Read Title (80 alphameric characters)

Read DIFF, KI, KF, INDI, INDF, NQ [F10.5, 5(I2,8x)].

DIFF is the energy of the gamma ray for the transition considered.

The KI and KF coefficients define a block data [i.e. a set of wave functions, ..., for a given final spin I]. These coefficients are printed by CORPAR I.

The INDI and INDF coefficients define the level considered with each block KI and KF respectively (see example). If NQ = 2, only static moments are calculated.

ITAG = 5

Read COEFK and CTWO (2F10.5)

If these values are not entered COEFK = k is set at 40 MeV;

CTWO =  $C_2$  is calculated from this value.

ITAG = 6

End of calculation.



## 2.2 Example

This is a sample input corresponding to calculations of e-m transitions in  $^{55}\text{Fe}$ . The data punched out by CORPAR I (defined by DATA hereafter) corresponded to  $\xi = 2.75$ ,  $\hbar\omega = 1.40$  MeV,  $\epsilon_1 = 2.02$  MeV,  $\epsilon_2 = 2.2$  MeV,  $1/2 \leq I \leq 11/2$ .

INPUT:

ITAG = 1

26.      55.      1.5      0.5      2.5      1.      1.      3.

ITAG = 0



DATA

ITAG = 0

ITAG = 3

0.5

ITAG = 4

55 FE CALCULATES STATIC

0.      2      2      16      16      2

[i.e. KI=KF=2, here spin  $I=3/2$ ;      INDI=INDF=16, here ground state;  
NQ=2: calculate static]

ITAG = 4

55 FE FIRST 1/2 TO G.S.

0.412      1      2      10      16

[i.e. KI=1: spin  $I=1/2$ ; INDI=10: lowest eigenvalue; to be  
calculated here the  $1/2 \rightarrow 3/2$ (g.s.) 0.412 MeV transition]

ITAG = 6

END



## Corresponding OUTPUT

1st Page:

Atomic number: 26.                      Mass number: 55.

THE G FACTORS USED HERE ARE:

GL=0.0                      GS=-3.8263                      GR=0.4727

THE FOLLOWING CALCULATIONS ARE DONE WITH A CHARGE EQUAL TO: 0.500 IN UNITS OF E  
 CALCULATIONS FOR XI=2.750                      HBAR-OMEGA=1.400 MeV

END OF DATA READING

THE PARTICLE HAS A SPIN  $J=3/2$  IN THE GROUND STATE. THE CORRESPONDING L IS 1  
 THE NEXT ORBITS AVAILABLE ARE:  $J_2=1/2$  WITH  $L=1$  AND  $J_3=5/2$  WITH  $L=3$

Next Page:

55FE CALCULATES STATIC

THE LEVEL WITH SPIN 1.500 HAS A  $Q_{EI}=-0.143$  E00 BARNSMAGNETIC DIPOLE MOMENT  $-0.162$  E01 N.M.55FE FIRST  $1/2$  TO G.S.

KI, KF, INDI, INDF AND NQ ARE RESPECTIVELY 1 2 10 16 0

DECAY FROM THE  $I=1/2$  STATE TO THE  $I=3/2$  STATE  $E(\text{GAMMA})=0.412$  MeV $B(M1) = 0.189E\ 01$  (N.M.)SQ  $T(M1) = 0.233E\ 13$  1/SEC  $\tau_{M1} = 0.430$  E-12 SEC $B(E2) = 0.167E\ 03$  E2-FM4  $T(E2) = 0.244E\ 10$  1/SEC  $\tau_{E2} = 0.411$  E-09 SEC

DELTA = - 1.85 DEGREES

DELSQ = 0.105 E-02

 $\tau = 0.429$  E-12                      GAMMA = 0.153 E-02 EV





All the variable names have their usual meaning. The B's and T's have already been defined (see eq. 1 and 2). TAU1 and TAU2 are the corresponding partial lifetimes; DELTA is the mixing ratio in degrees (i.e.  $\arctan \delta$ ); DELSQ is  $\delta^2$ ; TAU is the lifetime (in sec.) for the level decaying through this transition; GAMMA is the corresponding width in eV.

### 2.3 Machine Resources

CORPAR II is a fast program. For most of the calculations, i.e. for 20 to 30 transitions, the following requirements will be quite sufficient:

TIME:  $\leq 2mn$

LINES:  $\leq 2K$

SPACE: 100K

CLASS: A



## References

- Bl 52 J.M. Blatt and V.F. Weisskopf, Theoretical Nuclear Physics, John Wiley and Sons, Inc., New York, 1952.
- Bo 52 A. Bohr, Dan. Mat. Fys. Medd. 26, No. 14 (1952).
- Bo 53 A. Bohr and B.R. Mottelson, Dan. Mat. Fys. Medd. 27, No. 16 (1953).
- Bo 69 A. Bohr and B.R. Mottelson, Nuclear Structure - Vol. I - W.A. Benjamin, Inc. Press, 1969.
- Ch 54 D.C. Choudhury, Dan. Mat. Fys. Medd. 28, No. 4 (1954).
- Ch 67 D.C. Choudhury and T.F. O'Dwyer, Nucl. Phys. A93 (1967) 300.
- Fa 59 S. Fallieros and R.A. Ferrell, Phys. Rev. 116 (1959) 660.
- Fo 55 K.W. Ford and C. Levinson, Phys. Rev. 100 (1955) 1.
- Gl 60 N.K. Glendenning, Phys. Rev. 119 (1960) 213.
- Ha 63 M. Harvey, Nucl. Phys. 48 (1963) 578.
- Pa 70 T. Paradellis and S. Hontzeas, Nucl. Phys. A140 (1970) 400.
- Ra 63 K. Ramavataram, Phys. Rev. 132 (1963) 2255.
- Ro 57 M.E. Rose, Elementary theory of angular momentum, John Wiley and Sons, Inc., 1957.
- Ro 59 M. Rotenberg, R. Bivin, N. Metropolis, J.K. Wooten, Jr., The 3-j and 6-j symbols, Technology Press MIT, Cambridge, Mass., 1959.
- Ru 68 M.L. Rustgi, J.G. Lucas and S.N. Mukherjee, Nucl. Phys. A117 (1968) 321.









**B29965**